January 2010

Design, Synthesis and Characterization of Synthetic Ion Receptors as Biologically Functional Ion Carriers and Channels

Carl Yamnitz
Washington University in St. Louis

WASHINGTON UNIVERSITY IN ST. LOUIS

Department of Chemistry

Dissertation Examination Committee:
George W. Gokel, Co-Chairperson
Joshua A. Maurer, Co-Chairperson
Jianmin Cui
Peter P. Gaspar
Kevin D. Moeller
John-Stephen A. Taylor

Design, Synthesis and Characterization of Synthetic Ion Receptors as Biologically Functional Ion Carriers and Channels

By

Carl Robert Yamnitz

A dissertation presented to the Graduate School of Arts and Sciences
of Washington University in partial fulfillment of the
requirements for the degree of Doctor of Philosophy

August 2010

St. Louis, Missouri

ABSTRACT OF THE DISSERTATION

Design, Synthesis and Characterization of Synthetic Ion Receptors as Biologically Functional Ion Carriers and Channels

by

Carl Yamnitz

Doctor of Philosophy in Chemistry

Washington University, 2010

Dr. George W. Gokel, Thesis Advisor

The study of proteins and natural molecules that transport cations and anions across biological membranes has been a major focus of biochemistry and cellular biology for more than a century. The function of ion transporters is vital for all known forms of life. Natural and synthetic transporters can have applications as antimicrobial agents, in nerve impulse transduction and cell signaling.

The current work was performed to further the understanding of a diverse array of novel and previously-studied synthetic molecules as membrane-active ion transporters. In the process, important facets such as ion binding capacity, aggregation behavior, ion transport functionality, and antimicrobial activity are investigated. While these studies yield structural and mechanistic insights into our own research group's synthetic systems, they may also aid in understanding both other synthetic ion transporters as well as natural ion carriers and channels.

Among the studies that are performed, is the design, synthesis and characterization of members of the dipicolinic dianilide class of compounds as synthetic chloride channels. In originating this project, an array of both known and novel synthetic chloride receptors were modeled computationally. These compounds were selected for their synthetic accessibility and potential use as a chloride transporter. While some of the dipicolinic dianilides or closely-related isophthalic dianilides have been previously reported, few have been investigated for chloride-binding activity and none for chloride transport activity. Chloride binding and transport activity were correlated to the structural variations within the family, which entailed variation of aromatic substituents. This class of molecules are made in a one step synthesis from commercially-available materials. Some members elicit rapid chloride transport activity (over 80% in 10 minutes or less) at low micromolar concentrations. At least one of these select members displays channel functionality in planar bilayers—one of the smallest family of compounds known to do so. Molecular modeling and monitoring aggregation formation by fluorescence spectroscopy reveals that a stack of transporter monomers presents a geometric arrangement conducive of transmembrane pore formation.

This class of compounds, among others, is investigated for antimicrobial activity in Gram negative *E. coli*. While no activity is present for these chloride transporters, co-application with a known antimicrobial cation transporter diminishes the antimicrobial activity of the latter in Gram positive *S. epidermidis*.

Acknowledgements

There are many people in the past five years that have been extremely important in my development as a scientist. First, I would like to express my gratitude to my mentor and research advisor Dr. George Gokel, with whom I have had the pleasure of working with for over four years of my graduate studies. I thoroughly appreciate all of the support, encouragement and guidance that he has provided over the years. Words cannot possibly detail the level of indebtedness I have to this extraordinary individual. His success is evident in his over 400 publications and numerous awards and other accomplishments.

I would like to thank Dr. Peter Gaspar and Dr. Joshua Maurer for providing valuable input and guidance throughout the course of my project. Their insight and suggestions have led to a number of new directions for my research, yielding important discoveries. I also thank Dr. Kevin Moeller, Dr. John-Stephen Taylor, and Dr. Jianmin Cui for taking time out of their busy schedules to serve on my thesis committee.

My research could not have been possible without the strong knowledge base provided by courses instructed by a collection of exceptional professors. I thank Dr. Peter Gaspar, Dr. Kevin Moeller, Dr. Alfred Hortmann, Dr. John Bleeke, Dr. William Spees, Dr. Jingyue Liu, and the organic chemistry faculty members for sharing their wealth of knowledge with myself and my classmates.

I would also like to thank my co-workers in the Gokel research group, whose names should not go without mention. While the duration of my time with was short, the help of Dr. Robert Pajewski, Dr. Riccardo Ferdani, Mrs. Jola Pajewska and Zac Cusumano,

has been invaluable to my own research. I have been fortunate to have had more time to work with Dr. Elizabeth Elliott, Dr. Lei You and Dr. Ruiqiong Li, Dr. Natalie Barkey and Dr. Brock Levin who have provided both technical assistance as well as insightful suggestions for my research. Aside from their own insights, I have also had the pleasure of collaborating with Dr. Wei Wang, Dr. Oleg Kulikov, and Ms. Saeedeh Negin on research projects. While my time with them has also been short, it has been a pleasure to work with Mr. Matt Walsh and Mr. Jason Atkins during their undergraduate internships. Lastly within the Gokel group, I would like to thank Mr. Alex Carasel and Dr. Megan Daschbach Eckhardt, who have not only been exceptional collaborators and co-workers, but wonderful friends over the years as well.

Outside of the Gokel research group, I would like to thank Dr. Rudolph Winter, Dr. Jingyue Liu, Dr. Nigam Rath, Dr. Michael Nichols, Dr. Leo Seballos and Joseph Kramer at the University of Missouri-St. Louis for their collaborations and/or fruitful discussions. At Washington University, I would also like to thank Dr. Ed Hiss and Mrs. Norma Taylor for their tremendous help as well as Dr. Kit Mao for all of her efforts to accommodate her two commuting employees over the course of this last academic year.

Finally, I must thank my parents, Robert and Marilym, my brother Dustin and especially my wife, Jennifer, for all of their love and encouragement. Their optimism and unyielding belief in me has given me the strength to overcome what difficulties I have faced and continue towards this goal. Any past or future success of mine, I credit to their affection and support.

Table of Contents

List of Figures, Tables and Schemes

CHAPTER 1

The Design, Synthesis and Characterization of Synthetic Ion Receptors as Biologically Functional Ion Carriers and Channels

Background

Life and Compartmentalization

One of the seven pillars of life, as defined by Daniel Koshland,[1] is compartmentalization, or the separation of the other essentials of life from its environment. Compartmentalization is important as it allows for the regulation of chemical concentrations and, by proxy, regulation of chemical reactions. While in the simplest forms of cellular life, like prokaryotic bacteria, one level of compartmentalization is sufficient,[2] in more advanced forms, this compartmentalization is further manifested in cellular organelles such as the nucleus and mitochondria.[3] Without doubt, compartmentalization entails isolation, utilizing barriers to the ingress and egress of certain chemical species, but it cannot be fully achieved without the selective and regulated control of the transport of selected species.

To use a historical metaphor, the major cities of medieval and classical Eurasia could almost certainly not have existed without thick walls to keep out bandits and deter invaders. However, with the walls in place, there would have been no city at all without gates and guards to allow merchants, soldiers and citizens to pass through freely.

Phospholipid Membrane

In the most common forms of life, the isolation aspect of compartmentalization is accomplished via cellular membranes composed mainly of phospholipids.[4] Phospholipids, such as the dioleoylphosphatidylcholine molecule seen in Figure 1.1, are amphiphilic molecules with hydrophilic charged polar head-group moieties, a region of intermediate polarity, and long, hydrophobic acyl tails. A phospholipid membrane is composed of two leaflets or layers, a characteristic that gives rise to the alternate nomenclature of "phospholipid bilayer." Within a leaflet, the polar head-group of a phospholipid is aligned with the polar head-groups of other directly adjacent monomers. Likewise, the hydrophobic tails are in close contact with the acyl tails of adjacent monomers.[4] The leaflets themselves are arranged in a tail-to-tail fashion with the polar head-groups of each layer directed out toward the polar aqueous surroundings, minimizing the exposure of non-polar hydrophobic moieties to the polar aqueous environment.[5] If this bilayer were extended into a spherical or other hollow 3-dimensional shape, a vesicle or compartment would be formed. The end result is that a distinctly hydrophobic slab, located in the interior of the bilayer, separates the aqueous intracellular domain from the aqueous extracellular environment.

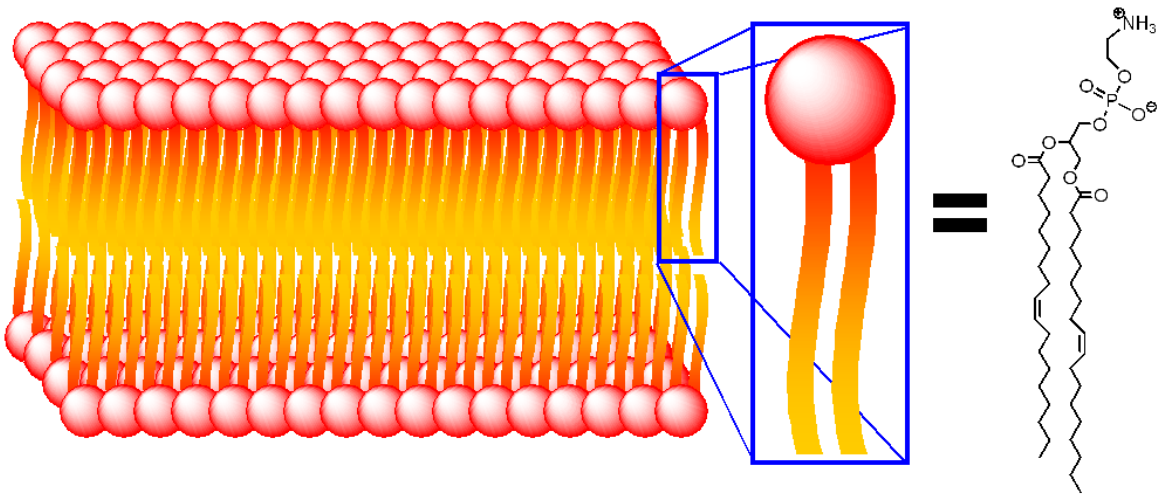

Figure 1.1 *Cartoon representation of a phospholipid bilayer showing phospholipid monomers (in box) aligning tail to tail, with hydrophilic head groups exposed to the aqueous environment. A monomer here represents a molecule of a typical phospholipid, dioleoylphosphatidyl choline (DOPC).*

Membrane Permeability

While lipophilic molecules can pass freely from one leaflet of the bilayer to the other, they cannot permeate into the aqueous surroundings. Conversely, for all but the smallest uncharged molecules exhibiting a polar surface (water, molecular oxygen, etc.) or densely-charged surface (sodium cation, chloride anion, adenosine triphosphate), the energy barrier required to permeate the non-polar region of the bilayer is too high to pass from aqueous phase to aqueous phase without assistance. However, these species can associate into the aqueous milieu as well as with the hydrophilic head-group domain of the phospholipid bilayer.[6] A summary of these different chemical species can be seen in Table 1.1.

Type	Examples	Membrane Permeable?
Non-polar	hexane	Yes
Large polar	glucose	**No**
Small polar	H_2O	Yes
Dense Surface Charge	Na^+, Cl^-, ATP^{4-}	**No**
Hindered or Diffuse Surface Charge	I^-	Yes

Table 1.1 *Summary of the permeability of chemical species through membranes.*

Concentration Gradients

As previously stated, the impermeability of ions through the phospholipid membrane imparts the ability to isolate aqueous environments from one another. Thus, through either natural circumstances or (more often) directed effort by a cell, ion concentrations can vary between the extracellular matrix and the cytosol. It is because of this aspect—ion homeostasis—that many cellular processes function. The regulation of intra- and extracellular ion concentrations is paramount to the maintenance of a fully functional cell. Undesired disruption of this regulation can cause apoptosis—programmed cell death—or in extreme cases, necrosis—immediate cell death. This latter event can occur from disruption of osmotic balance and cytolysis, or rupturing of the cell membrane, as water can move freely through the phospholipid bilayer. The general intra- and extracellular concentrations of common ions in mammals[7] are presented in Table 1.2. This relative trend in ion concentrations is seen throughout most biological systems, from mammals to *E. coli*.

Ion	Intracellular Concentration	Extracellular Concentration
K^+	139 mM	4 mM
Na^+	12 mM	145 mM
Cl^-	4 mM	116 mM

Table 1.2 *Intra- and extracellular ion concentrations of mammalian cells.*[7]

Amphiphilic Molecules

The mixed hydrophobic-hydrophilic nature of amphiphiles theoretically allows them, in an aggregated state, to permeate both the hydrophobic bilayer interior as well as the aqueous bilayer exterior. In aqueous milieu, the amphiphilic monomers arrange in such a way that their polar head-groups are directed externally into the polar aqueous exterior. Hydrophobic tails are directed inward, minimizing the number and degree of hydrophobic-hydrophilic contacts. Conversely, aggregates in a non-polar environment would be composed of polar head-groups in proximity to one another in three dimensions and lipophilic tails exposed to the similarly lipophilic surroundings. However, the formation of either of these types of aggregates is highly dependent on the geometric constraints of the molecules, and not every type of amphiphile would be able to form each type of aggregate.[8]

Either arrangement can result in (among others) flat bilayers or disks as with phospholipid bilayers, large hollow, spherical aggregates called vesicles or small single "layer" aggregates called micelles. The occurrence of each type of aggregate depends on a number of factors, including shape of the monomer, monomer concentration and temperature. While phospholipid membranes are themselves formed by amphiphiles,

many of the species that interact with them (or insert) in various ways are also amphiphiles.[9]

Natural Ion Carriers and Channels

With a phospholipid bilayer creating an appropriate isolating structure for cells, a mechanism for the selective transfer of ions and molecules into and out of a cell or organelle completes the compartmentalization requirement of life. Most of the larger polar species (sugars, membrane-impermeable proteins) pass into and out of the cell via endocytosis and exocytosis, respectively. While the transport of these species is of extreme importance and is well-studied,[10] the current work is concerned exclusively with the transport of ions across membranes.

Along with endo- and exocytosis, the transport of ions across a phospholipid membrane might have been one of the first processes developed in the evolution of life. In these early stages it is likely that a small amphiphilic molecule would bind with the ion in the aqueous media and ferry it through the membrane.

As evolution progressed, these simple molecules became more elaborate and complex; a new mode of ion transport developed in the form of the ion channel—a molecule or aggregate that spanned the lipid bilayer while forming a water-filled cavity through which ions could pass. Natural ion channels are amphiphilic protein molecules that insert into the membrane bilayer and span the distance between the separated aqueous domains.[11] In most cases, these ion channels present an outer hydrophobic surface to the similarly non-polar domain of the bilayer, while forming an ion-conducting pore lined with polar, hydrophilic residues.[12] The presence of these polar residues effectively lowers the

energetic barrier in the microenvironment of the pore for passage of the ion between aqueous domains.

These ion channels have been perfected by eons of evolution, as by trial and error, the best mix of amino acids in the best positions form pores of optimal geometry with selectivity filters and gating mechanisms able to determine what is transported and what conditions would be required for transport. Some channels evolved even further into pumps—structures able to actively transport ions or molecules against the concentration gradient. It is with these structures that cells are able to maintain ion homeostasis and concentration gradients.

Receptors, Carriers and Channels

Carriers Versus Channels

The carrier mechanism is often likened to a boat ferrying passengers back and forth across a river, while a channel is analogous to a bridge spanning the river, allowing the free and continuous passage of anyone wishing to cross. The metaphorical comparison extends to the rate of transport observed with the two separate mechanisms. An ion-carrying molecule first binds an ion on one side of the membrane barrier, diffuses across the membrane, and releases the ion on the far side of the barrier, repeating until equilibrium is established.

Potassium transport by valinomycin, one of the best known ion carriers, reaches a level of 10^4 ions per second[13] while a functional pore may conduct ions at a rate of 10^7 or even 10^8 ions per second.[14] However, the size of the channel is another issue, as only a certain number of ions can pass a confined space at any given time. Like a draw bridge,

the channel may open and close at intervals, with no ions or current passing across the barrier when the channel is closed. If two channels are open simultaneously in a cell or other system, the current and ion transport rate will be double that of a single channel.

Synthetic Versus Natural Channels and Carriers

The extremely large sizes of natural ion channels make them impossible to create without genetically-controlled biosynthesis. Protein crystallization,[13,15] sequencing[16] and induced mutation[17] has led to a wealth of discoveries about essential (conserved) residues and their contributions to pore,[18] gate[18] and selectivity filter geometries.[19] However, this work is extremely resource-intensive and difficult to achieve. Smaller synthetic compounds can offer a viable, easily-modifiable, and less resource-intensive alternative to research with natural ion channels. While such complexities as true ligand gating[20] (as opposed to pore blockage[21]) may be difficult or even impossible to achieve with smaller synthetic systems, such fundamentals as pore geometry and ion selectivity can be investigated.[22]

The work of chemical biologists is to create and utilize synthetic, often abiotic, compounds to elicit a desired activity in biological or biological model systems or to further the understanding of those systems. In the context of ion homeostasis and ion channels, a simpler synthetic molecule can yield important insights into exactly what can exhibit channel or carrier activity,[23] what can exhibit ion selectivity[24] and how channels can form by folding,[25] aggregation,[26] membrane reorganization[27] or some combination of the three.[28]

Measuring Carrier and Channel Activity

Both carriers and channels, by definition, must exhibit ion transport activity. An assay in a biological model system is often the first step in characterizing a molecule as such. Ion transport activity can be gauged by using a variety of biophysical techniques, with some methods seeing more use recently.[29]

An octanol/water partitioning has often been used for determining the hydophobicity of compounds (log P). Octanol provides a very rough approximation of the polarity and character of a phospholipid bilayer. Likewise, the partitioning of chloroform and water has been used in the same context to form discrete hydrophilic and hydrophobic layers. The U-tube test uses a U-shaped container to separate two aqueous layers with a layer of chloroform at the bottom of the "U." A salt containing the transport target ion is added to one of the aqueous layers along with a suspected transporter. After gentle stirring of the system, the ion will be present in the second aqueous layer if a transporter is present, as it has been carried through the hydrophobic layer by the transporting compound.[30]

While this system can impart important information, it is an extremely simplified version of very complex natural cell membranes that can vary significantly from species to species and even from cell type to cell type within the same species. Most importantly, the U-tube test can only characterize a transporter as a carrier. If a compound acts solely as a channel, it may not exhibit transport activity, as its ion transport dependence is based on insertion into a membrane and transport across a distance of roughly 30Å, not diffusion across a membrane. For a better assay, a better model of a natural system is required.

Liposomes, or phospholipid vesicles, are artificially created models of natural cells with an internal volume of aqueous buffer surrounded by a phospholipid bilayer. In most cases, these liposomes are formed exclusively with solutions of phospholipids, but

different phospholipids could be used in varied proportions, and amphiphilic molecules such as cholesterol can also be incorporated. After formation and purification, spherical liposomes of uniform size can be isolated with an internal aqueous solution that can be different from the external buffer. It is with these model systems that further investigations can be made.

Three common methods have been used in measuring ion transport in vesicles—NMR,[31] ion-selective electrode,[32] and fluorescent reporter.[33] All three methods are dependent on a reporter system that cannot cross the membrane and vesicles formed with an internal aqueous solution that is different from the external solution. Most importantly, all three methods use time-dependent measurements, allowing the characterization of not only transport activity, but also transport rate.

Receptors: Ion Recognition

In all cases of ion transport, the transporter must interact in some way with the ion. Thus, many synthetic ion transporters have their roots in supramolecular chemistry and ion receptors.[34] Most studies in the ion receptor field focus on solid-state binding geometries and maximizing ion-binding strength (with values usually achieved in less competitive non-polar solvents and counter-ions with diffuse charge densities). However, the field of transmembrane ion transport is more subtle—stronger binding is not always better and binding geometries in the solid state do not necessarily comport with binding in solution.

In aqueous solution, both direct transporter-ion interactions as well as indirect interactions via organized water molecules can occur. While direct transporter-ion interactions would seem to be the preferred method of interaction energetically, this is not necessarily the case. Aquated ions are surrounded by a hydration shell—a three-

dimensional array of water molecules with dipoles oriented toward the ion. Cations interact weakly with water's oxygen lone pairs, while anions act as hydrogen bond acceptors for water's protons. While a single water-ion interaction is relatively weak, an entire solvation shell as a whole is held tightly to the ion. Shedding a solvation shell or a part thereof can be energetically expensive. Any favorable binding energy present with a direct association of a transporter is counter-acted by this energy penalty.

Another aspect to consider is that an active transporter requires a dynamic interaction with the transported ion. Exceptionally strong binding with the ion could result in a binding equilibrium weighted heavily toward the complex, with ion uptake occurring rapidly, but ion release occurring slowly. Essentially, this would impede the passage of ions through the channel or preclude further uptake of ions by a carrier.

Considering this, a compound that orders water molecules or interacts with a solvation sphere, rather than with the ion itself may be a more active transporter than one that binds the ion directly. Therefore, while ion binding by a receptor and ion recognition by a transporter may be rooted in the same principles, the goals for each field are distinctly different when considering the design and implementation of an optimal set of compounds.

Supramolecular Interactions

Interactions of Receptors and Transporters with Ions

Reversible non-covalent interactions are of paramount importance in the fields of both ion binding and transmembrane ion transport. Electrostatic interactions are among the strongest non-covalent bonds, but depend significantly on the density of charge across the surface of the ionic species. More diffuse charges, such as seen with iodide anions, or

sterically-hindered charges lead to weaker electrostatic attractions. A chloride anion is attracted more strongly to a charge-dense sodium cation than it is to a tetrabutylammonium cation, which does not have a directly-accessible charge.

Solvent also has an effect on electrostatic attractions. The dearth of strong dipole moments in non-polar solvents such as methylene chloride and hexanes translates to a non-competitive environment. Assuming that both the anion and cation are completely soluble in this non-polar milieu, the only significant interaction is between the two ions. However, the strength of electrostatic attractions is greatly diminished in polar solvent as the dipoles of solvent molecules (as previously described with aquated ions) interact with the charged ions, forming solvation shells.

In either polar or non-polar solvent, host-guest interactions with these charged species can occur, given proper host or transporter binding geometries and strengths. These binding interactions, however, must at least be energetically and kinetically competitive with the counter ion and/or solvation shell if either is displaced. Whereas in non-polar solvents, binding competition comes mainly from the counter-ion, contact energies with the counter-ion are nearly negated in polar solvents, with competition from the ion's solvation sphere dominating.

Membrane Insertion

Whereas most interactions in the cytosol or aqueous cell exterior are driven by charge-charge, charge-dipole, or dipole-dipole contacts, the non-polar interior region of the membrane bilayer is characterized by moieties that are energetically driven to minimize contacts with polar and charged species. Other molecules that also have hydrophobic substructures, such as alkyl chains or arenes with minimal dipole moments, can insert into

membranes. Amphiphilic compounds must insert and interact as the surrounding phospholipids do, with polar or charged moieties directed outward and lipophilic residues directed in toward the membrane interior.

The hydrophobic residues of a membrane monomer or other amphiphiles are not inherently attracted to each other as cations are attracted to anions, but water is essentially repulsed by them—membrane insertion is entropy driven. No favorable hydrogen-bonding interactions exist between polar solvating water and non-polar substructures, so proximate water molecules lose the energetic advantage of full hydrogen bonding capacity. These water molecules, therefore, must maximize what favorable interactions are available to them by forming more rigid, "ice-like" contacts with surrounding water molecules, exacting a high entropic penalty in the process. When the quantity of rigid water contacts is minimized, the entropic energy penalty is proportionately diminished.

The lipophilic-lipophilic forces themselves are extremely weak, allowing free movement and lateral diffusion of amphiphilic and hydrophobic species laterally throughout the bilayer, in much the same way that charged and polar species diffuse in polar solvents. Given the proper conditions, amphiphiles that insert into one leaflet of the bilayer can flip to the other leaflet. Gramicidin, a well-studied natural cation transporter,[35] takes advantage of both of these characteristics in biological membranes. In fact, channel functionality is elicited by two monomers in each leaflet of the bilayer, diffusing across the face of its respective leaflet before aligning to form a transient pore.[36]

Self-Aggregation and Stacking

Another important aspect of weak-force binding that needs consideration is the energetic favorability of receptor and transporter molecules to aggregate in solution.

Aggregation of amphiphilic species in polar protic solvents is driven by the same forces that drive membrane insertion—minimization of contacts between hydrophobic moieties and solvent. In utilizing a molecule to elicit activity in a membrane, self-aggregation of the molecule in solution can be counterproductive.[37] Molecules that favor self-aggregation are less likely to insert into bilayer membranes—by definition, a necessary process for transmembrane ion transporters. While the compounds may be membrane active, the concentration required to effect the desired activity may be significantly higher for those that prefer self-aggregation.

One caveat to this self-aggregation concept is when the transporter is active *because of* self-aggregation, either in solution or in the membrane. For example, molecules that are too small to span the membrane bilayer as a monomer would be more likely to transport as a channel with increasing concentration.

Measuring Supramolecular Interactions

Both the association energies and geometries of these various supramolecular interactions have been studied over the past several decades. Structural information can be elucidated in the solid state by X-ray diffraction of grown crystals[38] or in solution by NMR.[39] Structural information can also be accurately modeled using computational methods.[40] This technique is extremely useful when crystals are difficult to obtain, and when NMR does not, or could not, yield sufficient structural information.

Relative binding strengths can also be modeled computationally[41] and can yield a significant amount of information relatively quickly, especially in the context of optimizing leads (or targets) before synthesis and experimental analysis. Quantitative characterization of interaction strengths, in the form of binding or association constants,

can be obtained using a variety of techniques, each with differing degrees of relevance or usefulness depending on the studied system and information gleaned.

For example, binding constants can be derived from the isotherms of host-guest titrations, monitoring the change in chemical shift ($\Delta\delta$) of binding protons by ^{1}H NMR spectroscopy.[42] Whereas in the case of anions, a set of hydrogen-bond donors should be present if any interaction exists, a cationic guest would not normally elicit a strong shift (if any) in a neutral host molecule. Thus, while ^{1}H NMR binding constants would be beneficial in measuring anion binding, it is often useless in measuring cation binding.

Summary of Dissertation Work

The following studies were performed to further the understanding of a diverse array of novel and previously-studied synthetic molecules as membrane-active ion transporters. In the process, important facets such as ion binding capacity, aggregation behavior, ion transport functionality, and antimicrobial activity are investigated. While these studies yield structural and mechanistic insights into our own research group's synthetic systems, they may also aid in understanding both other synthetic ion transporters as well as natural ion carriers and channels.

Chapter 2: Synthetic Anion Receptors

After completing an in-depth review of the synthetic anion receptor literature, a series of known uncharged anion receptors was modeled computationally to predict chloride-binding strengths. Comparison with experimentally-derived values for the known molecules aided in developing the calculation methods for later use with novel compounds

designed to be chloride hosts.

Upon completion of the method development, the known families of molecules and variations thereof, as well as novel families of uncharged molecules, were modeled and chloride-binding strengths were calculated. These calculations were used as a predictive tool for determining the best families of compounds to target and to better understand structure-activity relationships within a family of compounds. Such characteristics as number of hydrogen bond donors, proton acidity, and receptor flexibility were judged based on the calculated complexation energies, host and complex electrostatic potential maps, and analysis of host and complex geometries. Using the accrued data for the most promising candidates, targets were determined for further study based on predicted activity and synthetic accessibility.

Synthetic approaches were developed for all of the compounds studied, and efforts were made toward some of the more promising candidates. While one family of compounds (dipicolinic dianilides) is detailed in Chapter 3, the synthetic work and characterization for the remaining attempts are detailed in Chapter 2.

Chapter 3: Synthetic Anion Carriers and Channels

Dianilides of 2,6-pyridine dicarboxylic acid (dipicolinic acid), a family of compounds modeled in Chapter 2, were synthesized, characterized, and studied for carrier and channel activity in biological systems and biological model systems.

The first dipicolinic dianilides were made in a two-step synthetic process with overall yields of 40-70% and covered a range of substituent character from the electron-donating *para*-methyl substituent to the electron-withdrawing *para*-nitro. Initially, the compounds were investigated for chloride-binding activity in the context of chloride

receptor utilization. ^{1}H NMR binding constants were derived in both polar DMSO-d_6 and non-polar CD_2Cl_2, with the titrations showing that chloride binding activity was present even in the polar milieu of DMSO-d_6. These results were correlated with the previous molecular modeling studies, as well as with competitive electrospray ionization-MS studies performed by collaborators. The same trend in chloride binding strength was seen across the studied range of substituents: with increased substituent electron-withdrawing character comes increased chloride binding strength.

While elucidation of the solid-state structures of the host-guest complexes was attempted, molecular modeling and experimental work involving the measurement of the absorption spectra with increasing concentrations of a guest salt yielded significant insights into both the energetics and the geometries associated with the complexation.

Favorable chloride binding results signaled that the compounds could conceivably act as chloride carriers in biological model systems. Chloride influx into phospholipid vesicles was studied using a chloride-quenched internal fluorophore as an indicator of internal chloride concentration. Fluorescence intensity was monitored as a function of time, showing fluorescence quenching and, by extension, chloride transport in a dynamic setting. Again, the trend followed increased chloride transport activity with increasing substituent electron-withdrawing character.

The rapid chloride transport rate seen in the vesicle study suggested that a channel mechanism, not simply a carrier mechanism, may be present for at least some of the transporters studied. As stated previously, the simplest method to distinguish between the two mechanisms is the measurement of conductance between two aqueous environments electrically isolated by a bilayer membrane. A colleague measured the presence of this

electrical conductance using the planar-bilayer conductance technique. The results indicated channel functionality in the form of distinct open-close behavior.

A dipicolinic dianilide transporter monomer at its widest is approximately 15Å and is incapable of spanning the roughly 30Å of the hydrophobic region of the bilayer membrane. Thus, unable to work alone, the monomers must somehow aggregate to elicit the exhibited channel functionality. Using calculated geometries of stacked molecules, along with the concentration-dependent fluorescence profiles of the transporters, a stacking interaction was posited as the mechanism of channel formation.

Chapter 4: Solvent Dependence of Solid-State and Nanoscale Structure

Supramolecular interactions, are an extremely important part of understanding the morphology of aggregates of compounds and predicting the possible interactions of both monomers and aggregates in natural systems and biological model systems. The solvent environment often plays a key role in how molecules aggregate and interact with other species. Potential ion transporters, which are almost exclusively amphiphiles, can and will form aggregates of different morphologies under different solvent conditions.

The work detailed in this chapter seeks to bring these solvent effects on aggregate and crystal formation to the forefront in the context of understanding these molecules as potential ion transporters. The work presented in this chapter focuses on the solid-state and nanoscale morphologies of pyrogallol[4]arene macrocycles with branched sidechains. These compounds were analyzed for solid-state or "Angstrom-scale" geometry and morphology by X-ray crystallography and analyzed for nanoscale geometry and morphology by cryogenic transmission electron microscopy (cryo-TEM).

Both the crystallizations and EM sample preparations were performed in various solvent conditions—polar, non-polar, protic, aprotic—and in mixed solvents. While crystallizations were unsuccessful in many cases, EM sample preparation by slow evaporation generally yielded usable specimens. These specimens reveal that nanoscale aggregates self-assemble in polar media. Under 50000x magnification, these aggregates are shown to be formed from bundles of what appear to be short nanotubes of a diameter congruent with measurements taken from X-ray crystal structures.

Chapter 5: Biological Activity of Synthetic Ion Carriers and Channels

As stated previously, a major goal of a chemical biologist is to elicit biological activity from synthetic constructs. In this vein, assays of these constructs in biological model systems are cursory studies leading to investigation in biological systems. Pore-forming compounds, such as cation-conducting hydraphile channels,[43] as well as anion-conducting synthetic anion transporters (SATs),[25a,44] and dipicolinic dianilide channels[45] have the ability to conduct their respective ions rapidly across phospholipid membranes in biological model systems such as vesicles and planar bilayers. If that activity is present in biological systems such as bacterial and fungal cultures or human red blood cells, therapeutic applications might emerge.

The first of three projects associated with this chapter is an exploration of the antimicrobial activity for an array of novel ion transporters. In one part of this project, the family of compounds, known as hydraphiles, was investigated for activity with variation of growth culture pH. The subset of compounds tested had amide moieties present instead of amines that are generally present in the family. Additionally, both cation and anion transporters as well as suspected channel formers were studied using the minimum

inhibitory concentration (MIC) method in Gram-negative *Escherichia coli*. Only newly-studied members of the hydraphile family of known antimicrobial agents exhibit any biological activity in the studied bacterium.

The second project details the interaction between cation and anion transporters on antimicrobial activity was measured in Gram-positive *Staphylococcus epidermidis* using a co-application of two such compounds and comparing growth curves. While alone, the diaza-18-crown-6 sodium transporter that is studied exhibits antimicrobial activity, when co-applied with a dipicolinic dianilide chloride transporter these effects are completely negated.

The third and final project explored the development of antimicrobial resistance in *E. coli* to synthetic cation channel with known antimicrobial activity. The antimicrobial resistance was studied with regular application of sub-lethal concentrations of the hydraphile cation channel over 12 days. While resistance did develop over the time period, it plateaued after 6 days of growth, developing no further resistance.

1 D. E. Koshland, Jr.; *Science* **2002**, *295*, 2215-2216.

2 (a) Stanier, R. Y.; van Niel, C. B. *Arch. Microbiol.* **1962**, *42*, 17-35. (b) Whitman, W. B. *J. Bacteriol.* **2009**, *191*, 2000-2005.

3 Vellai, T.; Vida, G. *Proc. Biol. Sci.* **1999**, *266*, 1571-1577.

4 Singer, S. J.; Nicolson, G. L. *Science* **1972**, *175*, 720-731.

5 McBain, J.W. *Trans. Faraday Soc.* **1913**, *9*, 99.

6 Parsegian, A. *Nature* **1969**, *221*, 844-846.

7 Darnell, J.; Lodish, H.; Baltimore, D.; *Molecular Cell Biology*, **1986**; Scientific American Books, New York; (2nd ed., 1990) p. 618 and 725.

8 Israelachvili, J. N.; Mitchell, D. J.; Ninham, B. W. *J. Chem. Soc., Faraday Trans. 2*, **1976**, *72*, 1525-1568.

9 Yeagle, P. *The Structure of Biological Membranes*. CRC Press: Boca Raton, **1992**; p 1227.

10 Miaczynska, M.; Stenmark, H. *J. Cell Biol.* **2008**, *180*, 7-11.

11 Hille, B. *Ionic Channels of Excitable Membranes.* 3rd ed.; Sinauer Associates: Sunderland, MA, **2001**.

12 MacKinnon, R. *Angew. Chem. Int. Ed.* **2004**, *43*, 4265-4277.

13 Stark, G.; Ketterer, B.; Benz, R.; Lauger, P. *Biophys. J.* **1971**, *11*, 981-994.

14 Läuger, P. *Biochim. Biophys. Acta* **1973**, *311*, 423-441.

15 Dutzler, R.; Campbell, E. B.; Cadene, M.; Chait, B. T.; MacKinnon, R. *Nature* **2002,** *415*, 287-294.

16 (a) Edman, P. *Acta Chem. Scand.* **1950**, *4*, 283-293. (b) Noda, M.; Shimizu, S.; Tanabe, T.; *et al.*; *Nature* **1984**, *312*, 121-127.

17 Labarca, C.; Nowak, M. W.; Zhang, H.; Tang, L.; Deshpande, P.; Lester, H. A. *Nature* **1995**, *376*, 514-516.

18 Planells-Cases, R.; Ferrer-Montiel, A. V.; Patten, C. D.; Montal, M. *Proc. Nat. Acad. Sci. USA* **1995**, *92*, 9422-9426.

19 Yue, L.; Navarro, B.; Ren, D.; Ramos, A.; Clapham, D. E. *J. Gen. Physiol.* **2002**, *120*, 845-853.

20 Colquhoun, D.; Sivilotti, L. G. *Trends Neurosci.* **2004**, *27*, 337-344.

21 Kwon, D.-H.; Lu, C.-D. *Antimicrob. Ag. Chemother.* **2007**, *51*, 2070-2077.

22 (a) Gokel, G. W.; Mukhopadhyay, A.; *Chem. Soc. Rev.* **2001**, *30*, 274-286. (b) Dieckmann, G. R.; Lear, J. D.; Zhong, Q.; Klein, M. L.; DeGrado, W. F.; Sharp, K. A. *Biophys. J.* **1999**, *76*, 618-630.

23 (a) Sisson, A. L.; Shah, M. R.; Bhosale, S.; Matile, S. *Chem. Soc. Rev.* **2006**, 35, 1269-1286. (b) Davis, A. P.; Sheppard, D. N.; Smith, B. D. *Chem. Soc. Rev.* **2007**, *36*, 348-357. (c) Fyles, T. M. *Chem. Soc. Rev.* **2007**, *36*, 335-347.

24 (a) Schlesinger, P. H.; Ferdani, R.; Liu, J.; Pajewska, J.; Pajewski, R.; Mitsuyoshi, S.; Shabany, H.; Gokel, G. W. *J. Am. Chem. Soc.* **2002**, *124*, 1848-1849. (b) Gokel, G. W. *Chem. Commun.* **2000**, 1-9.

25 (a) Prince, R. B.; Barnes, S. A.; Moore, J. S. *J. Am. Chem. Soc.* **2000**, *122*, 2758-2762. (b) Goodman, C. M.; Choi, S.; Shandler, S.; DeGrado, W. F. *Nat. Chem. Biol.* **2007**, *3*, 252-262.

26 (a) Clark, T. D; Buehler, L. K.; Ghadiri M. R. *J. Am. Chem. Soc.* **1998**, *120*, 651-656. (b) Bhosale, S.; Sisson, A. L.; Sakai, N.; Matile, S. *Org. Biomol. Chem.,* **2006**, *4*, 3031. (c) Yang, J.; Dewal, M. B.; Sobransingh, D.; Smith, M. D.; Xu, Y.; Shimizu, L. S. *J. Org. Chem.* **2009**, *74*, 102 (d) Helsel, A. J.; Brown, A. L.; Yamato, K.; Feng, W.; Yuan, L.; Clements, A. J.; Harding, S. V.; Szabo, G.; Shao, Z.; Gong, B. *J. Am. Chem. Soc.* **2008**, *130*, 15784.

27 Plank, C.; Zauner, W.; Wagner, E. *Adv. Drug. Deliv. Rev.* **1998**, *34*, 21-35.

28 Pajewski, R.; Ferdani, R.; Pajewska, J.; Djedovic, N.; Schlesinger, P. H.; Gokel, G. W. *Org. Biomol. Chem.* **2005**, *3*, 619-625.

29 (a) Ashton, R.; Steinrauf, L. K. *J. Mol. Biol.* **1970**, *49*, 547-556. (b) Liu, C.; Hermann, T. E. *J. Biol. Chem.* **1978**, *253*, 5892-5894.

30 (a) Yamnitz, C. R.; Gokel, G. W. *Chem. Biodivers.* **2007,** *4*, 1395-1412. (b) Gokel, G. W.; Carasel, I. A. *Chem. Soc. Rev.* **2007,** *36*, 378-389.

31 Murray, C. L.; Gokel, G. W. *Chem. Commun.* **1998**, 2477-2478.

32 (a) Koulov, A. V.; Mahoney, J. M.; Smith, B. D. *Org. Biomol. Chem.* **2003**, *1*, 27-29. (b) Weber, M. E.; Schlesinger, P. H.; Gokel, G. W. *J. Am. Chem. Soc.* **2005**, *126*, 636-664.

33 (a) Sakai, N.; Matile, S. *J. Phys. Org. Chem.* **2006,** *19*, 452-460. (b) Ferdani, R.; Li, R.; Pajewski, R.; Pajewska, J.; Winter, R. K.; Gokel, G. W. *Org. Biomol. Chem.* **2007,** *5*, 2423-2432.

34 (a) Gatto, V. J.; Arnold, K. A.; Viscariello, A. M.; Miller, S. R.; Morgan, C. R.; Gokel, G. W. *J. Org. Chem.* **1986**, *51*, 5373-5384. (b) Leevy, W. M.; Weber, M. E.; Gokel, M. R.; Hughes-Strange, G. B.; Daranciang, D. D.; Ferdani, R.; Gokel, G. W. *Org. Biomol. Chem.* **2005**, *3*, 1647-1652.

35 (a) Urry, D. W. *Proc. Nat. Acad. Sci. (USA)* **1971**, *68*, 672-676. (b) Gowne, J. A.; Markham, J. C.; Morrison, S. E.; Cross, T. A.; Busath, D. D.; Mapes, E. J.; Schumaker, M. F. *Biophys. Chem.* **2002**, *83*, 880-898. (c) Huang, H. W.; *Novartis Foundation Symposium: Gramicidin and Related Ion Channel-Forming Peptides*, **1999**, *225*, 188–206.

36 Urry, D. W.; Goodall, M. C.; Glickson, J. D.; Mayers, D. F. *Proc. Nat. Acad. Sci. (USA)* **1971**, *68*, 1907-1911.

37 Elliott, E. K.; Daschbach, M. M.; Gokel, G. W. *Chem. Eur. J.* **2008**, *14*, 5871-5879.

38 Ladd, M. F. C.; Palmer, R. A. *Structure Determination by X-Ray Crystallography*; Plenum Press: New York, **1985**.

39 Pons, M., ed. *NMR in Supramolecular Chemistry*, Kluwer Academic Publishers: Dordrecht, Netherlands, **1999**.

40 Wu, Y.-D.; Wang, D.-F.; Sessler, J. L. *J. Org. Chem.* **2001**, *66*, 3739-3746.

41 Lybrand, T. P.; McCammon, J. A.; Wipff, G. *Proc. Natl. Acad. Sci. USA* **1986**, *83*, 833-835.

42 Connors, K. A. *Binding Constants*, 1st ed.; John Wiley & Sons: New York, **1987**, 189-215.

43 Gokel, G. W. *Chem. Commun.* **2000**, 1-9.

44 Schlesinger, P. H.; Ferdani, R.; Pajewski, R.; Pajewska, J.; Gokel, G. W. *Chem. Commun*. **2002**, 840-841.

45 Yamnitz, C. R.; Negin, S.; Carasel, I. A.; Winter, R. K.; Gokel, G. W. *Chem. Commun.* **2010**, *46*, 2838-2840.

CHAPTER 2

Design and Computational Investigation of Novel Synthetic Anion Receptors for Use as Anion Transporters

Summary and Contributions to this Work

The work presented in this chapter focuses on the implementation of a computational method to design and optimize families of molecules as potential anion receptors with the goal of utilizing them as transmembrane chloride transporters. 40 potential receptors of 5 different types were modeled and studied computationally at the density-functional level of theory. Structural variations within families include the number and type of neutral hydrogen bond donor moieties, as well as substitutions in π-systems that are in conjugation with the hydrogen bond donors.

After optimization of a computational method, the investigation yielded a number of insights into the design of anion receptors. First, the use of urea or thiourea in the binding cleft can lead to a significant complexation energy advantage over carbamates or amides. In practical terms, however, the solubility of these compounds may limit their use as receptors. Second, larger molecules with more hydrogen bond donor moieties may not be advantageous when considering the design of an anion receptor or transporter. Intramolecular hydrogen bonds would need to be broken to and complexation with an anion may not be as energetically favored. Finally, electron-withdrawing substituents in a

π-system including anion-binding moieties dramatically lowers the binding energy of those systems due to increased proton acidity.

One family of these compounds studied, the dipicolinic dianilides, was investigated further. They are shown in Chapter 3 to bind chloride in polar solvent, transport chloride across phospholipid vesicles, and function as a synthetic anion channel.

I performed all of the computational work, synthesis, and characterization described below.

Introduction

The essence of supramolecular chemistry has been, from its inception, weak force interactions.[1] While some early work was devoted to the complexation of anions,[2] initial studies focused primarily on host-guest interactions involving neutral hosts and cationic guests. The field of anion binding remained only modestly active for many years, and work did not gain momentum until recently. During the past decade, however, there has been a burgeoning interest in both anion binding and transport.[3] The anion-binding and anion-transport fields have found utility in applications as diverse as the detection of chemical weapons[4] and therapeutic value in mitigating the symptomatic manifestations of cystic fibrosis.[5]

The most common complexation mode for such anions as fluoride and chloride is hydrogen bonding. Amides, ureas and thioureas, alcohols and protonated amines have all proven to be effective hydrogen bond donor sources for these interactions,[3b] although the latter has found more use in anion receptor studies than ion transporter studies. A successful ion carrier is dependent on at least three rates: the rate of binding the ion outside

the cell, the rate of diffusion across the membrane into the cytosol, and the rate of decomplexation—solvation of the ion by cytosolic water.[6] Naturally, the former and latter rates are inversely related, and the effectiveness of a transporting agent is held to a true Goldilocks standard: a carrier that binds an ion too weakly prevents any meaningful host-guest interaction; a carrier that binds an ion too strongly will not release the ion once in the cytosol. Logically, the best ion carrier is one that binds a target ion at an intermediate magnitude of strength, being able to both bind an ion on one side of the membrane and release it on the other side.

Incorporating a moiety with a charge opposite the target ion would render a carrier host too strongly bound to its guest. The carrier must be uncharged but incorporate a series of dipoles that favorably interact with the target ion. After such a molecule or aggregation of molecules meets these criteria, it must pass the final test—permeate the lipid bilayer, ion in tote.

Results and Discussion

Families of compounds modeled

As mentioned previously, numerous neutral and charged anion receptors have been developed recently.[3b] Therefore, preliminary work consisted of identifying, as fully as possible, the range of novel synthetic molecules already used as ion hosts, specifically halide anion hosts. A development process, detailed below, followed to determine likely combinations of anion-complexing moieties using readily available starting materials to identify likely anion host targets.

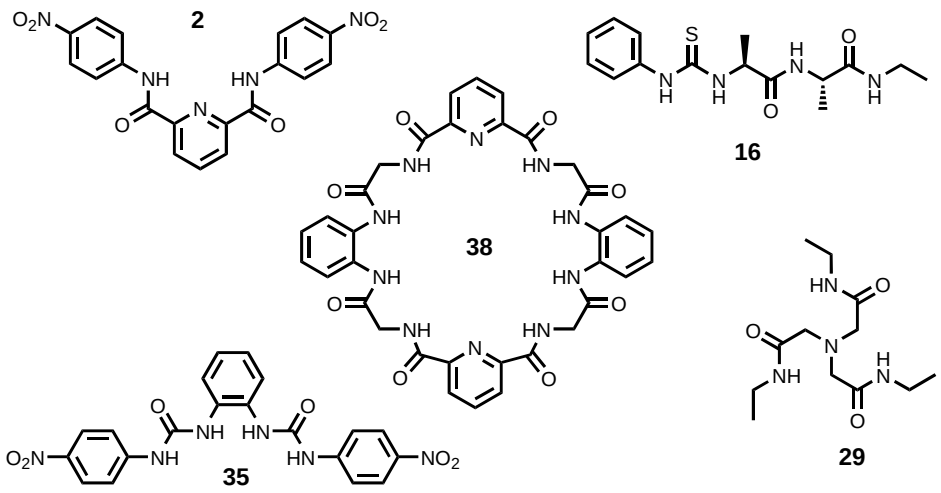

Figure 2.1 *Examples of the five categories of transporter candidates modeled.*

From this process, a number of candidates were determined. The candidate field was winnowed down by eliminating structures that might present solubility problems, that could not adopt a favorable complexation geometry, or were overly-large or complex to target synthetically. The final candidates, therefore, were those that were synthetically accessible, smaller, easier to model computationally and easily modifiable in order to introduce a wide variety of compounds from a core or base structure. These candidates fell into one of five distinct categories (examples given in Figure 2.1):

1. Dianilides of dipicolinic acid (compound **2**) and of the structurally-similar isophthalic acid—such as those discovered by Crabtree's group[7] and championed by Gale and co-workers,[8]
2. Highly modified peptide chains akin to our group's SCMTR[9] (**16**),
3. Metal-chelating poly-acids that have been amidated to bind anions (**29**),
4. Alkyl and arylureas (**35**), and

5. Macrocycles incorporating some combination of *o*-phenylenediamine, dipicolinic acid and optional amino acids (**38**).

Dipicolinic and isophthalic diamides

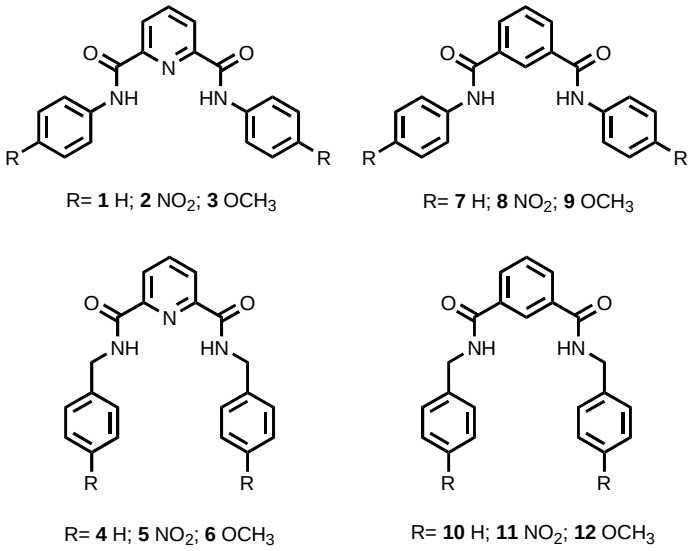

Figure 2.2 *Synthetic anion receptors formed from the coupling of dipicolinic acid or isophthalic acid and a substituted/unsubstituted aniline or benzylamine.*

Method Version	Conformer Search	1st Geometry Optimization	2nd Geometry Optimization	Energy Calculation
I	MMFF *10 of 10000*	AM1	-	B3LYP
II	MMFF *10 of 10000*	PM3	-	B3LYP
III	MMFF *20 of 10000*	RM1	B3LYP	B3LYP/MP2

Table 2.1 *Summary of the study methodology as developed over three versions*

Using the set of molecules, **1-12** seen in Figure 2.2, the methodology for the study was developed and perfected over three iterations, summarized in Table 2.1. In all three iterations, a subset of lowest energy conformers (LECs) as determined from a set of up to

ten thousand conformations generated at random and energy minimized using a low cost molecular mechanics level of theory. Method versions I and II found ten such LECs, while version III found twenty LECs. In all three versions, the optimized geometries of these LECs were found using a slightly more computationally-expensive semi-empirical method (AM1[10] in version I, PM3[11] in version II and RM1[12] in version III). Version III included a further geometry optimization performed at the density functional level of theory (DFT) using the B3LYP method[13] with a 6-31G* basis set. B3LYP combines Becke's three-parameter function[14] with the non-local correlation provided by the correlation function of Lee, Yang and Parr,[13] and finds common usage at this level of theory. Finally, the single-point energy was calculated for all versions using the B3LYP method and 6-31G* basis set. Version III also attempted an electron correlated Möeller-Plesset MP2[15] calculation for most molecules, but a lack of computational resources prevented this calculation from being performed on all but the smallest molecules and complexes. Thus, for comparison, both sets of values are listed where appropriate.

The dipicolinic and isophthalic acid-derivatized receptors **1-12** were thus evaluated using all three versions of methodology. Version III's use of a second geometry optimization at the density functional level of theory proved worthwhile in evaluating the receptors, as the calculated LEC of the semi-empirically-optimized molecules in versions I and II were, at times, significantly inaccurate. The calculated complexation energies of receptors **1-12,** using each version, are shown in Table 2.2. Of note is the significant difference in the calculated energies of compounds **1**, **3**, and **6** from version to version, as well as the comparatively high calculated chloride complexation energies of the *para*-nitro compounds.

Diacid	Amine	*para* Substituent	Compound Number	Version I (kcal/mol)	Version II (kcal/mol)	Version III (kcal/mol)
2,6-Pyridine Dicarboxylic Acid	Aniline	H	**1**	*-43.6*	*-9.8*	*-29.8*
		NO_2	**2**	-45.8	-45.7	**-50.7**
		OCH_3	**3**	*-14.7*	*-16.8*	*-32.6*
	Benzylamine	H	**4**	-21.9	-18.6	-27.5
		NO_2	**5**	-44.3	-41.8	**-45.6**
		OCH_3	**6**	*-2.6*	*-30.4*	*-33.6*
Isophthalic Acid	Aniline	H	**7**	-34.7	-33.2	-30.3
		NO_2	**8**	-48.9	-49.3	**-49.7**
		OCH_3	**9**	-33.5	-31.8	-35.0
	Benzylamine	H	**10**	-21.8	-34.0	-39.4
		NO_2	**11**	-39.6	-48.7	**-48.5**
		OCH_3	**12**	-25.8	-30.2	-35.8

Table 2.2 *Calculated chloride complexation energies for compounds **1-12** as calculated by each previously-described method. Of note are the inaccurate early-version calculations of compounds **1**, **3**, and **6** (italicized in gray boxes) and the comparatively high calculated complexation energies of the* para*-nitro compounds **2**, **5**, **8**, and **11** (bolded typeface).*

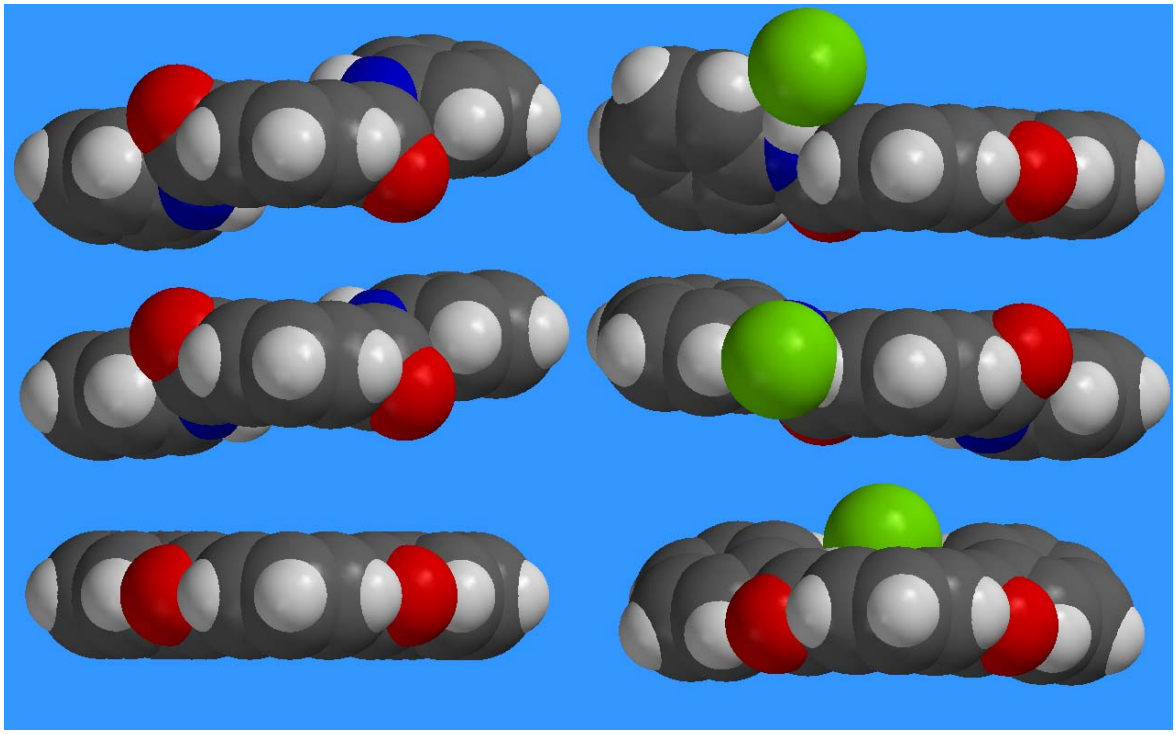

Figure 2.3 *Left: Top-down view of geometry-optimized CPK structures of receptor **1** as calculated by version I (top), version II (middle) and version III (bottom) of the calculation method. Right: Geometry-optimized CPK structures of the chloride complexes corresponding to the receptors on the left.*

Using compound **1** as an illustrative example of the limits of the first and second calculation method version, it can be seen in Figure 2.3 that different geometry optimizations can yield significantly different geometries. Superficially, the results seem the same, as in all cases, the receptor adopts a *syn-syn* conformation as a native host and an *anti-syn* conformation to bind the chloride anion guest with one amide N-H moiety. The top-down view, however, allows us to see that using version I, shows a higher-energy LEC host in a non-planar conformation (Figure 2.3 top left)—the amides are rotated 58° from the plane of the central pyridine and 13° from the plane of the side arm phenyls, eliminating any energy advantage gained from a fully planar, fully conjugated system. However, in the chloride complex (top right), planarity and conjugation exist in the *syn*-conforming side arm. The chloride-binding *anti*-conforming side arm, however, is rotated by 34° away from the central pyridine plane in order to favorably complex chloride.

The version II geometry also shows a rotation away from planarity in the native host, though the rotation is less extreme than its version I counterpart. As a result, an energy calculation yields a lower energy than that calculated with the former version. The complexing host in version II, however, shows no amide-arene planarity in either the *syn* or *anti* side arm resulting in a higher complex energy and a lower energy advantage for complexation.

Version III, using two sets of geometry optimizations—the final at the density functional level—predicts a low energy fully conjugated, fully planar conformation in the native host and a 18° side-arm rotation in the chloride-binding host. The inclusion of the density-functional level geometry optimization is the most important step in this 3rd version. Other computational studies with anion receptors have used similar procedures

with geometry optimization performed at the DFT level of theory,[16] so its use here is prudent.

The design of receptors **1-12** was based on a proposed *syn-syn* binding mode making use of both amide protons for hydrogen bonding in an "internal cavity" between the two side arms. The complex LECs for all receptors with substituted side arms show this behavior using all calculation method versions. However, as seen in receptor **1** as well as in others with unsubstituted side arms (**4**, **7**) a one hydrogen bond *syn-anti* mode is observed in the LEC optimized geometries of the first two calculation methods. However, when geometry is optimized at the density functional level of theory as with Version III, all of the receptors bind chloride in a *syn-syn* fashion. The dianilides, specifically, bind chloride out of the central arene plane, requiring a rotation of the amide moieties out of this plane as well.

A closer investigation of the aniline derivatives **1-3** and **7-9**, show an interesting relationship between the inductive strength of the *para* substituent and the chloride binding strength of the amide. This trend, is explored more fully in Chapter 3 of this work, including a wider breadth of substituents used. In addition, a computational investigation is conducted that studies the energetic advantages and penalties for a rotation out of the plane of the central arene to bind chloride.

Modified peptide chains

After optimization of the energy calculation process with compounds **1-12**, method version III was applied to the remaining receptor candidates, starting with C- and N-capped peptide chains. Taking experience and expertise from our similar, already-established SAT anion transporters,[9] such a synthetic thrust, involving peptide coupling

and modification seemed reasonable. With adequate computational study, the groundwork could be laid to properly direct such a foray.

The first issue studied in this category of carrier candidates was the effect of substituting N-terminus capping moieties. In our SAT family of compounds, the N-termini of the peptide chains are capped with a diglycolic acid anhydride derivative terminated with a dialkylamine lipophilic membrane anchor. The C-termini are also protected and are implicated in a secondary anchoring capacity.[17] A new approach to these peptide chains would be to reverse the function of the N- and C-termini, modifying the C-terminus with a main hydrophobic anchoring moiety and availing the N-terminus for additional anion complexation.

Structure	Compound	B3LYP $E_{complexation}$ (kcal mol^{-1})	MP2 $E_{complexation}$ (kcal mol^{-1})
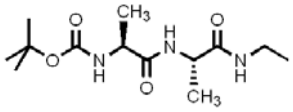	**13**	-27.3	-41.0
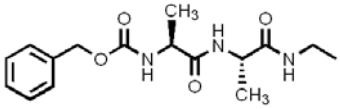	**14**	-26.2	-42.1
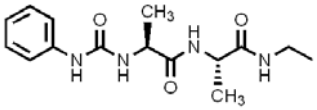	**15**	-40.4	-49.1
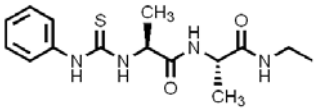	**16**	-45.9	-56.0
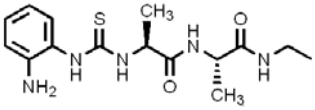	**17**	-40.4	-50.8

Table 2.3 *Structures and calculated chloride complexation energies for Ala-Ala sequence compounds varying the N-terminal moieties. Energies shown are calculated using the B3LYP or MP2 method with the 6-31G* basis set.*

In order to study the effects of varying the N-terminus capping moiety, a simple alanine-alanine dipeptide chain was modeled with an ethyl amidated C-terminus and a variably-capped N-terminus. Compounds **13-17** include two commonly used N-protecting groups, carboxybenzyl (CBZ) and *tert*-Butoxycarbonyl (t-BOC), a phenyl urea, a phenylthiourea, and a phenylthiourea with an *ortho*-amino substituent. The alanine-alanine sequence was chosen to (1) preclude any backside amino NH···carbonyl O hydrogen bonding in the native host, (2) introduce chirality leaving open the possibility for a later chirality-based complexation study, and (3) produce models that are relatively easy to calculate using the more stringent MP2 method. These structures, and the calculated chloride complexation energies are seen in Table 2.3.

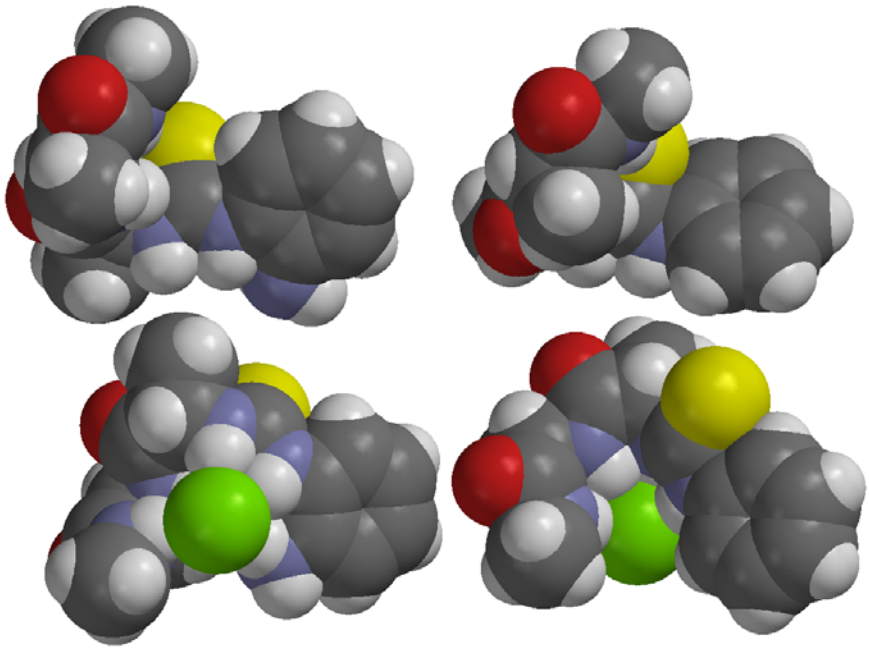

Figure 2.4 *Top: Geometry-optimized space-filling structures of* ortho-*amino phenylthiourea receptor* ***17*** *(left) and phenylthiourea receptor* ***16*** *(right). Bottom: Corresponding geometry-optimized CPK structures of the chloride complexes of the receptors above.*

The addition of a fourth potential hydrogen bond donor in a switch from carbamates in **13** and **14** to ureas in **15**, **16**, and **17** lends an estimated 7 kcal mol^{-1} energy advantage using the MP2 method for energy calculation. Substituting the urea for a thiourea yields an additional 7 kcal mol^{-1} in **16**. However, the addition of an *ortho* amino substituent to the phenylthiourea cap in **17** reduces this energy advantage to one comparable to the urea, **15**.

As seen in Figure 2.4, this latter phenomenon may have to do with the fact that, at most, only 4 N-H moieties bind the chloride anion in either geometry-optimized complex. The extra amino substituent in **17** replaces the non-binding N-H moiety, the first alanine backbone N-H which is geometrically unable to bind.

The interplay between the addition of anion-binding moieties and intramolecular hydrogen bonding in the host is further investigated by lengthening the peptide to 3, 4 and 5 residues. The urea and thiourea N-capping moieties were used in a study of the effect of peptide length on chloride binding. A poly-alanine peptide sequence was thus used for this study with extension out to 5 amino acid residues. Further extension of the chain would have raised the computational costs significantly, and as the results imply (Figure 2.5), additional amino acid residues past three would lend no significant change in complexation ability.

N-Terminus Cap	Alanine Chain Length	Host	B3LYP $E_{complexation}$ (kcal mol^{-1})	MP2 $E_{complexation}$ (kcal mol^{-1})	Intramolecular H-Bonds		Complex NH···Cl$^-$ Contacts
					Host	Complex	
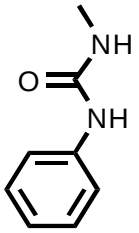	1	**18**	-37.1	-46.2	1	0	3 of 3
	2	**15**	-40.4	-49.1	1	0	4 of 4
	3	**19**	-50.9	-	2	0	5 of 5
	4	**20**	-50.6	-	3	0	5 of 6
	5	**21**	-51.0	-	4	3	4 of 8
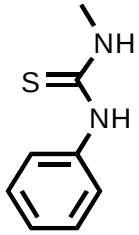	1	**22**	-37.8	-46.7	1	0	3 of 3
	2	**16**	-45.9	-56.0	1	1	3 of 4
	3	**23**	-55.1	-	2	1	4 of 5
	4	**24**	-54.8	-	3	0	5 of 6
	5	**25**	-56.0	-	4	0	6 of 7

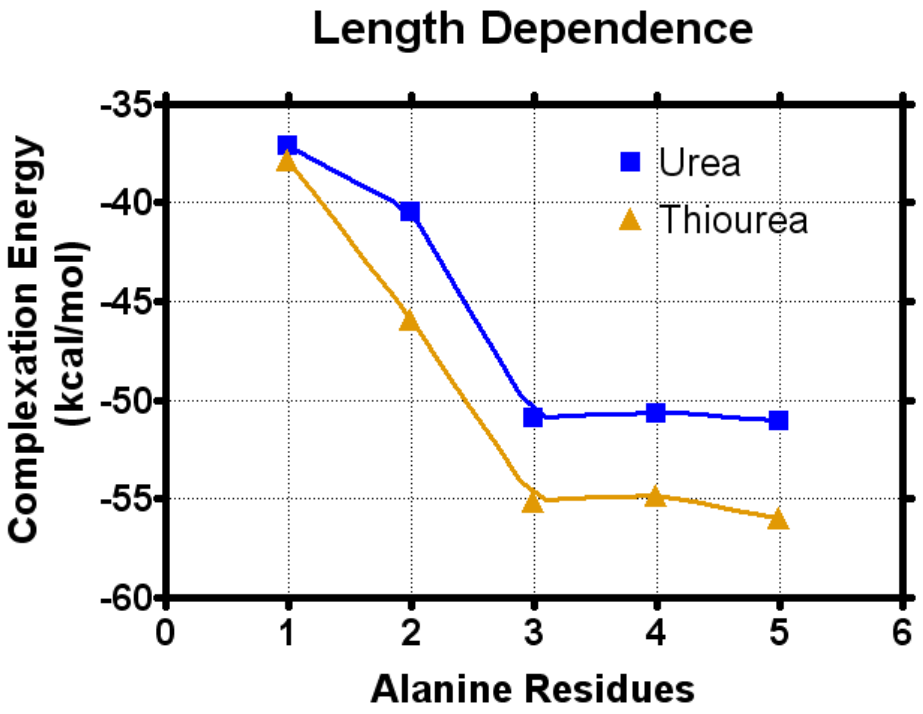

Figure 2.5 *Tabular and graphical representations of complexation energies of urea (**15, 18-21**) and thiourea (**16, 22-25**) N-capped poly-Alanine peptides of various length. No additional complexation energy advantage is expected past three alanine residues.*

The study suggests that for simplicity's sake (both for calculations and synthesis), a tripeptide is the optimal length for chloride binding via the peptide backbone. Intramolecular hydrogen bonding is present in the smallest native hosts (**18** and **22**), and increases proportionately with the addition of each hydrogen bond donor past a peptide chain length of two. The thiourea series shows an increasing degree of chloride complexation with increasing length. In the 5-mer, 6 N-H···Cl^- contacts are present of 7 possible. This compares to the same urea with 4 N-H···Cl^- contacts of 7 possible and three intramolecular hydrogen bonds in the host molecule. However, a closer examination of the 5 lowest energy conformations for these two hosts shows that in both cases, the higher energy conformers (+ < 1.0 kcal mol^{-1}) have variations in the amount of intramolecular hydrogen bonding and chloride coordination. The trade-off between intramolecular hydrogen bonds and binding to the chloride guest is roughly the same when considering the degree of intramolecular hydrogen bonding present in the host.

A final computational study in this area surveyed different amino acids used in urea-terminated dipeptides. Once again, the compounds are compared to **15** as a standard to compare across the three discrete studies performed. As seen in Table 2.4, four amino acids have been studied in this capacity. In compounds **27** and **28**, two additional hydrogen bond donors are present in the form of the serine and threonine residue side chains, respectively. Compared to host **15**, which contains only 4 hydrogen bond donors instead of 6, the calculated chloride binding energy of **27** and **28** is 5 to 8 kcal mol^{-1} better.

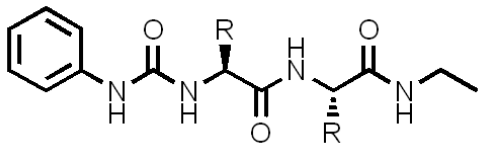

R =	Amino Acid	Host	B3LYP $E_{complexation}$ (kcal mol^{-1})	MP2 $E_{complexation}$ (kcal mol^{-1})	Intramolecular H-Bonds		Complex $NH\cdots Cl^-$ or $OH\cdots Cl^-$ Contacts
					Host	Complex	
H	Gly	**26**	-40.5	-47.1	1	0	4 of 4
CH_3	Ala	**15**	-40.4	-49.1	1	0	4 of 4
CH_2OH	Ser	**27**	-44.7	-	1	1	5 of 6
$CH(OH)CH_3$	Thr	**28**	-47.7	-	1	1	5 of 6

Table 2.4 *Structures and calculated chloride complexation energies for dipeptide compounds varying the amino acid composition. Energies shown are calculated using the B3LYP or MP2 method with the 6-31G* basis set.*

Examination of the geometries of the **27·Cl⁻** and **28·Cl⁻** complexes reveals that the geometries of the host peptides are essentially identical in the complex. Both of the side-chain hydroxyl moieties bind the chloride guest along with both urea N-H protons and the first amino acid amide proton. The N-H proton of the second amino acid residue is hydrogen-bonded to the oxygen atom of the urea in both complexes.

The diglycine compound, **26**, is predicted to be as good a host as the dialanine compound. When compared to the dialanine compound, **15**, it can be understood that the presence of a methyl side-chain has no disruptive effect on the calculated binding energy. Analysis of the host and complex geometries of **15** and **26** shows that they nearly overlap. As with the other receptors modeled, the lowest energy conformer of **26** has one intramolecular hydrogen bond present in the native host. When bound to chloride, however, this interaction is broken in favor of a fourth interaction with the guest molecule.

Amides of tri- and tetraacids

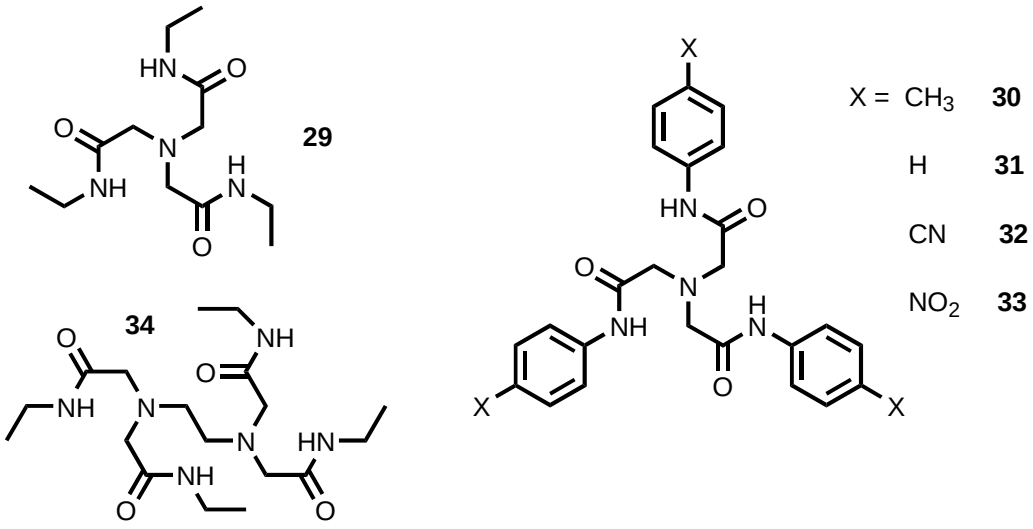

Figure 2.6 *Structures of the computationally-modeled amidated metal-chelates. Compounds **29-33** are triamides of nitrilotriacetic acid, while **34** is the tetraethylamide ethylene diamine tetracetic acid.*

The third category of compounds (examples seen in Figure 2.6) studied are fully-amidated multi-carboxylates normally used for metal chelation. One of the most well known of these metal chelates is EDTA, ethylenediaminetetraacetic acid. Amidation of the four carboxylic acids yields a tetraamide—four covalently-bound moieties capable of complexing a halide anion. When the ethyltetraamide, **34**, is subjected to the established calculation method, a tetracomplexation conformation is lacking in the twenty lowest energy conformers (LECs), with only two halide-amide interactions present in the overall LEC (Figure 2.7). Although other low energy conformers have three binding amide moieties, presumably the energy-lowering backside amide to amide intramolecular hydrogen bonding negates any advantage gained by extra complexing interactions.

Host	Chelate Acid	B3LYP $E_{complexation}$ (kcal mol^{-1})	*Host H-Bonds*		*Contacts in Complex*	
			Intra-	Extra-	N-H···Cl^-	N-H···O
29	NTA	-44.2	2	-	3	0
29·29	NTA	-43.8	3	2	6	0
34	EDTA	-37.2	4	-	2	2

Table 2.5 *H-bonds and complexation energies of modeled ethylamides of metal-chelating agents nitrilotriacetic acid (NTA) and ethylenediaminetetraacetic acid (EDTA).* ***29*** *was modeled as a dimeric host as well.*

However, computational study of a tripodal receptor candidate, **29**, shows that all three amide N-H moieties are in close contact with the chloride anion (<2.31Å) with the entire complex in C_3 symmetry as seen in Figure 2.8. The clockwise or counter-clockwise nature of the side chains (clockwise from the anion-binding face in Figure 2.8) could mean induced chirality in aggregates of molecules with larger alkyl or aryl side chains. The short-chained compound **29** was modeled not as a real-world synthetic target, but as a computationally-friendly model of such targets. The core of the investigation of this family of compounds is the central amide residues retained in all variations of this family.

With compound, **29**, yielding a -44.2 kcal mol^{-1} complexation energy advantage, a synthetic targeting of this receptor type seems prudent. Lack of similar structures used as anion receptors and the relative ease of synthesis (see synthetic approach, below) further argued for this synthetic target. Utilization of alkylamides can aid in optimization of the solubility and membrane permeability of this class of compounds. The addition of amino acid moieties or peptide chains with N-termini coupled to the triacids can yield additional structural variability.

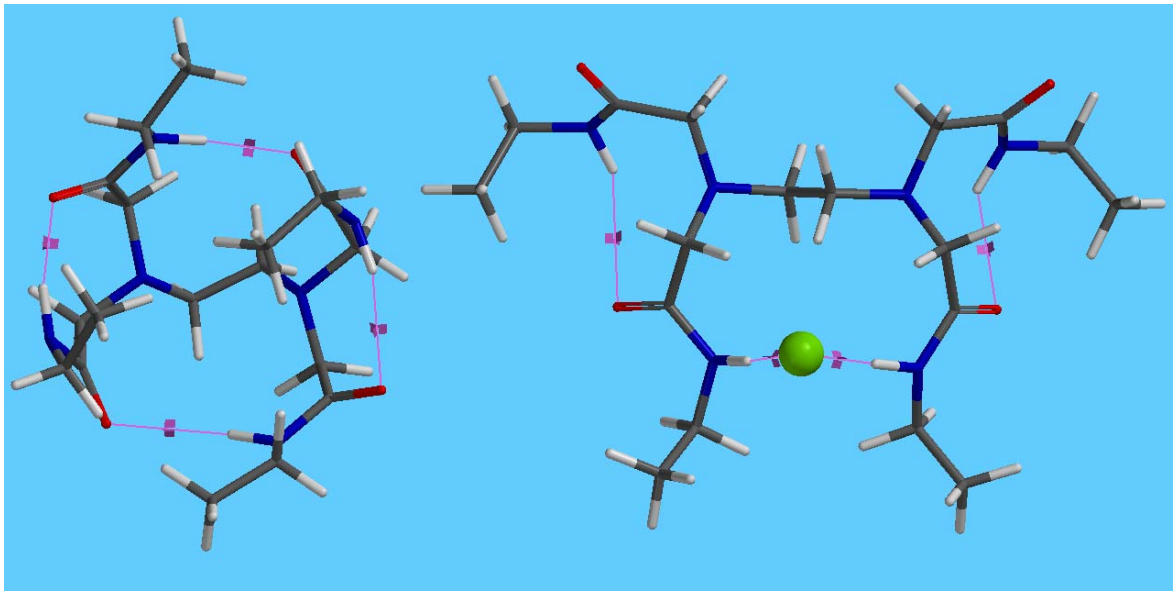

Figure 2.7 *(Left) Lowest energy conformer of* ***33*** *exhibiting 4 intramolecular N-H···O contacts (Right) Lowest energy conformer of* ***33****-Cl*$^{-}$ *complex. Two amide N-H moieties bind chloride with close contacts as shown in the foreground, while the remaining amide N-H moieties are in close contact with the carbonyl oxygen atoms of the former.*

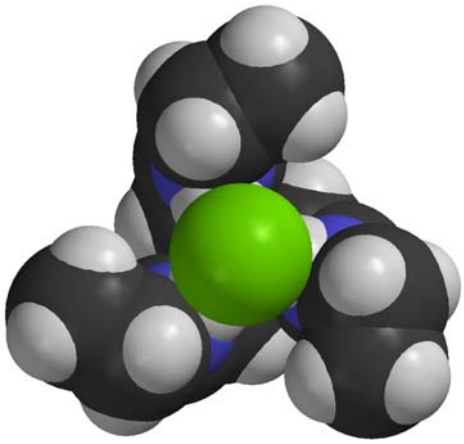

Figure 2.8 *Lowest energy conformer of* ***29****-Cl- complex. All three amide N-H moieties bind chloride with close contacts on the same face of the receptor as the central nitrogen lone pair (hidden behind the chloride ion).*

During modeling and geometry calculations, an idea took hold for receptor **29** (and by extension any similar nitrilotriacetamide) binding in a 2:1 host to guest ratio with chloride. This possibility was modeled in the gas phase and the relevant host and guest energies were calculated. However, the drop in the complexation energy advantage expected from the addition of three complexing amide N-H moieties was not seen in the

final energy calculations. In fact, the energy advantage was statistically even with a slight drop from -44.2 kcal mol^{-1} to -43.8 kcal mol^{-1}.

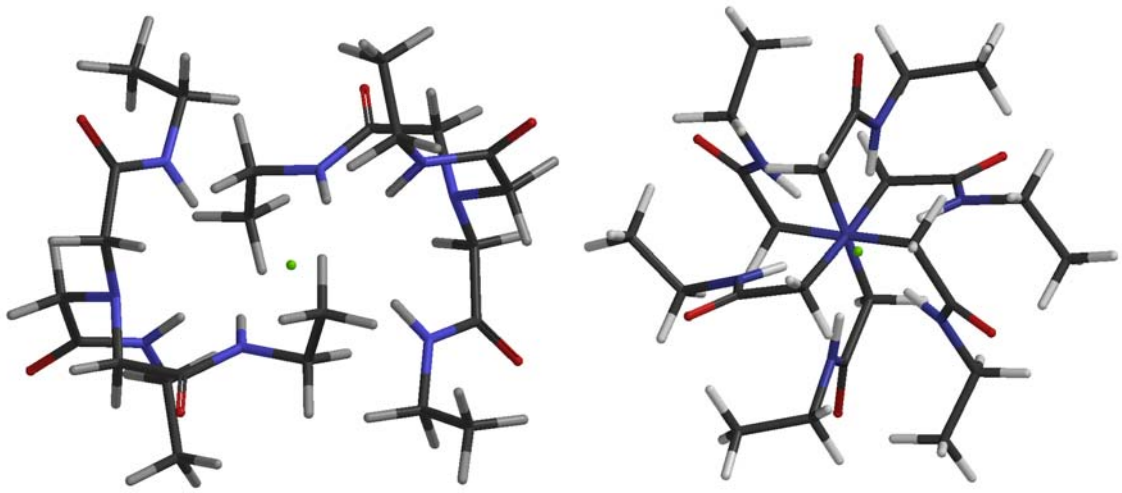

Figure 2.9 *Orthogonal views of the tube model of the lowest energy conformer of* ***29·29·****Cl- complex with six amide N-H moieties binding chloride with close contacts. The complex has a pseudo-octahedral geometry with an extended midsection. The angles of the opposite N-H vertices, passing through the guest at the center average are offset between 8° and 12° from linearity. Additionally, the central nitrogen atoms are offset 11° from linearity through the central guest ion.*

The optimized LEC of the **29·29·**Cl^- complex (Figure 2.9) shows, as expected, both hosts complexing the chloride anion with a total of 6 amide N-H residues, but the N-H···Cl^- distances have increased from <2.31 Å to between 2.42 Å and 2.44 Å. In contrast, the N-H···Cl^- bond angles have decreased from 27° to about 24°. The marginal bond angle decrease (3°) paired with a significant N-H···Cl^- contact distance increase (>0.1 Å) leads to no significant change if both host molecules are taken separately. Essentially, it is the interactions within the host molecule dimer in the gas phase that leads to the lack of change in the complexation energy. Apart from the two intramolecular hydrogen bonds already present in the monomer, the two remaining non-interacting moieties on each monomer hydrogen bond intermolecularly as seen in the center of Figure 2.10. This gas-phase dimerization leads to an energy difference of -22.7 kcal mol^{-1} in the host dimer

(compared to two monomers) and no net energy advantage to using a 2:1 host to guest complex.

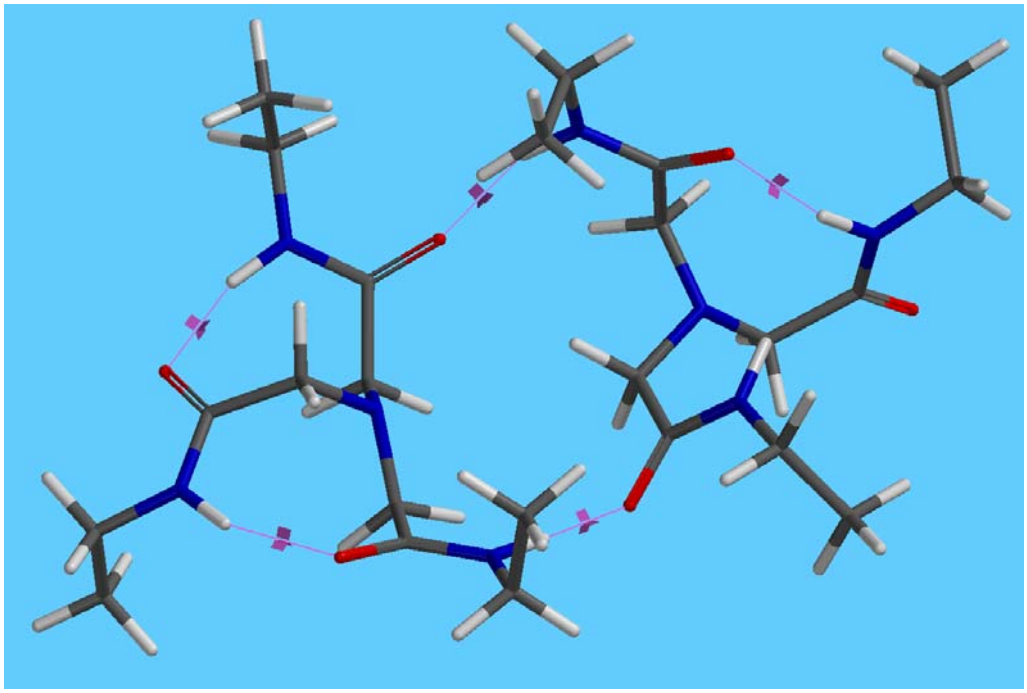

Figure 2.10 *Tube representation of the lowest energy conformer of the* ***29·29*** *homodimer. Extensive hydrogen bonding (3 intramolecular and 2 intermolecular) lowers the gas phase energy of the host and negates any energy complexation advantage from the three additional amide N-H moieties in the complex seen in Figure 2.9.*

While the modeling of **29** as a 2:1 dimer does not yield an additional complexation advantage, the geometry of the complex—which fully encapsulates the guest chloride ion—is intriguing. This encapsulation strategy was used in the development of cryptands as cation binding agents[18] and synthetic cation carriers.[19] The 2:1 host to guest complex was modeled for *para*-substituted trinitrilotriacetanilides **30**-**34**. As seen below in Figure 2.11, The rigid *tris*-anilide side-arms interdigitate in the complex at interatomic distances as close as 3.7 Å. In all of the complexes, six N-H···Cl^- are present at an average H···Cl^- distance below 2.17 Å and a bond angle that does not exceed more than an 11° deviation from linearity. This information is summarized in Table 2.6.

Dimeric Host	*para*-substituent	B3LYP $E_{complexation}$ (kcal mol^{-1})	Average N-H-Cl Bond Angle (°)	Average N-H···Cl Distance (Å)	N-H Electrostatic Potential (kcal mol^{-1})
30·30	CH_3	-72.7	171.6	2.163	84.2
31·31	H	-77.8	171.7	2.163	87.7
32·32	CN	-104.3	171.1	2.160	113.4
33·33	NO_2	-106.3	169.9	2.169	115.7

Table 2.6 *Summary of the calculated energies and relevant geometric measurements of the* para*-substituted trinitrilotriacetanilides, hosts* ***30-34*** *modeled as the 2:1 dimer complex.*

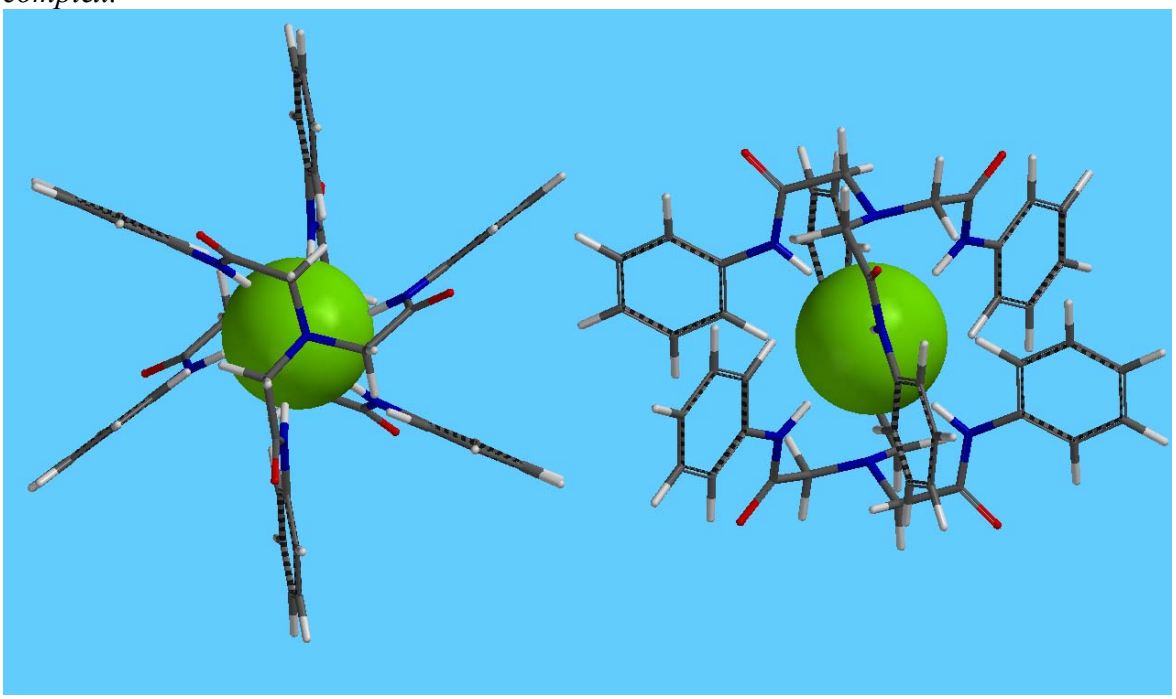

Figure 2.11 *Orthogonal views of the* ***31·31·****Cl^- complex.*

While the geometry of each of these complexes is essentially identical, the most telling aspect gleaned from the calculations is the electrostatic potential of the chloride-binding cleft. The electrostatic potential is the measure of attraction or repulsion of a positive charge on an isodensity surface.[20] This potential is negative (energetically favored) at more electron rich regions of the molecule such as the oxygen atom of a ketone. Conversely, this potential is positive (energetically disfavored) at more electron

poor regions of the molecule, such as the carbon atom of a ketone, or in the present case, the hydrogen atom of an amide. This calculated prediction of localized proton acidity correlates well with the calculated complexation energies.

Alkyl- and arylureas

The fourth of five categories of host candidates includes the urea non-peptidic compounds shown in Figure 2.11. The favorable interactions of the urea and thiourea-capped peptides led to the idea of extending the moiety to simple non-peptidic compounds—a 4-nitrophenyl alkyl urea (**36**) and an *ortho*-phenylene *bis*(4-nitrophenyl)urea (**35**). Both compounds have been made previously, with the former studied for antimicrobial activity[21] and the latter used as an anion binding agent.[22]

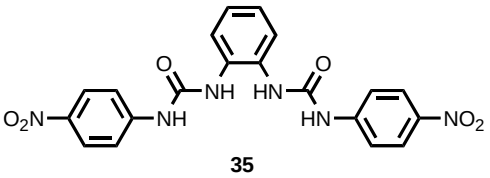

35

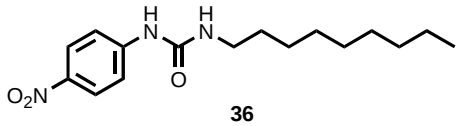

36

Compound	N-H Donor(s)	B3LYP $E_{complexation}$ (kcal mol^{-1})
35	(2x) Urea	-83.6
36	Urea	-46.5

Figure 2.12 *Structures of the p-NO_2 urea compounds **35** and **36**.*

Compound **35**, the chloride complex of which is seen in space-filling form in Figure 2.13, produces the largest calculated energy advantage from a 1:1 complexation of all of the compounds studied with -83.6 kcal mol^{-1}.

Unlike the dipicolinic and isophthalic acid receptors, the geometry of the native host is nearly planar while, upon rotation of one of the side arms, becomes completely planar in the complex. The host forms four close contacts between urea N-H moieties and the chloride guest. The anion receptor cleft is in such a geometry that the N-H···Cl^-

hydrogen bonds are very close to linearity (169.2° and 162.9°) and in close contact (2.27Å and 2.32Å) with no real deviation from the lowest energy conformation of the native host. While Gale and co-workers have shown that this compound does bind chloride in DMSO-d_6,[22] it has a preference for trigonal planar anions.

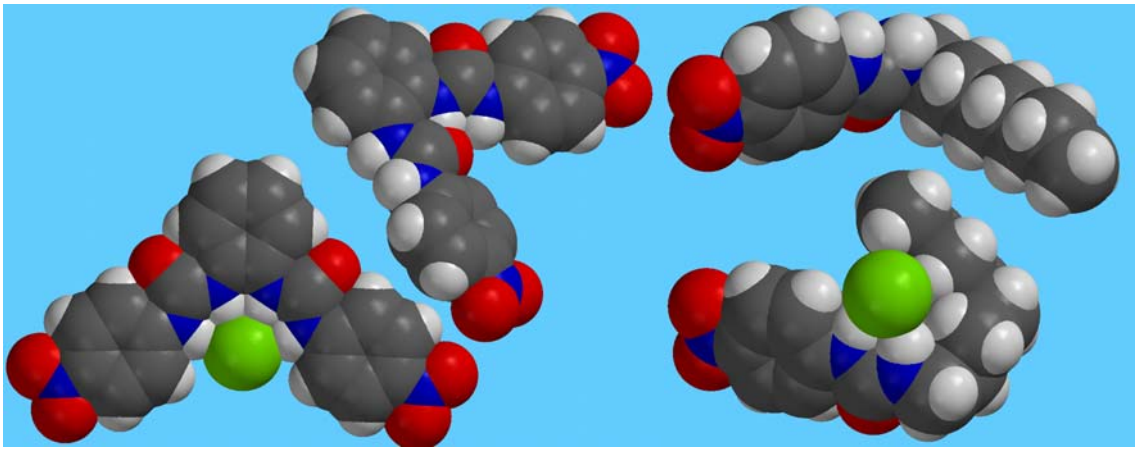

Figure 2.13 *(Left)Space-filling models of the lowest energy conformers of the native host* ***35*** *(top) and the* ***35-Cl*** *complex (bottom). The chloride-bound host is in a low energy fully-planar and fully-conjugated system, while the host deviates by < 7° from planarity. (Right) Structures of the lowest energy conformers of the native host* ***36*** *(top) and the* ***36-Cl*** *complex (bottom).*

The alkylurea compound, **36**, contains only one urea moiety. Conjugation with the electron-withdrawing *p*-NO_2 substituent creates a more acidic urea moiety. The chloride binding moieties deviate more from linearity than the interactions seen with **35** (N-H···Cl^- angles = 164.9° and 156.2°), but are in closer contact (2.13Å and 2.28Å). Observed in the lowest energy conformation of the complex, hydrogen atoms of the 3-,6-, and 8- carbons of the octyl chain are in close contact with the chloride anion (H···Cl^- distance = 3.02Å, 3.33Å and 3.00Å, for the 3-, 6-, and 8- carbons, respectively). These C-H···Cl^- interactions are normally seen with aromatic carbons (the hydrogen atom *ortho* to the urea substituent in 36 is at a contact distance of 3.32Å). The limited energy that must be associated with these C-H···Cl^- interactions could be roughly equal to the energetic penalty of the

methylene carbons rotating out of the all-*gauche* conformation. All of the twenty lowest energy conformers have at least one non-*gauche* rotation, but the second lowest energy conformer has only one, signifying that the all-*gauche* conformation is energetically favorable as well.

Dipicolinic acid / *ortho*-phenylene diamine macrocycles

The fifth and final category of candidate receptors includes macrocycles incorporating *ortho*-phenylenediamine and dipicolinic acid. The *ortho*-phenylenediamine moiety was chosen as it presents 2 hydrogen bond donors in close proximity to one another, as ureas and thioureas do. The dipicolinic acid residue was used as the lone pair electrons of the pyridine nitrogen can pre-organize the amide N-H moieties to interact with anions. The geometry of the two components also complement each other.

The macrocyclic compound, **37**, was targeted for its structural rigidity, as pre-organized receptors do not have significant energetic penalties associated with rotation into the optimal guest-binding conformation. The leftmost half of Figure 2.14 shows the geometry-optimized structure of the native host. The host is held rigidly in a puckered geometry with two adjacent arenes related by a dihedral angle of 36°. The dihedral angle between *ortho*-phenylenediamine and each amide C-N bond is approximately 23° while the dihedral angle between each C-N bond and pyridine is approximately 13.° The geometry of the host in the calculated complex, however, reverses these angles, with the amide moiety more closely aligned with the phenylene plane rather than the pyridine plane.

The chloride binding strength of macrocycle **37** is comparable to the other reported hosts. The binding geometry is not ideal, as the average N-H···Cl^- bond angle deviates approximately 22° from linearity and the average H···Cl^- distance is 2.57Å. The rigidity

and pre-organization of the host is a key aspect in explaining the favorable chloride complexation energies. However, a chloride ion of a diameter of 3.56Å is too large to fit into the pre-organized binding cavity which is approximately 1.6Å in diameter, when including the van der Waals radii of the binding amide protons. Fluoride (d = 3.02Å) may be a better suited guest for this receptor.

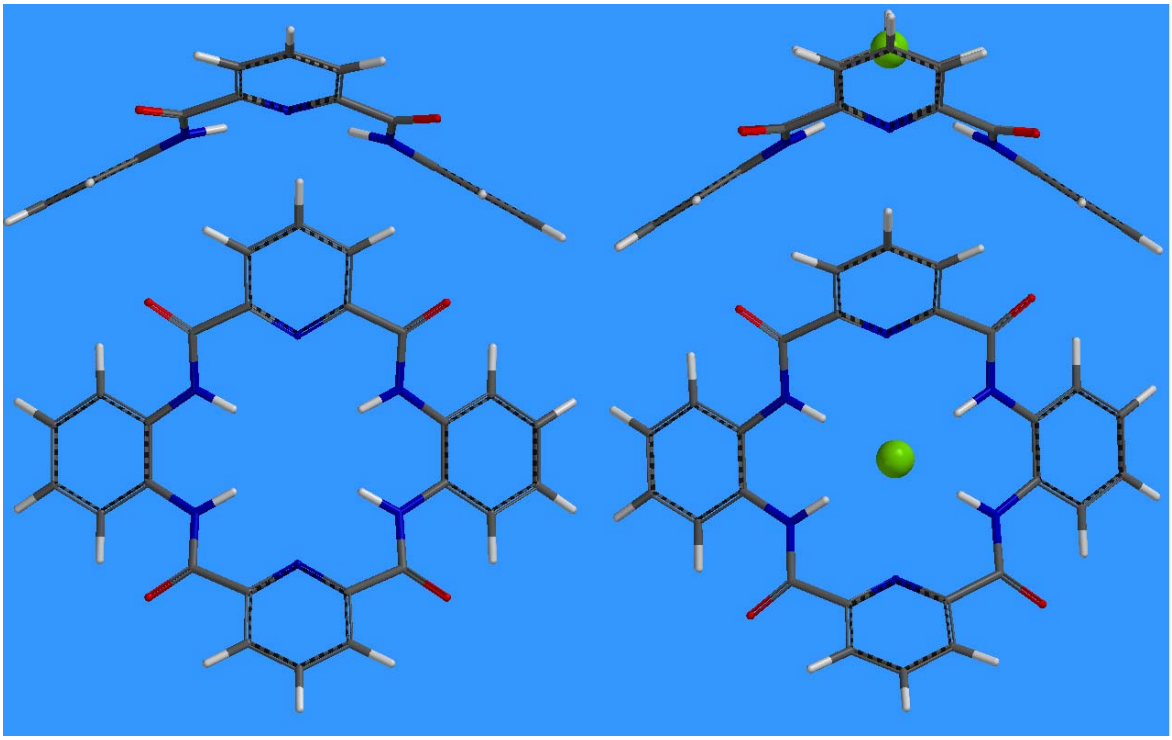

Structure	Dihedral Angle			Average H···Cl⁻ Distance	Average N-H···Cl⁻ Angle	B3LYP $E_{complexation}$ (kcal mol^{-1})
	Pyridine/ Amide	Amide/ Phenylene	Pyridine/ Phenylene			
37	13.1°	22.7°	35.8°	-	-	-42.5
37·Cl	33.5°	16.1°	50.6°	2.57Å	158.1°	

Figure 2.14 *Orthogonal views of the the lowest energy conformer of the* ***37*** *host (left) and the* ***37****-Cl⁻ complex. "Puckering" of the ring allows for a better chloride binding geometry in the complex, although the hydrogen bonds deviate by about 22° from linearity.*

Unfortunately, macrocycle **37** was reported in the literature during the initial phase of this investigation.[23] Therefore, a second type of macrocycle was envisioned that made use of a repeating sequence of *ortho*-phenylenediamine, amino acid, dipicolinic acid, and amino acid. This larger macrocycle may better complement larger anion guests with a more favorable binding geometry.

This second design approach also allows for the incorporation of either D- or L-, hydrophobic or hydrophilic, or natural or artificial amino acids to either aid in solubility or anion binding or resist biodegradation. Only macrocycles incorporating four arenes and four amino acids were modeled and binding energies were calculated. Any larger macrocycles would require greater computational and synthetic resources and were ruled out. However, the macrocycles present, at a minimum, 8 hydrogen bond donors available for chloride complexation. Additional binding moieties can be integrated using appropriate amino acids such as serine and threonine (used previously with compounds **27** and **28**) or others such as asparagine, which have two hydrogen bond donors.

Three of the two-repeat macrocycles have been modeled and analyzed—the tetraglycine version, **38**, the tetraserine version, **39**, and the tetraasparagine version, **40**, all seen in Figure 2.15. The latter two were modeled with the idea in mind of increasing the available hydrogen-bonding moieties, and in turn increasing binding strength while the former gives a good reference to the effects of adding different side chains into the mix. Compound **40** also lends an increase in side arm flexibility (from the added length) resulting in a high number of low energy conformers and increasingly difficult and computationally-expensive geometries to optimize.

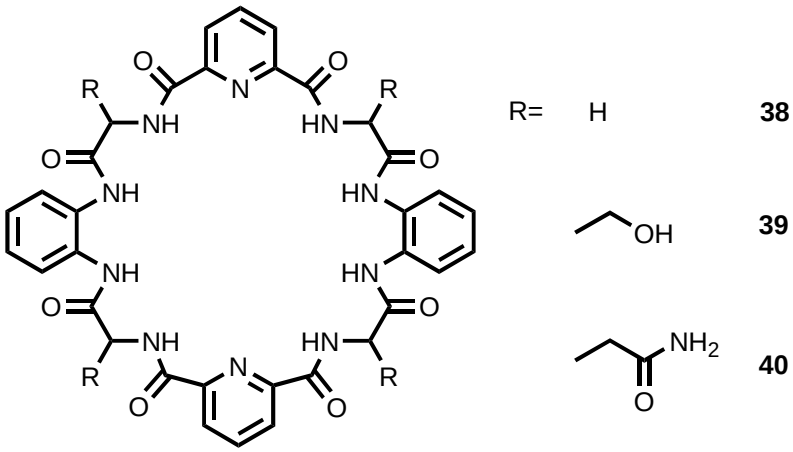

Figure 2.15 *Structures of the tetraarene, tetraamino acid macrocycles **38-40**. In compound **38**, an array of 8 possible hydrogen bond donors are presented while compounds **39** and **40** present 12 and 16 donors, respectively. Note that the amount of hydrogen bond acceptors also increases from 10 for **38** to 14 for **39** and **40**.*

Focusing the discussion on the differences between compounds **38** and **39**, we can see in the orthogonal views of the two chloride complexes (Figure 2.16) that host **39** nearly encapsulates the chloride ion from the back, front, and sides. Notably, in the front, relative to viewpoints on the left-hand side of Figure 2.16, the serine side chain alcohol moieties are binding and better encapsulating the chloride anion. Three of the four serine side chains are binding the chloride anion, yet they replace the same number of amide hydrogen bond donors, resulting in no net gain in close contacts. While an intramolecular hydrogen bond is retained in the host molecule within the complex, host **39** starts out with eight intramolecular hydrogen bonds in its native form and thus must sacrifice seven of them to bind chloride. In contrast, host **38** only has four intramolecular hydrogen bonds to sacrifice and a binding event involves the same number of hydrogen bond donors. As a result, host **38** has a greater net complexation energy advantage than its serine counterpart (see Table 2.7 for full details)

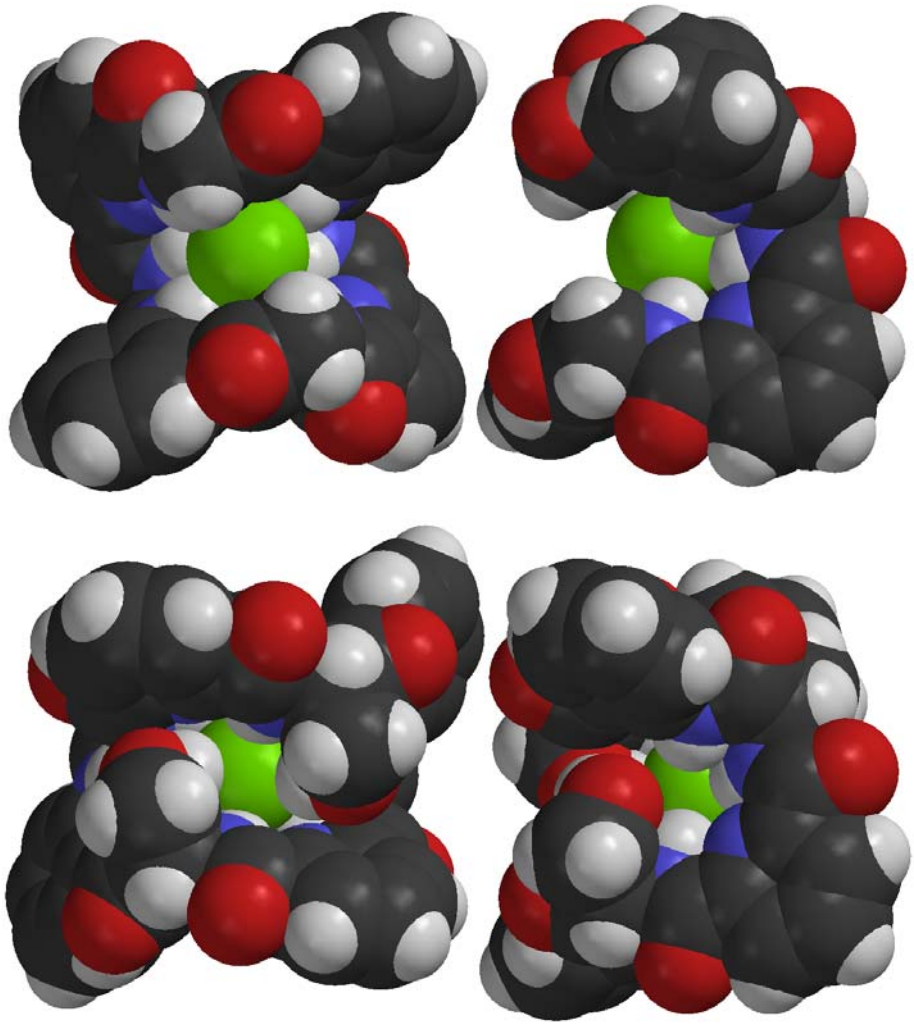

Figure 2.16 *Orthogonal views of the CPK model of the tetraglycine compound* ***38****, top, and the tetraserine compound* ***39****, bottom. In compound* ***38****, six of eight amide hydrogen-bond donors are in close contact (H···Cl*$^{-}$ *<2.75Å) at reasonable ion-dipole interaction angles (>150°). Two hydrogen-bond donors are geometrically forbidden from anion binding. A noticeable exposure to the outside environment is seen in the leftmost view. This exposure is somewhat diminished with* ***39*** *as host molecule in which three of the amide-chloride interactions are replaced with three serine side chain hydroxyl-chloride interactions, forming a more octahedral binding domain as seen in chloride complex of the dimer of the nitrilotriacetamide* ***29****.*

Compound	Amino Acid	Complexation Energy (kcal/mol)	*Contacts in Complex*		*Intramolecular H-Bonds*	
			N-H···Cl^-	O-H···Cl^-	Host	Complex
38	Gly	-58.0	6	-	4	0
39	Ser	-50.6	3	3	8	3
40	Asp	-52.3	4	-	9	9

Table 2.7 *Comparison of compounds **38** and **39**. **38** is predicted to complex chloride more efficiently as the incorporation of the serine alcohol side chains in **39** affords no additional chloride-dipole close contacts and results in the breaking of seven intramolecular hydrogen bonds rather than four broken in **38** to bind chloride. Close contacts and hydrogen bonds are defined as those with less than or equal to a 2.75Å hydrogen-heteroatom or hydrogen-chloride distance, the presumed bifurcated hydrogen bonds observed in the dipicolinic diamide system are not counted as binding with the pyridine nitrogen lone pair.*

Synthetic approaches and synthesis of selected modeled anion receptors

The receptors outlined in this study were designed and investigated for their simplicity and ability to be structurally-modified. Both of these traits are highly desirable in the context of new applications—the former for minimizing the use of resources and the latter for optimizing a desired function. The families outlined above make use of amino acid residues, alkyl or aryl moieties, or some combination of the three.

The use of alkyl substructures in a family of compounds allows for the optimization of solubility and membrane permeability. Ethyl substituents were used as a stand-in for any length alkyl chain in the modeling studies, as this minimized computational cost. The exception to this is the octyl urea compound, **36**. Utilization of substituted aryls allows for the optimization of the strength of chloride interaction. Insertion of amino acids into receptor molecules allows for further optimization of membrane permeability and chloride-binding characteristics with variation of the amino acid side-chains. With these key aspects in mind, receptors **1-40** were targeted to both allow these structural variations and minimize the synthetic steps (and resources used) to access these compounds.

With 40 proposed synthetic receptors modeled computationally, the accessibility for all of the families were assessed by the development of a synthetic approach for each. The synthesis and characterization of the dianilides **1**, **2**, **7** and **8**, as well as similar compounds not enumerated here, are detailed in Chapter 3 in the context of the full investigation of that family of compounds for anion binding, transport and channel functionality.

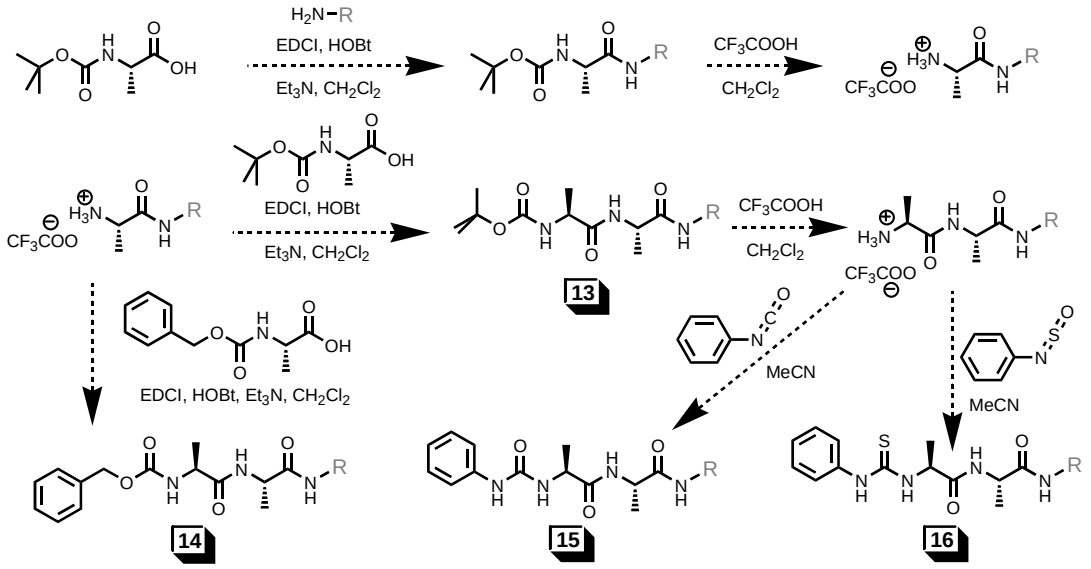

Scheme 2.1 *Synthesis of modified peptides **13-16**. Peptide length can be varied by the use of extra peptide coupling steps while different amino acids can be used at any step to vary the side-chains, giving access to the remainder of the modified peptides outlined above. "EDCI" = 1-ethyl-3-(3-dimethylaminopropyl) carbodiimide; "HOBt" = 1-hydroxybenzotriazole.*

The protected peptides **13**-**28**, are similar to the SAT molecules studied in the Gokel lab, and are accessed through a similar synthetic approach. Standard solution coupling methods would be used to prepare these modified peptides. Scheme 2.1 shows the approach used to access the N-terminal-varied dialanine compounds **13**-**16**. This same approach can be used to access the remaining protected peptides, **17-28**, and peptides of

the same class. This is accomplished by variation of the amino acids used or the number of amino acids coupled (for longer chains).

The approach consists of first coupling the alkylamine to the C-terminus of the peptide, accomplished in the first step using EDCI or 1-ethyl-3-(3-dimethylaminopropyl), a carbodiimide amide coupling agent[24] and HOBt or 1-hydroxybenzotriazole, a racemization suppressor.[25]

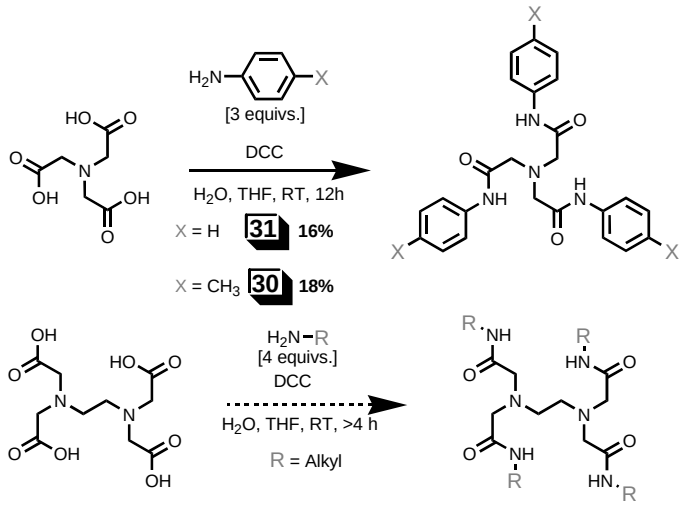

Scheme 2.2 *Synthesis of nitrilotriacetanilides **30** and **31** and the proposed approach for the synthesis of the N,N',N'',N'''-alkyl* tetrakis*(ethylenediaminetetraacetic)acetamide, (modeled by **34**) from the corresponding tri- or tetraacid and the appropriate equivalents of aniline or alkylamine. "DCC" = 1,3-dicyclohexylcarbodiimide.*

A coupling agent is also used in the synthesis of nitrilotriacetanilides **30** and **31** as shown in Scheme 2.2. DCC, or 1,3-dicyclohexylcarbodiimide, is an older variety of the carbodiimide family of compounds. As no stereocenters are present in the proposed receptors, a racemization suppressor is not utilized in this coupling interaction. Unfortunately, the yields for these two compounds are relatively low, and a different coupling reagent or different conditions may be used to optimize the synthetic efficiency if future work were to progress with this type of anion receptor. Scheme 2.2 also shows a synthetic approach for the tetraamides of EDTA. This methodology can be used for

compounds in both classes. The poor solubility of the tri- and tetraacids in organic solvent necessitates a reaction performed in an aqueous environment, and this is accomplished using this procedure.

The N-(4-nitrophenyl)-N'-octylurea, **36**,[21] and *bis*(4-nitrophenyl)urea, **35**,[22] have both been made previously. However, a synthetic method developed by Barbiou and co-workers[26] was used to synthesize these receptors as seen in Scheme 2.3. The compounds were made in one step from commercially available material in quantitative or near-quantitative yields. Variation of the substituents present on the phenyl isocyanate ring can be used to optimize the chloride binding strengths of both **35** and **36** while variation of the alkylamine (R) used in the synthesis of **36** can be used to optimize solubility and membrane permeability of this type of receptor.

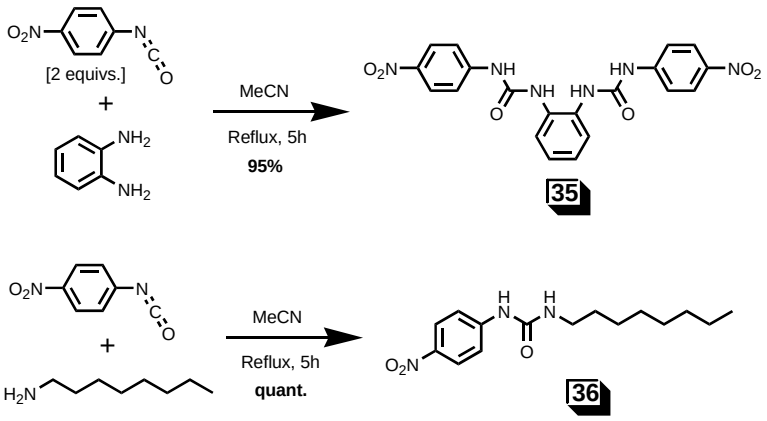

Scheme 2.3 *Synthesis of urea **36** and* bis-*urea **35** from 4-nitroisocyanate.*

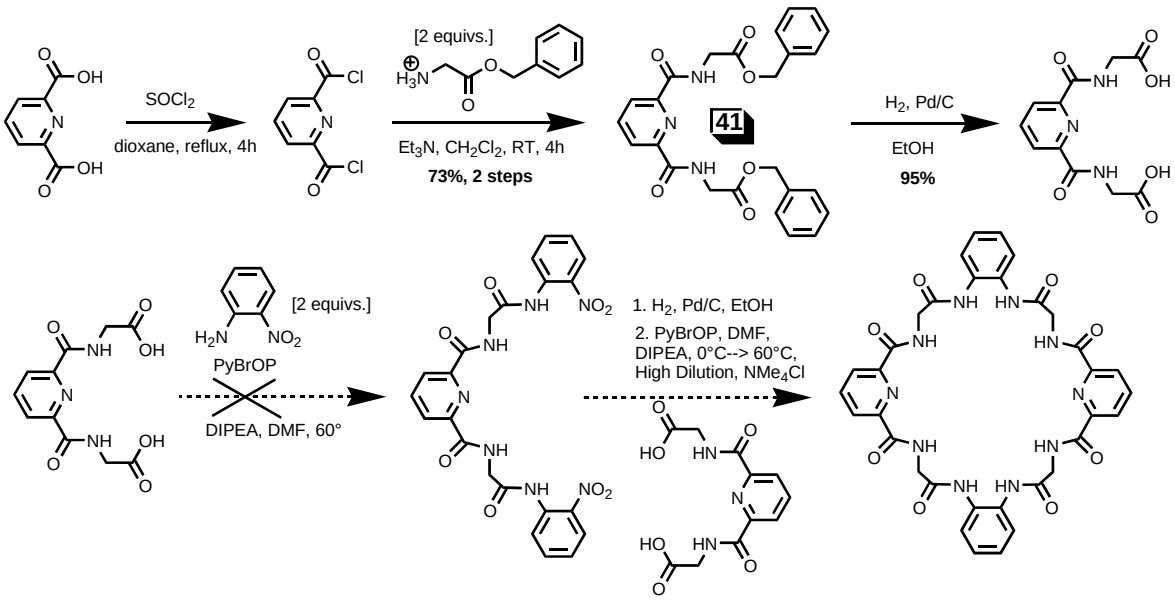

Scheme 2.4 *Synthetic approach to macrocycle **38** from dipicolinic acid, glycine benzyl ester, and 2-nitroaniline. While the acyclic receptor **41** was accessed, the later coupling with 2-nitroaniline was unsuccessful. "PyBrOP" = Bromo-*tris*(pyrrolidino)phosphonium hexafluorophosphate; "DIPEA" = N,N-diisopropylethylamine.*

The tetraarene / tetraamide macrocycle, **37**, has been made previously,[23] along with a number of other similar compounds,[27] so the synthetic approach to this molecule is not outlined here. However, the macrocycles incorporating amino acid residues, **38**-**40**, have not, to our knowledge, been made previously. The synthetic approach to access the tetraglycine compound, **38**, is shown above in Scheme 2.4. The first two steps include the coupling of dipicolinic acid to two equivalents of C-protected glycine through formation of the dicarbonyl chloride to yield the acyclic bis-glycine dipicolinamide, **41**. This compound was studied in Chapter 5 for antimicrobial activity.

After hydrogenolysis of the benzyl esters, attempts were made to couple the resulting diacid with 2-nitroaniline. However, the electron-withdrawing nature of this substituent significantly decreases the nucleophilicity of the aniline amino moiety, resulting in no reaction. While the coupling reagent, bromo-*tris*(pyrrolidino)phosphonium

hexafluorophosphate, or PyBrOP, is shown in Scheme 2.4, EDCI was also used unsuccessfully as a coupling reagent.

A second strategy to access this class of compounds could make use of coupling N-protected amino acid residues to 1,2-phenylenediamine through the C-termini. After deprotection, the N-termini could be coupled to a dipicolinic acid that has been monobenzylated. After hydrogenolysis and a cyclization coupling step, the desired marocycle could be achieved. As detailed in Chapter 3, the success of the dipicolinic dianilides as anion receptors and transporters precluded further synthetic exploration of the tetraamino acid, tetraarene macrocycle family.

Conclusions

This survey of a vast number of novel structures has yielded better insight into which anion-binding moieties and how many should be used in a successful anion receptor. Modeling of the N-capped peptides has shown that the use of urea and especially thiourea in the binding cleft can lead to a significant complexation energy advantage over carbamates or amides.

The lengthening N-capped peptides, nitrilotriacetamide dimers, and the tetraamino acid tetraarene macrocycles has shown that larger, more complex molecules with more hydrogen bond donor moieties may not be advantageous when considering the design of an anion receptor or transporter. Utilization of amides or ureas as hydrogen bond donors in a binding motif also presents hydrogen bond acceptors in the native host. If a significant amount of intramolecular hydrogen bonding exists in the host because of this, then intramolecular host hydrogen bond would need to be broken and complexation may not be

as energetically favored as one would anticipate. The best approach, therefore, would be one that considers just a few amide or urea residues rather than many.

Modeling of the 2:1 host to guest complexes of 4,4',4''-substituted nitrilotriacetanilides and chloride has shown that that electron withdrawing substituents in a π-system including anion-binding moieties dramatically lowers the binding energy. Correlation with the calculated electrostatic potential maps reveals that this is caused by increasing proton acidity. This characteristic is exploited more fully in the investigation of the dipicolinic dianilide chloride transporters in Chapter 3.

These calculations give good predictions of actual molecules, yielding insight into what substructures should be incorporated and how variations of those structures can optimize the desired activity. However, once a family is designed and leads are made, they must be correlated with experimental data to truly yield relevant information. The calculations performed for the dipicolinic dianilides are further expanded upon in Chapter 3 leading to work done with these compounds as synthetic ion channels. A few of the other compounds modeled in this survey are approached synthetically, and the resulting compounds are tested for antimicrobial activity as detailed in Chapter 5.

Experimental

General.

Reagents were the best (non-LC) grade commercially available and were distilled, recrystallized or used without further purification, as appropriate. CH_2Cl_2 was distilled from calcium hydride. Unless otherwise stated, all chemicals were purchased from Sigma-Aldrich (St. Louis, MO).

Melting points were determined on a Thomas Hoover apparatus in open capillaries and are uncorrected. All ^{1}H NMR spectra were recorded on a Bruker Avance 300 spectrometer at 300 MHz and all chemical shifts are reported in ppm (δ), calibrated to literature values for internal solvent with integrated intensity (X H) and multiplicity (b = broad, s = singlet, d = doublet, t = triplet, q = quartet, bs = broad singlet, m = multiplet, etc.) and coupling constants in Hz. ^{13}C-NMR spectra were obtained on a Bruker Avance 300 spectrometer at 75.4 MHz and referenced to solvent literature values for chemical shifts. All Mass Spectrometry experiments were performed at high resolution on a JEOL MStation, JMS-700, double focusing high-resolution instrument using the fast-atom bombardment ionization technique in the positive ion detection mode. Calculations were run using the Spartan 2006 software package on a Dell Dimension DXP061 desktop with a 2.40GHz Intel® Core™2 Processor and 2.00GB of RAM.

Molecular Modeling

The following calculation method is the third such version as described in this method. All calculations and visualizations are performed using Spartan '06 software from Wavefunction Inc. The Monte Carlo simulated annealing method was used to determine the twenty lowest energy conformations (LECs) from ten thousand conformations using the Merck Molecular Force Field, a molecular mechanics level of theory. In some cases, fewer than twenty LECs are generated when conformational flexibility is limited. The geometry of these twenty LECs were then optimized first using the RM1 semi-empirical method and then at the density functional level of theory using the B3LYP method with a 6-31G* basis set. The final single point, ground state energy calculations and electrostatic

potential mapping were performed with the B3LYP method and the 6-31G* basis set. For a specific set of final energy calculations, the electron-correlating MP2 method was used.

In every case, the conformer with the lowest calculated single point energy was used for the calculation of the complexation energy. This calculation was performed by adding the energies of the host and guest, then subtracting the energy of the complex. The complexation energy is listed as a negative value if the interaction is favorable, the more negative a value the more favorable an interaction.

***N*,*N'*,*N''*-*tris*(phenyl)nitrilotriacetamide, 31**

This compound was made previously by Greco and Schrock[28] as an intermediate for a metal coordination complex. The synthetic procedure from that work was used here. No melting point was reported, but the spectral data agrees with what was determined previously.

Aniline (1.84 g, 19.8 mmol) was added to a stirring suspension of nitrilotriacetic acid (1.25g, 6.5 mmol) in water (14.0 mL) and stirred until a solution is formed (complete proton exchange forming the salt). To this solution is added a solution of 1,3-dicyclohexylcarbodiimide (4.10 g, 19.9 mmol) in tetrahydrofuran (21.0 mL). The reaction was stirred under N_2 overnight. The resulting suspension was filtered over a glass frit, retaining the crude product as a white solid. This was suspended and filtered with methanol (3x15mL) and diethyl ether (3x15 mL). The white solid was suspended in dimethylformamide (4x25mL) and filtered over a glass frit, with the filtrate reduced *in vacuo* to yield an off-white solid. This was suspended in a 2:1 mixture of diethyl ether and chloroform (50 mL) before filtering, retaining the white solid. Trace solvent was removed *in vacuo* to yield the pure product as a white solid (0.421 g, 16%, m.p. = 217°-220°C). ^{1}H-

NMR (DMSO-d_6): 3.67 (6H, s, NC***H*****$_2$**C(O)), 7.06 (3H, t, *J* = 7.3 Hz, Anil ***4-H***), 7.33 (6H, dd, J_1 = 8.0 Hz, J_2 = 7.3 Hz Anil ***3/5-H***), 7.66 (6H, d, *J* = 8.0 Hz, Anil ***2/6-H***), 10.47 (3H, s, C(O)N***H***-Anil).^{13}C-NMR (DMSO-d_6): 58.9 (N***C***H_2C(O)), 119.4 (Anil ***2/6-C***), 123.7 (Anil ***4-C***), 129.2 (Anil ***3/5-C***), 139.2 (Anil ***1-C***), 170.4 (CH_2***C***(O)NH). FAB-MS: m/z calc for $[M+H]^+$ 417.1926, found: 417.1926.

N,N',N''-tris(4-methylphenyl)nitrilotriacetamide, 30

The synthetic method for of this compound is similar to that used for *N,N',N''-tris*(phenyl)nitrilotriacetamide, above, using an approach developed by Greco and Schrock.[28] *p*-Toluidine (2.18 g, 20.3 mmol) was added to a stirring suspension of nitrilotriacetic acid (1.28g, 6.7 mmol) in water (25.0 mL), heated to 58°C and stirred until a solution is formed. To this solution is added a solution of 1,3-dicyclohexylcarbodiimide (4.21 g, 20.4 mmol) in tetrahydrofuran (15.0 mL). The reaction was stirred under N_2 overnight. The remaining work-up is identical to above. Trace solvent was removed *in vacuo* to yield the pure product as a white solid (0.562 g, 18%, m.p. = 216°-218°C). ^{1}H-NMR (DMSO-d_6): 2.25 (9H, s, Anil-C***H*****$_3$**), 3.63 (6H, s, NC***H*****$_2$**C(O)), 7.12 (6H, d, *J* = 8.3 Hz, Anil ***3/5-H***), 7.53 (6H, d, *J* = 8.3 Hz, Anil ***2/6-H***), 10.21 (3H, s, C(O)N***H***-Anil).^{13}C-NMR (DMSO-d_6): 20.4 (Anil ***C***H_3), 58.5 (N***C***H_2C(O)), 119.1 (Anil ***2/6-C***), 129.1 (Anil ***3/5-C***), 132.2 (Anil ***4-C***), 136.3 (Anil ***1-C***), 169.7 (CH_2***C***(O)NH). FAB-MS: m/z calc for $[M+H]^+$ 459.2396, found: 459.2379.

N,N'-(1,2-Phenylene)*bis*([4-Nitrophenyl]urea), 35

This compound was made previously by Gale and co-workers[22] as a carboxylate receptor. No melting point was reported, but the spectral data agree with what was

determined previously. A synthetic procedure derived from the work of Barbiou and co-workers[26] was used.

A solution of 1,2-phenylenediamine (0.2880g, 2.66 mmol) in acetonitrile (20 mL) is added dropwise to a stirring solution of 4-nitrophenylisocyanate (1.0163 g, 6.19 mmol) dissolved in acetonitrile (50 mL for 70 mL total). The reaction was heated to reflux and stirred for 5 hours. After cooling, the resulting yellow suspension was filtered and washed with acetonitrile (1 x 10 mL) and dichloromethane (2 x 10 mL) before drying under high vacuum. The resulting yellow solid is retained as the pure product (1.1088 g, 95%, m.p. = 293°-297°C). ^{1}H-NMR (DMSO-d_6): 7.19 (2H, m, *o*-Phen ***4/5-H***), 7.71 (2H, m, *o*-Phen ***3/6-H***), 7.78 (4H, d, *J* = 9.2 Hz, Isocyan ***3/5-H***), 8.19 (4H, d, *J* = 9.2 Hz, Isocyan ***2/6-H***), 8.83 (2H, bs, Urea N-***H***), 9.32 (2H, bs, Urea N-***H***).

N-(4-Nitrophenyl)-N'-octylurea, 36

This compound was made previously by Micich.[21] The observed melting point agrees with the literature value. A synthetic procedure derived from the work of Barbiou and co-workers[26] was used.

A solution of octylamine (0.32g, 2.5 mmol) in acetonitrile (10 mL) is added dropwise to a stirring solution of 4-nitrophenylisocyanate (0.30 g, 1.8 mmol) dissolved in acetonitrile (10 mL for 20 mL total). The reaction was heated to reflux and stirred for 5 hours. After cooling, the resulting yellow suspension was filtered and washed with dichloromethane (2 x 10 mL) before drying under high vacuum. The resulting yellow-orange solid is retained as the pure product (0.53 g, 97%, m.p. = 110°-113°C, Lit.[21] = 113°-114°C). ^{1}H-NMR (DMSO-d_6): 0.86 (3H, t, -C***H$_3$***), 1.25-1.28 (10H, *pseudo*-s, CH_2C***H$_2$***CH_2), 1.55 (2H, m, -C***H$_2$***CH_3), 3.47 (2H, bdt, *J* = 5.7 Hz, NHC***H$_2$***CH_2), 7.84 (2H,

d, *J* = 9.2 Hz, Isocyan ***3/5-H***), 8.16 (2H, d, *J* = 9.2 Hz, Isocyan ***2/6-H***), 8.38 (1H, bt, NHC(O)N***H***CH_2), 10.21 (1H, bs, ArN***H***C(O)NH). ^{13}C-MR (DMSO-d_6): 14.0 (CH_2***C***H_3), 22.1 (CH_2***C***H_2CH_3), 26.5 + 28.1 + 28.7 + 28.7 + 31.3 (CH_2***C***H_2CH_2), 43.9 (NH***C***H_2CH_2), 120.2 (Isocyan ***2/6-C***), 124.5 (Isocyan ***3/5-C***), 141.9 (Isocyan ***4-C***), 147.1 (Isocyan ***1-C***), 179.9 (NH***C***(O)NH).

***N*^{2},*N*^{6}*-bis*(glycine benzyl ester)pyridine-2,6-dicarboxamide, 41**

2,6-pyridinedicarbonyldichloride (3.24 g, 15.88 mmol) was dissolved in dichloromethane (40 mL) and was added dropwise to a stirring solution of the tosyl salt of glycine benzyl ester (12.81 g, 37.8 mmol) and triethylamine (20.0 mL, 143.6 mmol) in dichloromethane (60 mL additional for 100 mL total) held at 0°C in an ice bath. Upon completion of the addition, the system was returned to room temperature and stirred for 4 hours. The reaction was quenched with the addition of 100 mL of 5% (w/w) ammonium chloride in water. The organic layer was washed with 5% sodium carbonate (2 x 50 mL) and water (2 x 25 mL), dried over magnesium sulfate and filtered before removing solvent *in vacuo* to yield the crude product as a dark red oil. The crude was chromatographed over silica with 1:1 hexane to ethyl acetate → ethyl acetate → methanol to yield the pure product as a light orange oil (7.18 g, 73%, oil). ^{1}H-NMR ($CDCl_3$): 5.18 (4H, s, OC***H$_2$***Ar), 4.16 (4H, d, *J* = 5.9 Hz, NHC***H$_2$***C(O)), 7.29-7.37 (10H, m, Bn-***H***) 7.89 (1H, t, *J* = 7.8 Hz, Pyr ***4-H***), 8.16 (2H, d, *J* = 7.8 Hz, Pyr ***3/5-H***), 8.43 (2H, bt, *J* = 5.8 Hz, C(O)N***H***CH2). ^{13}C-NMR ($CDCl_3$): 41.7 (NH***C***H_2C(O)), 67.6 (O***C***H_2Ar), 125.4 (Pyr ***3/5-C***), 128.7 + 128.9 + 129.1 (Bn ***2/3/4/5/6-C***), 136.0 (Pyr ***4-C***), 139.4 (Bn ***1-C***), 148.5 (Pyr ***2/6-C***), 164.1 (Pyr-***C***OCH_2), 171.0 (CH_2***C***(O)O). FAB-MS: m/z calc for $[M+H]^+$ 462.1665, found: 462.1658.

1 Lehn, J.-M. *Supramolecular Chemistry*; Wiley-VCH: Weinheim, **1995**.

2 (a) Dietrich, B.; Fyles, T. M.; Lehn, J.-M.; Pease, L. G.; Fyles, D. L. *J. Chem. Soc., Chem. Commun.* **1978**, 934-936. (b) Dietrich, B.; Hosseini, M. W.; Lehn, J.-M.; Sessions, R. B.; *J. Am. Chem. Soc.* **1981**, *103*, 1282-1283.

3 (a) Bianchi, A.; Bowman-James, K.; Garcia-Espana, E., Ed. *Anion Receptor Chemistry*; Wiley-VCH: New York, **1997**. (b) Sessler, J. L.; Gale, P.; Cho, W.-S. *Anion Receptor Chemistry*; Royal Society of Chemistry: Cambridge, **2006**.

4 Camioli, S.; Gale, P. A.; Hursthouse, M. B.; Light, M. E. *Org. Biomol. Chem.* **2003**, *1*, 741-744.

5 (a) Collins, F. S. *Science* **1992**, *256*, 774-779. (b) Pajewski, R.; Garcia-Medina, R.; Brody, S. L.; Leevy, W. M.; Schlesinger, P. H.; Gokel, G. W. *Chem. Commun.* **2006**, 329-331.

6 (a) Läuger, P.; Stark, G. *Biochim. Biophys. Acta* **1970**, *211*, 458-466. (b) Behr, J.-P.; Kirch, M.; Lehn, J.-M. *J. Am. Chem. Soc.* **1985**, *107*, 241-246. (c) Tümmler, B.; Maass, G.; Vögtle, F.; Sieger, H.; Heimann, U.; Weber, E. *J. Am. Chem. Soc.* **1979**, *101*, 2588-2598.

7 Kavallieratos, K.; de Gala, S. R.; Austin, D. J.; Crabtree, R. H.*; J. Am. Chem. Soc.* **1997**, *119*, 2325-2326.

8 Gale, P. A.; *Acc. Chem. Res.* **2006**, *39*, 465.

9 Schlesinger, P. H.; Ferdani, R.; Liu, J.; Pajewska, J.; Pajewski, R.; Saito, M.; Shabany, H.; Gokel, G. W.; *J. Am. Chem. Soc.* **2002**, *147*, 1848-1849.

10 Dewar, M. J. S.; Zoebisch, E. G.; Healy, E. F.; Stewart, J. J. P.; *J. Am. Chem. Soc.* **1985**, *107*, 3902-3909.

11 Stewart, J.J.P.; *J. Comput. Chem.* **1989**, *10*, 209-220.

12 Rocha, G. B.; Freire, R. O.; Simas, A. M.; Stewart, J. J. P.; *J. Comput. Chem.* **2006**, *27* (10), 1101-1111.

13 Lee, C.; Yang, W.; Parr, R.G.; *Phys. Rev. B* **1988**, *37,* 785-789.

14 Becke, A. D. *J. Chem. Phys*. **1993**, *98*, 5648-5652.

15 Møller, C.; Plesset, M.S.; *Phys. Rev.* **1934**, *46*, 618-622.

16 Wu, Y.-D.; Wang, D.-F.; Sessler, J. L. *J. Org. Chem.* **2001**, *66*, 3739-3746.

17 Djedovic, N.; Ferdani, R.; Harder, E.; Pajewska, J.; Pajewski, R.; Weber, M.E.; Schlesinger, P.H.; Gokel, G.W.; *New. J. Chem*. **2005**, *29*, 291-305.

18 Gokel, G. W.; *Crown Ethers and Cryptands*; Royal Society of Chemistry: Cambridge, **1991**.

19 Fyles, T. M. *Can. J. Chem.* **1987**, *65*, 884-891.

20 (a) Anslyn, E. V.; Dougherty, D. A. *Modern Physical Organic Chemistry*; University Science Books: Sausalito, CA, **2006**; pp.14. (b) Cramer, C.J. *Essentials of Computational Chemistry*; John Wiley & Sons: New York, **2004** (2^{nd} ed., 2005); pp. 308-309.

21 Michich, T. J.; *J. Am. Oil Chem. Soc.* **1982**, *59*, 448-452.

22 Brooks, S. J.; Edwards, P. R.; Gale, P. A.; Light, M. E. *New J. Chem.* **2006**, *30*, 65-70.

23 Vandromme, L.; Monchaud, D.; Teulade-Fichou, M.-P. *Synlett* **2006**, 3423-3426.

24 Sheehan, J. C.; Hlavka, J. J. *J. Org. Chem.* **1956**, *21*, 439-441.

25 Carpino, L. A. *J. Am. Chem. Soc.* **1993**, *115*, 4397-4398.

26 Arnal-Herault, C.; Barbiou, M.; Petit, E.; Michau, M.; van der Lee, A. *New J. Chem.* **2005**, *29*, 1535-1539.

27 (a) Chmielewski, M J.; Jurczak, J.; *Chem. Eur. J.* **2006**, *12*, 7652. (b) Sessler, J. L.; Katayev, E.; Pantos, G. D.; Ustynyuk, Y. A. *Chem. Commun.* **2004**, 1276.

28 Greco, G. E.; Schrock, R. R. *Inorg. Chem.* **2001**, *40*, 3850-3860.

CHAPTER 3

Chloride Binding, Transport, and Channel Functionality of Dianilides of Dipicolinic Acid and Isophthalic Acid

Summary and Contributions to this Work

Dianilides of 2,6-pyridine dicarboxylic acid (dipicolinic acid), a family of compounds modeled in Chapter 2, were synthesized, characterized, and studied for carrier and channel activity in biological systems and biological model systems.

The first dipicolinic dianilides were made in a two-step synthetic process with overall yields of 40-70% and covered a range of substituent character from the electron-donating *para*-methyl substituent to the electron-withdrawing *para*-nitro. Initially, the compounds were investigated for chloride-binding activity in the context of chloride receptor utilization. ^{1}H NMR binding constants were derived in both polar DMSO-d_6 and non-polar CD_2Cl_2, with the titrations showing that chloride binding activity was present even in the polar milieu of DMSO-d_6. These results were correlated with the previous molecular modeling studies, as well as with competitive electrospray ionization-mass spectrometry studies performed by collaborators. Amide proton acidity and chloride binding strength both increase with increasing anilide substituent electron-withdrawing character.

A fluorescence-quenching assay was used to monitor chloride influx mediated by this series of compounds into phospholipid vesicles over time. These studies show that dianilides with more acidic protons attain approximately 80% of chloride transport, while

those with less acidic protons elicit approximately 20% of chloride transport. In both cases, the maximal chloride transport is achieved within 600 s of application.

Using the planar bilayer conductance technique, a collaborator, Saeedeh Negin, confirmed channel functionality, showing that one of the highly-active chloride transporters exhibits classic open-close behavior. A dipicolinic dianilide transporter monomer at its widest is approximately 15Å and is incapable of spanning the roughly 30Å of the hydrophobic region of the bilayer membrane. Thus, unable to work alone, the monomers must somehow aggregate to elicit the exhibited channel functionality. Using calculated geometries of stacked molecules, along with the concentration-dependent fluorescence profiles of the transporters, a stacking interaction was posited as the mechanism of channel formation.

I performed all calculations, syntheses and characterization, proton NMR binding studies, chloride transport studies, and optical spectroscopy detailed here. A fellow Gokel research group member, Alex Carasel of Washington University, along with Joseph Kramer and Dr. Rudolph Winter of the University of Missouri-St. Louis, performed the electrospray-ionization mass spectrometry studies. Saeedeh Negin, another member of the Gokel research group and a graduate student at the University of Missouri-St. Louis, performed the planar bilayer studies.

A portion of this work is included in a paper published in *Chemical Communications* in 2010. [1]

Introduction

The transport of anions is limited by the same constraints that are common to all

transport processes.[2] Similar to the demands of ion receptors, selectivity is dictated by a binding or complexation interaction. These complexation forces must be strong enough so that recognition can occur but, unlike receptors, weak enough to maintain a dynamic system in order to effect transport. Once this dynamic characteristic is established, a successful transporter may elicit functionality through one of two mechanisms—carrier or channel.

The carrier mechanism is often likened to a boat ferrying passengers back and forth across a river, while a channel is analogous to a bridge spanning the river, allowing the free and continuous passage of anyone wishing to cross. The metaphorical comparison extends to the rate of transport observed with the two separate mechanisms. An ion-carrier molecule first binds an ion on one side of the membrane barrier, diffuses across the membrane, and releases the ion on the far side of the barrier, repeating until equilibrium is established. Potassium transport by valinomycin, one of the best known ion carriers, reaches a level of 10^4 ions per second[3] while a functional pore such as gramicidin may conduct ions at a rate of 10^8 or even 10^9 ions per second.[4]

The roughly thousand-fold difference in transport rate is attributable to the rate-limiting diffusion process required of a carrier.[5] Since a protein channel, at the very least, spans the width of the hydrophobic bilayer domain, no diffusion is required for the channel to elicit transport activity.

However, the size of the channel is another issue, as only a certain number of ions can pass a confined space at any given time. Like a draw bridge, the channel may open and close at intervals, with no ions or current passing across the barrier when the channel is closed. If two channels are open simultaneously, the current will be double that of a single channel.

Many of the particulars of binding interactions for various anion hosts have been obtained from binding constant determinations and X-ray crystal structure studies.[6] While the latter can yield valuable insights into static binding arrangements, the geometries and stabilizing interactions of the solid-state may be altered in the presence of solvent molecules. Binding constants can gauge the strength of the interactions in solution, but ion transport is a dynamic process that cannot truly be verified without the use of dynamic tools in biological model systems.

Several techniques have been developed over the past decades to assess ion transport functionality. These methods range from the U-tube technique using a water-organic partitioning to gauge carrier functionality[7] to vesicle-based systems that monitor intra- or extravesicular ion concentration levels.[8]

The complexation of anions was explored nearly concurrently with the development of cation complexation by crown ethers.[9] Examples include studies reported by Simmons,[10] Schmidtchen,[11] Lehn,[12] de Mendoza,[13] Newcomb,[14] and others.[6] Great interest and activity in this area burgeoned only recently, however. By far, the most common complexation mode for such anions as fluoride and chloride has been hydrogen bonding, particularly by amides or protonated amines. Characterization of anion complexes has often been accomplished by X-ray crystallographic methods, although solution studies[15] and much more rarely, dynamic transport studies[16] have also been reported.

In 1999, Crabtree and coworkers reported a much emulated isophthalic acid dianilide anion host.[17] This isophthalic dianilide bound Br^- in the solid state and Cl^- in $CHCl_3$ solution. Since these first reports, the family of studied isophthalic acid dianilides has been greatly expanded by Gale and coworkers,[18] the receptor has been incorporated as an anion-binding subunit into ion-pair hosts,[19] while isophthalamides have been reported

that replace the aniline subunit with other aromatics such as aminoindoles[20] or with alkylamines.[16e] Numerous pyridine-2,6-dicarboxylic acid dianilides are known as well although most were prepared for study in a context other than anion complexation.[21] Dipicolinamides have been incorporated as subunits into structures such as Lehn's helices[22] and Anslyn's cyclophane receptor for trigonal planar anions.[23]

For a potential new chloride channel or carrier to transport its quarry, either must recognize and bind chloride or at least organize solvent molecules to indirectly bind the anion. For the most part, compounds that are thought to form channels or pores are of a length at sufficient to penetrate a single leaflet of a bilayer membrane, while most span both leaflets of the bilayer. An exception exists in the system developed by Sakai, Matile and coworkers that appears to stack dendritic folate rosettes within the bilayer.[24] Using planar bilayer conductance studies, transport of various cations was demonstrated for this assembly. The arrangement of multiple individual elements in an organized membrane-spanning stack seems unlikely from an energetic point of view but essential in the light of the experimental evidence. That transport occurs is unequivocal, so some type of organized assembly that mediates transport must form.

While several synthetic chloride ion channels have been prepared,[25] only one example of channel function by an isophthalamide, and none by a dipicolinamide, has appeared before completion of the current work.[1] Li *et al*. showed that a *bis*(α-aminoxyamide) derivative of isophthalic acid can form Cl^--conducting channels in phospholipid bilayers.[26] This is remarkable because the isophthalamides are small molecules that seem incapable of spanning a bilayer membrane and would require both aggregation and organization to function as a channel. Li *et al*. have offered no structural suggestion to account for pore formation.

Recent work published by Yang and co-workers[26b] has expanded upon the biological and biophysical effects of their chloride channels in living cells, but have yet to offer an explanation for the mechanism of chloride channel formation. The goals of this study of the dipicolinic dianilides were therefore twofold: to compare the chloride-binding abilities of these dipicolinamide compounds, and to determine the efficacy and mechanism of chloride transport activity.

Results and Discussion

Compounds prepared for the current study

Compounds **1-4, 7** and **8** were prepared as outlined in Scheme 3.1 by converting 2,6-pyridinedicarboxylic acid into the corresponding dichloride using $SOCl_2$, followed by coupling with two equivalents of amine in the presence of triethylamine.[27] Compounds **9-12** were prepared in one step from the commercially-available 2,6-pyridinedicarbonyl dichloride. The well known isophthalamide, **5**,[17b] was used as a control in the ion-binding studies. Previously-unstudied **6**[28] was prepared as a comparison to the deeply-investigated compound **4**. Both of these compounds were prepared in one step from commercially-available isophthaloyl dichloride. All products were characterized by ^{1}H- and ^{13}C-NMR and mass spectrometry. Structural data were as expected, and agreed with published values where available.

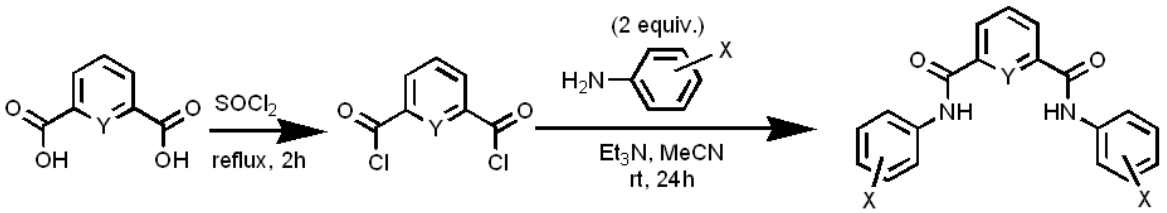

Compound	Y =	X =	Yield	m.p. (°C)
1	N:	4-CH_3	42%	223-224
2	N:	H	86%	277-278
3	N:	4-CN	34%	304-306
4	N:	4-NO_2	52%	> 330
5	CH	H	67%	291-294
6	CH	4-NO_2	40%	> 330
7	N:	4-$NHC(O)CH_3$	72%	195-196
8	N:	4-C(O)CH3	76%	>330
9	N:	3- CH_3	78%	211-214
10	N:	3-CN	37%	260-261
11	N:	3- CF_3	41%	288-291
12	N:	3-Cl	70%	245-247

Scheme 3.1. *Synthesis of compounds **1-12** with yields reported over one or two steps as appropriate. Compounds **5**, **6**, and **9-12** were made in one step from the appropriate commercially-available dicarbonyl chloride. Compounds **1-4** and **7-8** were made in two steps.*

Comparison of calculated and solid state structures

Much of the work with dipicolinamides and isophthalamides has focused on solid-state structures and anion binding. Accordingly, there are a number of crystal structures and binding constants of these hosts or closely related molecules available in the literature. To give us a sense of chloride-binding strength we can model these hosts and their complexes and calculate their associated energies (see the "Calculated gas-phase chloride-binding energies" section below), but the structures themselves yield insights into host and complex geometries outside of the solid-state and the influence of crystal-packing forces.

Comparison of solid-state and calculated gas-phase structures, therefore, seemed a necessary step in developing of our binding models.

Figure 3.1 shows calculated gas-phase structures for the related isophthalic and 2,6-dipicolinic acid dianilides. The geometries of the unbound host molecules are significantly different from one another. The dipicolinamide adopts a *syn-syn* conformation of side-arms, with amide protons directed inward, while the isophthalamide host adopts a *syn-anti* side-arm conformation with only one amide proton directed inward. All of the dipicolinic dianilide hosts were calculated to be planar in their unbound forms, maintaining an extended conjugated π-system while minimizing molecular dipoles. The pyridyl lone pair offers little or no steric hindrance of the type the 2-hydrogen does in isophthalic acid. While the solid-state structure of the 4-CH_3 isophthalamide (CSD:ATIQAV) reported by Nimmanpipug *et al*.[29] confirms this *syn-anti* conformation, the unsubstituted isophthalamide (CSD: PULHUZ)[27b] adopts the *syn-syn* conformation seen in the calculated gas-phase and experimental solid-state structures of dipicolinamides. This difference may be attributable to a more favorable crystal packing geometry arising from the *syn-syn* conformation.

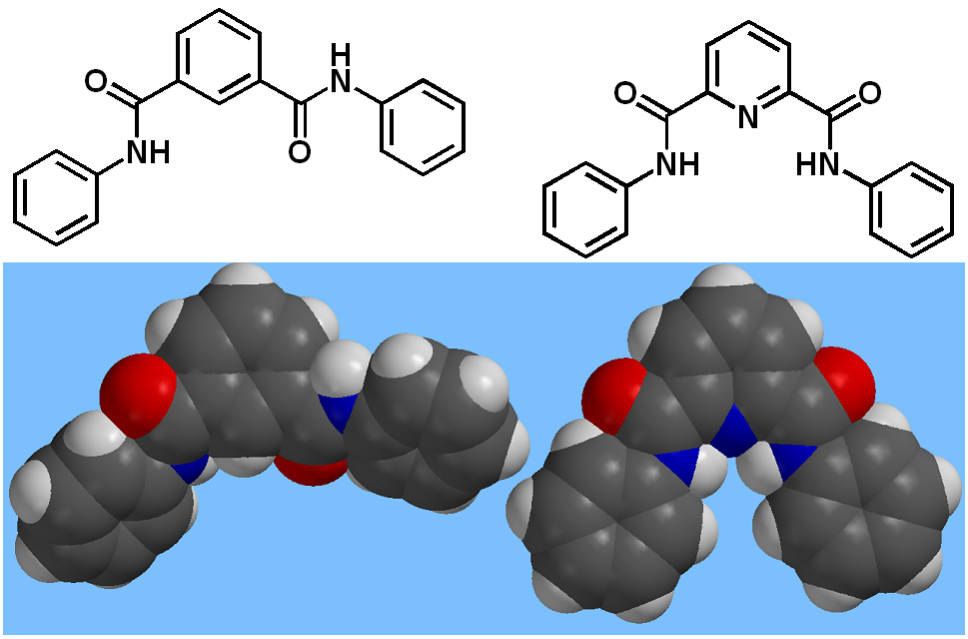

Figure 3.1. *Structural comparison of dianilides of isophthalic acid (left) and dipicolinic acid. Space filling models are of the DFT energy-minimized conformer of the unsubstituted dianilides*

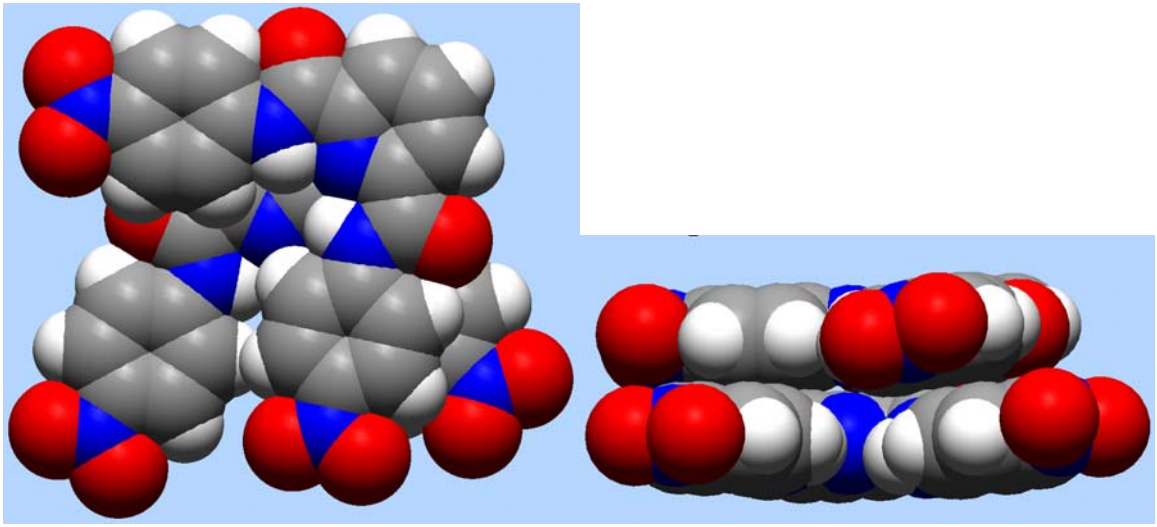

Figure 3.2.*Orthogonal depictions of the solid-state structure of the DMSO pseudo-polymorph of* ***4****, as determined by X-ray analysis.*

Solid-state structures of **1** (CSD: RABZUK),[30] **2** (CSD: PULJAH), [27b] and of **4** have previously been reported. The latter was crystallized by Yin *et al*.[31] from several different solvents but not in the presence of Cl^{-}. The study rather described the formation of *pseudo*-polymorphs in which **4** was solvated by DMSO (CSD: NEDSAR), DMF (CSD:

NEDRUK), or MeCN (CSD: NEDROE). In that work, the oxygen atom of a single DMSO molecule in **4**•DMSO was coordinated to the amide hydrogen atoms of the dipicolinamide. Along with the original report by Kavalleratos *et al.* of the isophthalamide•Br^- complex,[17b] structures have been reported by Gale and coworkers[32] of compounds related to **4**, namely N^1,N^3-*bis*(3-nitrophenyl)isophthalamide co-crystallized with Bu_4NPF_6 (CSD: QAGFAG) and N^1,N^3-*bis*(3,5-dinitrophenyl)isophthalamide with Bu_4NF (CSD: QAGFEK). The existence of these structures led to our desire to deduce a complex of the more biologically-relevant chloride ion with receptor **4**. Numerous attempts to co-crystallize **4** as a chloride complex (in DMSO with NBu_4Cl or NaCl) afforded only the uncomplexed receptor. Therefore, the previously published structure with DMSO (CSD: NEDSAR)[31] was compared with the calculated host **4** geometry. No direct solid-state comparison could be made with the calculated **4**• Cl^- complex.

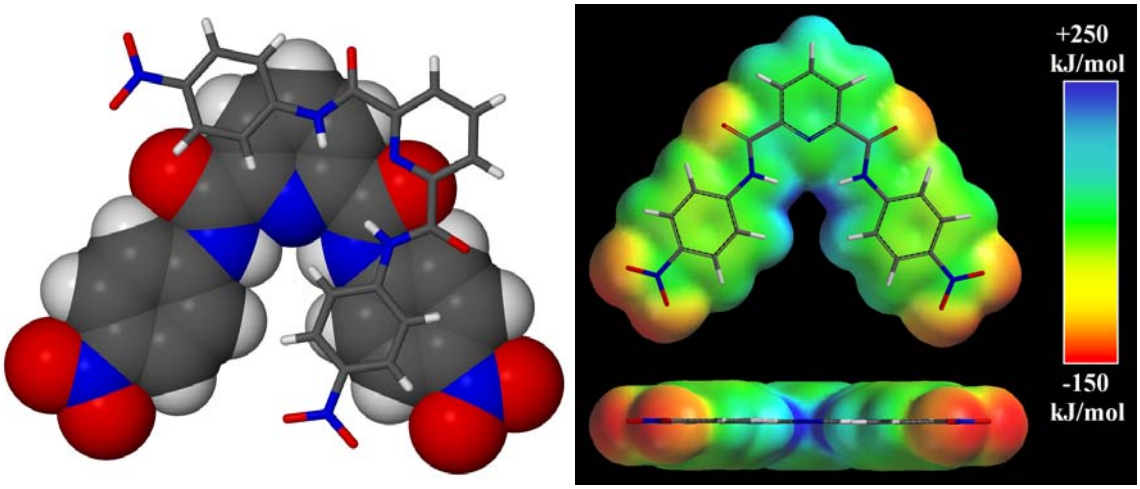

Figure 3.3. *(**A**) Solid state structure of **4** viewed from above, derived from the work of Yin* et al.[31] *The top molecule is represented as sticks and the lower in the space-filling metaphor. The two molecules are offset by ~60° and the interplanar distance is ~3.4 Å. (**B**) The gas-phase calculated electrostatic potential map (DFT/B3LYP/6-31G*) of receptor **4** with a capped-stick structural overlay depicting the underlying geometry. The more electronegative portions (amide and nitro oxygen atoms) are shown in red on the map with the electropositive chloride-binding cleft (amide protons) shown in darker blue. Regions of intermediate potential are shown spanning the spectrum from red to blue.*

Of particular interest is the orientation of the adjacent (*i.e*. stacked) molecules of **4**. The left panel of Figure 3.3, derived from the crystal structure of **4** by Yin *et al.*[31] shows that two receptors in the unit cell are stacked at van der Waals distances (~3.4 Å) and rotated by ~60^{o} with respect to one another. The DMSO molecules have been omitted for clarity. The right panel of Figure 3.3 shows the calculated electrostatic potential map for **4**. The color scale runs from blue (most positive) to red (most negative). Four areas that are relatively negative owing to the presence of electronegative oxygen are found at the termini of the inverted V and proximate to pyridine's 2- and 6-positions. The most electropositive regime is comprised of two amide protons surrounding the pyridyl nitrogen. A comparison of the calculated electron densities and the crystal structure (above) suggests that the orientation of the two molecules of **4** is determined primarily by the overlap of this most electropositive region with one of the electronegative carbonyl oxygen atoms.

However, in agreement with crystal structures of similar complexes,[17b,33] the geometry-optimized dipicolinic dianilide hosts adopt a non-planar conformation with rotation about the pyridine-CO bond to bind chloride and other anions above the pyridine plane. This rotation leads to an energetically unfavorable conformation that breaks the π-conjugated system. Thus, an energy trade-off is required to maximize chloride binding and minimize the energy of the complex. Calculations investigating this energetic relationship are detailed below.

Calculated gas-phase proton acidities, chloride-binding energies and complex geometries

As seen in the left panel of Figure 3.4, an analysis of electrostatic potential maps calculated at the density-functional level of theory reveal that the electrostatic potential at

the amide protons closely correlate (R^2 =0.881) to the Hammett σ_p and σ_m constants for the substituents modeled. The electrostatic potential is the measure of attraction or repulsion of a positive charge on an isodensity surface.[34] This potential is negative (energetically favored) at more electron rich regions of the molecule such as the oxygen atom of a ketone. Conversely, this potential is positive (energetically disfavored) at more electron poor regions of the molecule, such as the carbon atom of a ketone, or in the present case, the hydrogen atom of an amide.

This measure of acidity can also be correlated to experimentally-derived data. In the right panel of Figure 3.4, the calculated electrostatic potentials are plotted against the observed chemical shifts (ppm) of the amide protons of dipicolinic dianilides **1-4** and **7-10** in DMSO-d_6. The straight line fit to these data shows a good correlation (R^2 =0.897) between calculated and experimental values.

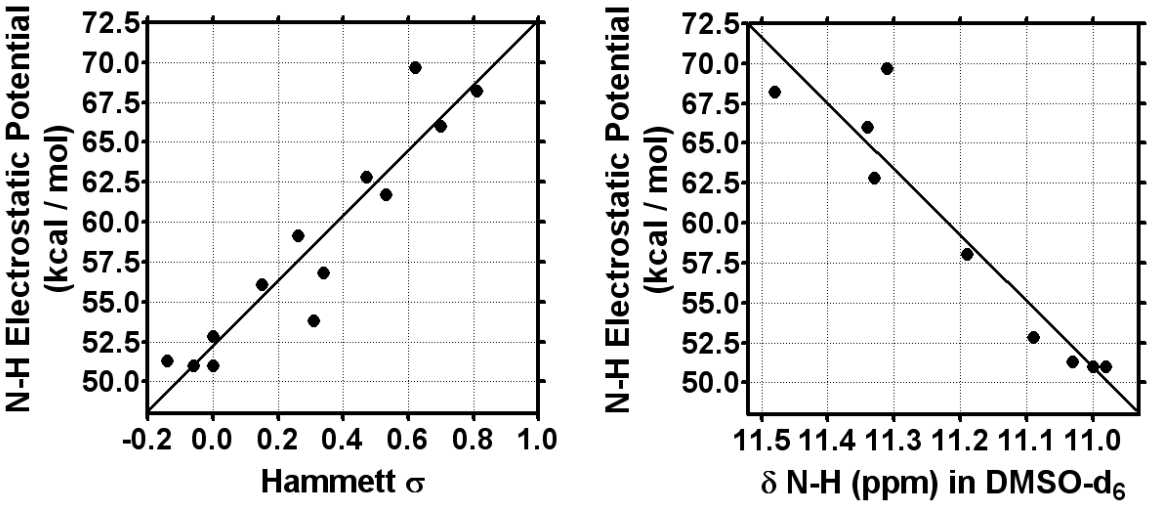

Figure 3.4: *(Left) Linear correlation (R^2 =0.881) between Hammett σ values[35] of dipicolinic dianilide substituents and the DFT-calculated electrostatic potential at the N-H amide protons. (Right) Linear correlation (R^2 =0.897) between the calculated N-H amide electrostatic potential and the observed chemical shift of the same moiety in DMSO-d_6.*

Binding energies were also calculated for chloride complexation by nine of the *para*-substituted dipicolinic dianilides at the density-functional level of theory (DFT-B3LYP)[36] using the 6-31G* basis set. Likewise, the calculated binding energies (1:1 host:Cl^-) obeyed a Hammett relationship,[37] with the strongest Cl^- binding calculated to occur when the 4,4'-substituents were most electron withdrawing. The plot shown in Figure 3.5 includes data for compounds **1**-**4** (black dots), which were examined experimentally as well as by computational methods. The calculated energies for those compounds that were not further studied are shown as gray, rather than black, points. The range of substituents and their Hammett σ_p constants[35] were CH_3, -0.14 (**1**); OCH_3, -0.12; H, 0.00 (2); F, 0.15; Br, 0.26; $COCH_3$, 0.47; CF_3, 0.53; CN, 0.70 (**3**); and NO_2, 0.81 (**4**). A graph of the calculated data produced a straight line having R^2 =0.96.

Two phenomena are observed with increasing substituent electron withdrawing nature: increased acidity (and H-bond donor ability) of the amide proton as well as better facilitation of rotation away from planarity and full conjugation with decreased electron density over the rotating π-bonds. The latter observation was investigated by measuring the energy penalty associated with rotating away from co-planarity in the unbound host.

The energetic effects of this non-planarity were studied in further computational detail for the *p*-NO_2 variant **4** by incrementally and symmetrically rotating the pyridine-CO bond in the unbound host, freezing the host geometry and optimizing the geometry of the complex with an unconstrained chloride guest, calculating energies at each step. With no rotation, there is no direct N-H···Cl^- interaction, so a rotation must occur to yield a binding event.

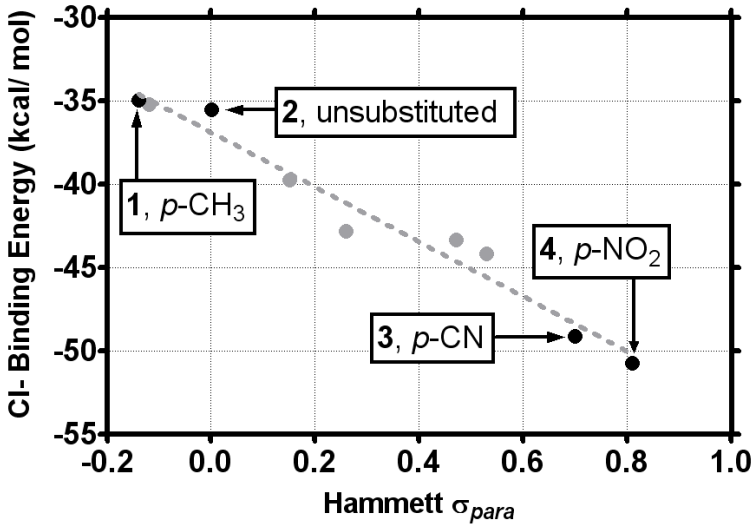

Figure 3.5: *DFT-calculated binding energies plotted against the Hammett* σ_{para}[35] *for each* para-*substituent modeled in the survey* (R^2 *=0.965).*

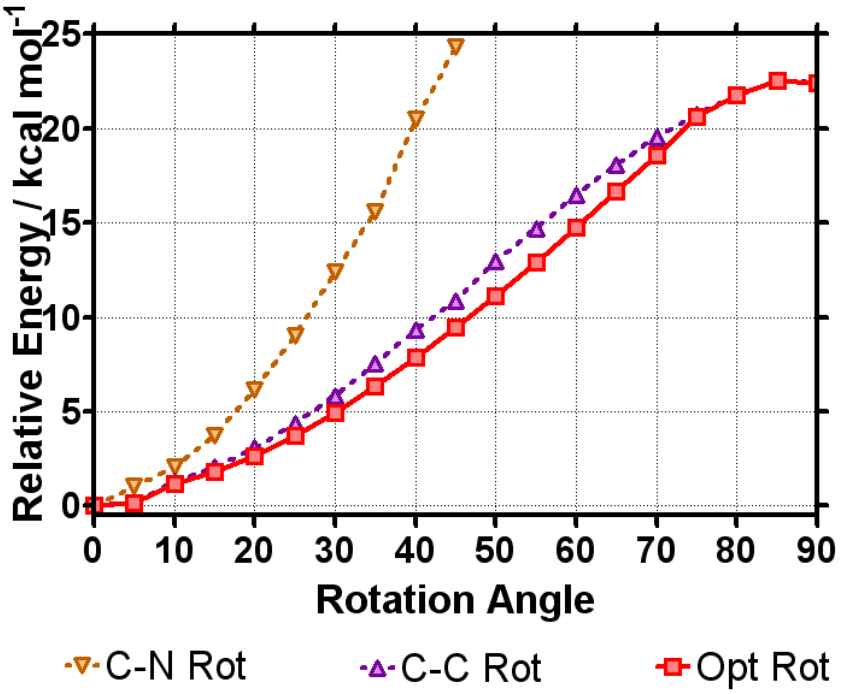

Figure 3.6 *Energy penalty of rotation away from the central arene plane in host* ***4*** *("Opt Rot"), compared to the rotation of each bond. The significantly higher energy penalty of rotating the C-N amide bond precludes any rotation of this angle above 11°.*

In rotating away from the central arene, two of the three interarene bonds (those proximal to the central arene) result in decreased steric repulsion and better geometry for

binding chloride by the amide hydrogen bond donors. However, rotation of the distal N_{amide}-C_{arene} bond has no effect on geometry of the amide proton moieties and yields little to no steric advantage. Thus, this distal bond is neglected in considering the rotation of the side-arm arenes to bind halides.

For compound **4**, the optimum bond angles for the two proximal bonds were established by calculating the DFT energy of the host resulting from each 5° rotation (up to 90°) of either the C_{arene}-C_{amide} (proximal) bond or the C_{amide}-N_{amide} (middle) bond. These energy distributions were fit to polynomial functions then related to predict the lowest energy combination of rotations for both bonds to yield a total 5° rotation from the central arene plane. The energy of each optimized rotation was then calculated and compared to the lowest energy conformation of 0° rotation. These results are graphically summarized in Figure 3.6.

After these host geometries were established at each 5° interval, the host was frozen and an unfrozen chloride anion was added to the structure before geometry optimization (essentially optimizing the host-guest interactive distances and geometry). The energy for each optimized complex was calculated by comparing the energy of the host and guest separately to the energy of the complex. Finally, the total relative energy was calculated by adding the energy advantage from complexation to the energy penalty from bond rotation.

As summarized graphically in the relative energy profile seen in Figure 3.7, this conformational change incurs an energetic penalty (squares) to the unbound host, but yields an optimized binding geometry. Whereas the energetic penalty is due primarily to the disruption of the conjugated π-system, steric interactions and the intramolecular pyridine nitrogen—amide hydrogen bonds play minor roles. The advantage of binding Cl^-

ion is greatest at between a 50° and 60° rotation (circles). Closer examination of the calculated geometries of the host-guest complexes show that with increased pyridine-CO bond rotation, the N-H···Cl^- angle gradually approaches 180° while simultaneously shortening the H···Cl^- distance until only one amide proton can bind the guest chloride ion. However, the summation of the rotation energy penalty and the binding energy advantage (diamonds) shows that a shallow energy trough between 20° and 40° yields the best combination of minimized π-system disruption and optimized N-H···Cl^- binding geometry.

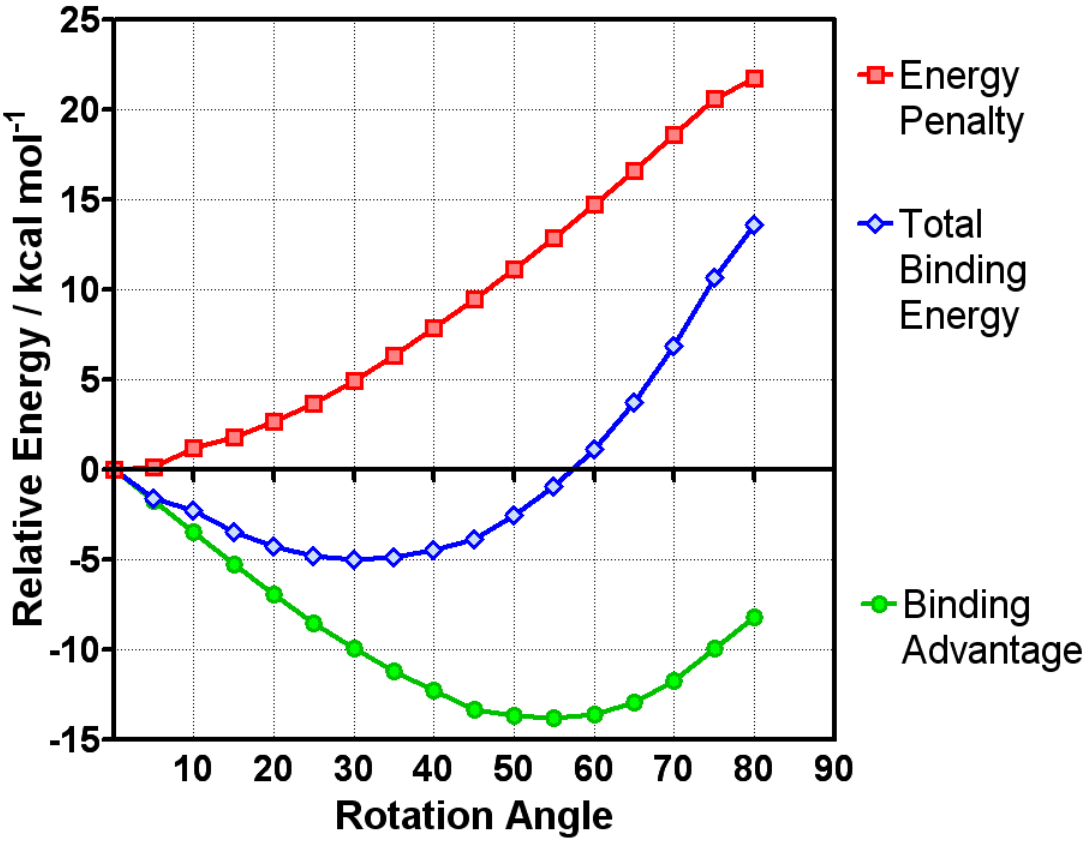

Figure 3.7 *Total relative energies for each conformation of host* ***4*** *rotated at 5° intervals from the central arene plane. The energy penalty arises from the breaking of planar conjugation in the π-system whereas the energy advantage is gained from more favorable halide complexation geometry. Note that the overall greatest energy advantage occurs at around 55°, but is negated by a higher energy penalty. As a result, the lowest total relative binding energy is present at around 30°.*

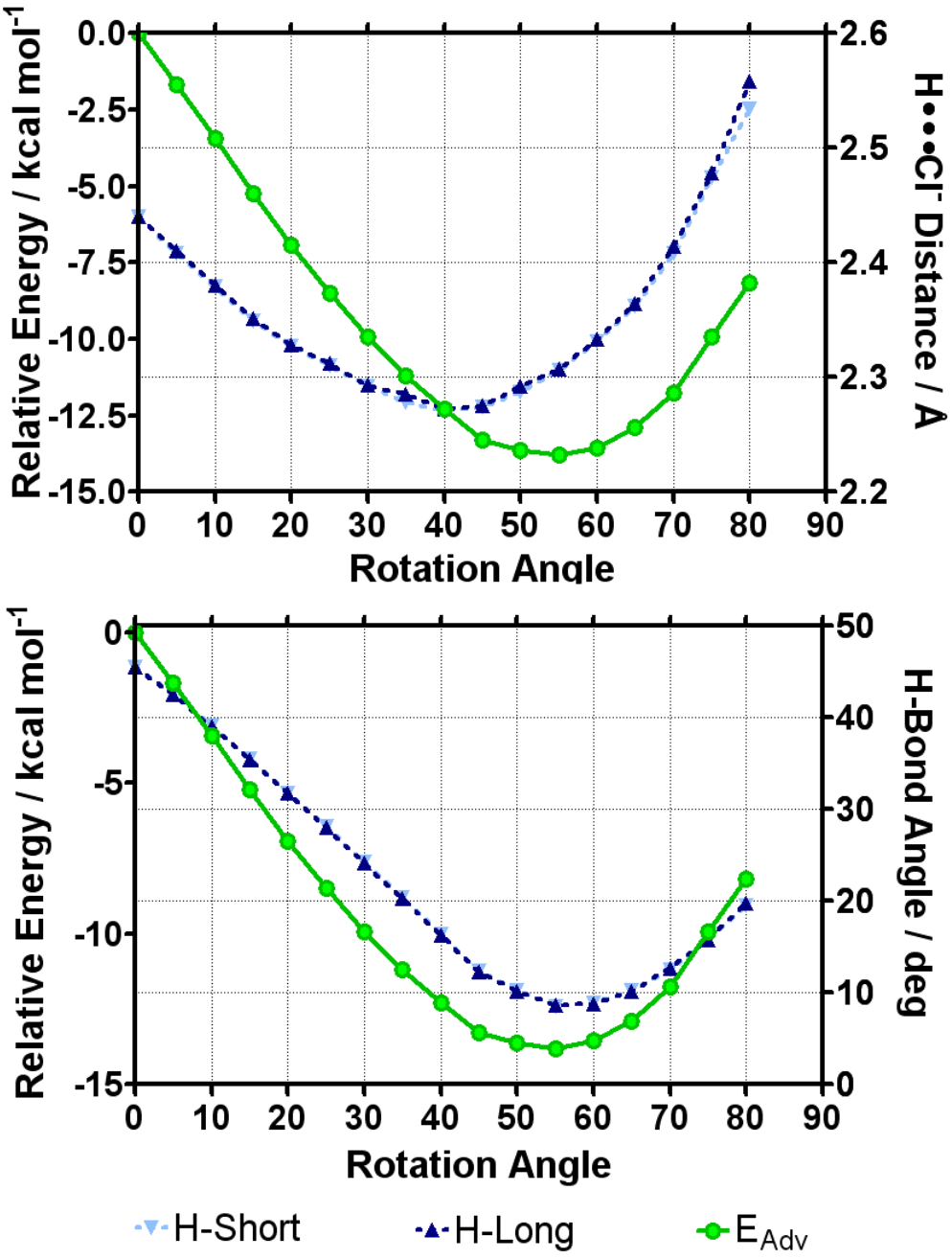

Figure 3.8 *Energy advantage for conformation of host* ***4*** *optimally rotated at 5° intervals from the central arene plane compared with the N-H…Cl⁻ bond distance (top panel) and N-H…Cl⁻ bond angle (bottom panel). The increased energy advantage appears more dependent on a lower angle of deviation from linearity in the H-bond, as the conformation with the smallest such angle corresponds to the conformation with the greatest energy advantage.*

While the energy penalty of rotation increases as rotation away from the central arene plane occurs, a large energy advantage is gained by creating a better complexation geometry through a closer N-H···Cl^- contact and a bond geometry closer to 0° through the three atoms. A survey of these interactions (Figure 3.8) in these optimized geometries show that, while close contact reaches its peak at 40° with a 2.27Å H-bond distance (upper panel), optimum bond geometry occurs at 55° with a bond angle of 8.6° (lower panel). The energy calculations show that indeed it is at this latter angle that the lowest energy is achieved (greatest energy advantage), predicting that bond geometry trumps contact distance when considering a difference of less than 0.1Å.

Binding constants determined by ^{1}H-NMR.

The chloride association constants (K_s) of compounds **1-6** and were determined by ^{1}H NMR spectroscopy in DMSO-d_6 and CD_2Cl_2 by titration of a solution of 10:1 Bu_4NCl guest to dianilide host into a solution of host only, monitoring the chemical shift change ($\Delta\delta$) of the amide N-H peak. In all cases, the amide N-H peak shifts downfield upon addition of chloride guest. Donation of electron density from the anionic guest to the unfilled N-H σ* antibonding orbitals leads to less N-H bonding character and a downfield shift. Job plots[38] were constructed for each determined binding constant and with a maximal N-H amide shift at χ_{Host}= 0.5, a 1:1 binding stoichiometry is indicated for all complexes. Using this 1:1 host to guest complex stoichiometry, constants were determined at [host] = 1.8 mM. The data points, derived from three independent titrations each, were fit to eq. 1,[17b] where "$[H]_0$" is the initial host concentration, "$[G]_0$" is the initial

guest concentration, "Δδ" is the change in chemical shift of the proton peak of interest, and "K_a" is the association constant.

$$\Delta\delta = \frac{\left([H]_0 + [G]_0 + \frac{1}{K_a} - \left(\sqrt{\left([H]_0 + [G]_0 + \frac{1}{K_a}\right)^2 - 4[G]_0[H]_0}\right)\right)\Delta\delta_{max}}{2[H]_0} \quad \textbf{(Eq. 1)}$$

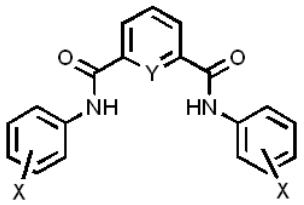

	Host		DMSO-d_6	CD_2Cl_2
No.	Y =	X =	K_s (M^{-1})[a]	K_s (M^{-1})[a]
1	N:	*p*-CH_3	NB[b]	63 ± 5
2	N:	H	26 ± 8	222 ± 14
3	N:	*p*-CN	50 ± 7	Insol[c]
4	N:	*p*-NO_2	44 ± 4	Insol[c]
5	CH	H	16 ± 1	NP[d]
6	CH	*p*-NO_2	46 ± 8	NP[d]

Table 3.1: *Chloride association constants K_s (M^{-1}) and maximal amide N-H shifts for 1-6. [a][Host] = 1.8 mM. Guest Cl^- (as NBu_4Cl) up to 18.0mM in DMSO-d_6 and CD_2Cl_2 at 298 K. [b]NB = no binding [c]Insol = the host is insoluble. [d]Not Performed.*

Direct comparison of binding by **1-4** was complicated by differing solubilities. Compounds **1** and **2** were soluble in CD_2Cl_2, but hosts **3** and **4**, were not. Although **1-4** were all soluble in DMSO-d_6, its polarity diminishes the binding to such an extent that an encompassing comparison could not be completed in that solvent. As shown in Table 3.1, the isophthalamide receptor **5** bound chloride significantly better than its dipicolinamide counterparts **1** and **2** in non-polar CD_2Cl_2. However, in the more polar milieu of DMSO-d_6, **3** and **4** bound chloride more strongly than **2** and far more strongly than **1**, which did not yield a fittable curve.

Job Plots and titration curves leading to the values seen in Table 3.1 can be seen in Appendix A of the dissertation.

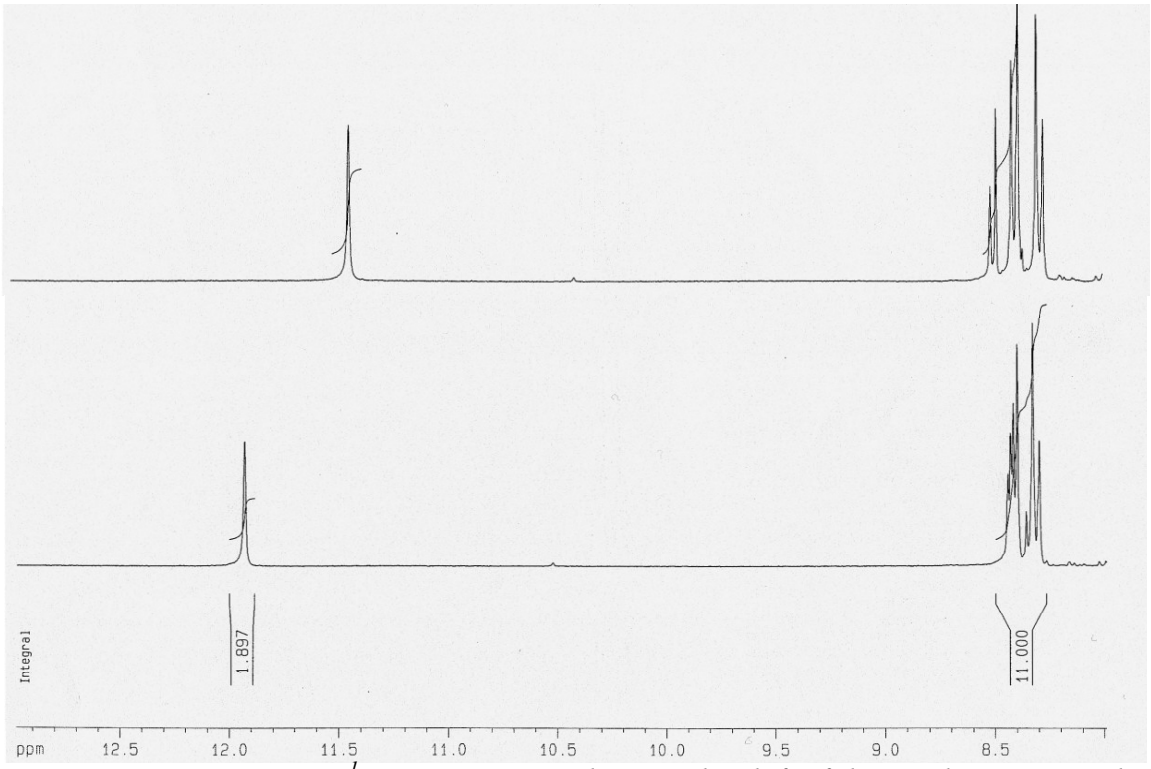

Figure 3.9: *Representative ^{1}H NMR spectra showing the shift of the amide proton peak of **4** upon addition of Bu_4NCl guest. The uppermost panel is the spectrum with no guest present (δ NH = 11.438 ppm). The lower panel is the spectrum acquired with 16 equivalents of guest present (δ NH = 11.933 ppm).*

Competitive chloride binding assayed by electrospray mass spectrometry

As noted above, our desire to directly compare binding in a single solvent was thwarted. Alex Carasel, Joseph Kramer, and Dr. Rudolph Winter thus undertook an electrospray ionization mass spectrometry (ESI-MS) study that would permit comparison of all of the compounds under similar conditions. Although mass spectrometry is a gas phase technique, the electrospray method gives data that are reflective of the solution at the time of ionization and limits or eliminates fragmentation.[39] The electrospray study of **1-6** was conducted in CH_3OH, using Bu_4NCl as the Cl^- source. Methanol is not identical to

either solvent system used in the ^{1}H NMR studies, but it permits a uniform evaluation for all of these receptors.

In each experiment, competing hosts were present in equimolar concentrations (50 μM) and chloride (as NBu_4Cl salt) was kept sub-stoichiometric (5 μM) so that competition for the guest would be obvious. The excess neutral host molecules are not observed in mass spectrometry unless they are complexed by Cl^-, so excess neutral host could be ignored. The ratios shown in Table 1 were calculated from the total integration of relevant M/z peaks for host-Cl^- adducts. Five charged adducts were observed at significant abundances: $[host^A \bullet Cl]^-$, $[host^B \bullet Cl]^-$, $[(host^A)_2 \bullet Cl]^-$, $[(host^B)_2 \bullet Cl]^-$, and $[host^A \bullet host^B \bullet Cl]^-$. In each case, the lowest relative abundance was normalized to 1. Errors are the calculated standard deviations of ratios from at least three independent experiments.

No.	**Host** Compound	**^{1}H NMR Ratio** *vs*. Control (**5**)[a]	**ESI-MS Ratio** *vs*. Control (**5**)[b]
1	Dipic *p*-CH_3	NB[c]	0.14 ± 0.01
2	Dipic unsub	1.63 ± 0.56	0.13 ± 0.02
3	Dipic *p*-CN	3.13 ± 0.44	3.27 ± 0.26
4	Dipic *p*-NO_2	2.75 ± 0.25	2.82 ± 0.07
5	Isophth unsub	**1.00**	**1.00**
6	Isophth *p*-NO_2	2.88 ± 0.51	5.44 ± 0.65

Table 3.2: *Comparison of ratio of chloride association constants to ESI-MS competitive ratio.* [a]*K_A (M^{-1}) in DMSO-d_6 at 298 K normalized to K_A of* **5** [b]*Competitive complexation with host* **5** *[Host] = 50 μM, 10% DMSO in MeOH.* [c]*NB = no binding.*

Table 3.2 shows that Cl^- binding by dipicolinamides **3** (*p*-CN) or **4** (*p*-NO_2) was similar. The K_S values obtained in DMSO-d_6 were 50.2 ± 7.3 and 44.0 ± 3.8, respectively with a ratio of binding constants equal to 1.14:1. The results of mass spectrometric

competition experiments for these two hosts were similar, with a ratio of 1.2:1 obtained by ESI-MS.

When **3** and **4** were used as hosts, they behaved in a relatively similar manner showing roughly equal abilities to bind chloride. When either **3** or **4** was compared with control **5**, each showed a much higher affinity for chloride. When all three compounds were mixed together, again **3** was slightly better than **4**, and both were much better than **5** with a ratio of the adducts of **3** to **4** (~1.2:1) preserved, even in the presence of **5**. When **3**, **4** or **5** were compared all at once with compounds **1** and **2**, no chloride adducts of **1** and **2** were observed, indicating very weak binding. These data are in accordance with the calculated binding energies and provides further support for our findings.

Chloride transport through vesicular phospholipid bilayers

Compounds **1-4** and **6** as well as the control **5** were tested for mediation of chloride influx into dioleoylphosphatidylcholine (DOPC) vesicles as indicated by quenching of a vesicle-entrapped chloride-sensitive fluorescent indicator.

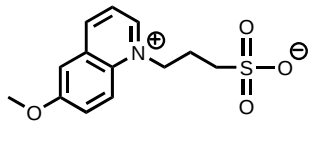

6-Methoxy-*N*-(3-sulfopropyl)quinolinium
SPQ

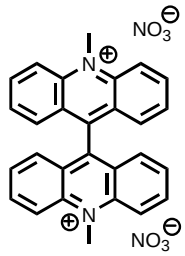

N,*N*'-Dimethyl-9,9'-bisacridinium nitrate
Lucigenin

Phospholipid vesicles were prepared as previously described[40] to obtain liposomes of a uniform 200 nm size. The indicator 6-methoxy-*N*-(3-sulfopropyl)quinolinium, or SPQ, has been used in previous chloride-transport studies using synthetic transporters[26a] but was unsuitable in the present context because the excitation and emission bands of **4** were

found to overlap with SPQ. While the fluorescence and absorption profiles of **4** were further investigated (see the "Absorbance and fluorescence of the *p*-NO_2 derivative" section), an alternative chloride-sensitive dye, *N*,*N'*-dimethyl-9,9'-bisacridinium nitrate, or lucigenin, was used. This fluorescent probe was also used in previous transport studies[40,41] and was found to be optimal with no excitation and emission overlap with any of the compounds to be tested. Lucigenin's use requires it to be trapped in the Cl^--free interior of vesicles where it fluoresces (λ_{exc} = 368 nm, λ_{em} = 506 nm). However, if an agent mediates the passage of Cl^- through the bilayer from the external buffer, the fluorescence intensity decreases due to collisional quenching. After a specified time, Triton X-100 is added to lyse the vesicles, and a baseline intensity for complete quenching is established. This baseline fluorescence intensity value is subtracted from the raw fluorescence intensity data and fractionally normalized to F_0, the unquenched fluorescence value. Thus, a value of 0.2 indicates 80% chloride influx.

Figure 3.10 compares Cl^- transport mediated across dioleoylphosphatidyl choline (DOPC) vesicles over the course of 600 s by **1**-**6** at a host concentration of 10 μM. Transport mediated by weak chloride binders **1** and **2**, was far less effective than transport mediated by the stronger binders **3** and **4**. In direct correlation with the molecular modeling predictions, the experimental binding constants and the mass spectrometry competition experiments, receptors **3, 4,** and **5** exhibited the highest levels of chloride-transport activity with ~80% chloride influx after 600 s, respectively. Receptors **1** and **2** and the control, **5**, showed diminished activity under the same conditions. The ideal chloride transporter (carrier or channel) needs to bind the ion strongly enough for recognition to occur but weak enough to maintain a dynamic system. While **1**, **2**, and **6**

can be considered to bind chloride too weakly in a polar environment, the stronger interactions observed for **3, 4** and **5** are weak enough that a dynamic system is maintained.

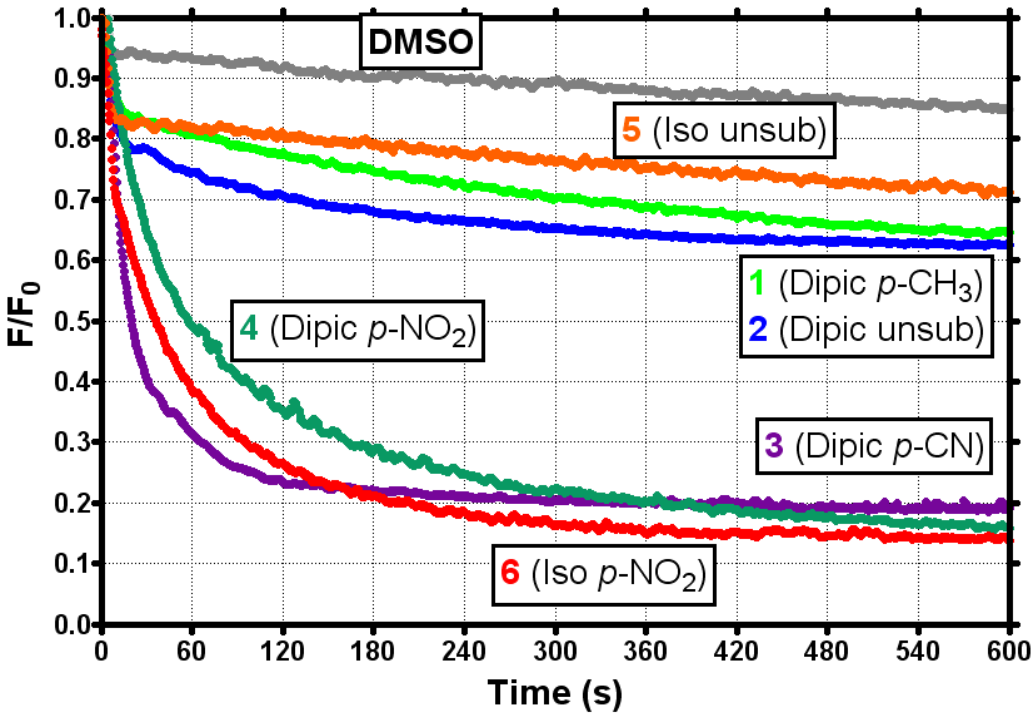

Figure 3.10. *Chloride transport through DOPC vesicles mediated by dianilides **1-4** and isopthalamides **5** and **6** as determined by lucigenin quenching.*[42] *All hosts are added as DMSO solutions with a final concentration of 10 μM. Maximal quenching is reached within 10 minutes in all cases. Data points for all replications are within 7% of the mean.*

The relatively rapid chloride influx rate, observed at low micromolar concentrations of receptors **3** and **4**, suggests that a channel mechanism versus a carrier mechanism is responsible for transport. Thus, a definitive test for channel activity, a planar-bilayer conductance study, was performed to confirm the theory (see the "Planar bilayer conductance" section).

While the lucigenin quenching experiment characterizes chloride transport activity at a given transporter concentration, variation of the transporter concentration can yield insights into the aggregation mechanics of transport activity. Systems using vesicles at a

fixed lipid concentration of 0.31 mM and transporter **4** in a range of concentrations from 20 μM to 50 nM were used to study the concentration dependence of chloride transport activity. The results, shown in Figure 3.11, can be used to construct a Hill Plot[43] (Figure 3.12) to determine the concentration dependence of the active channel or carrier.

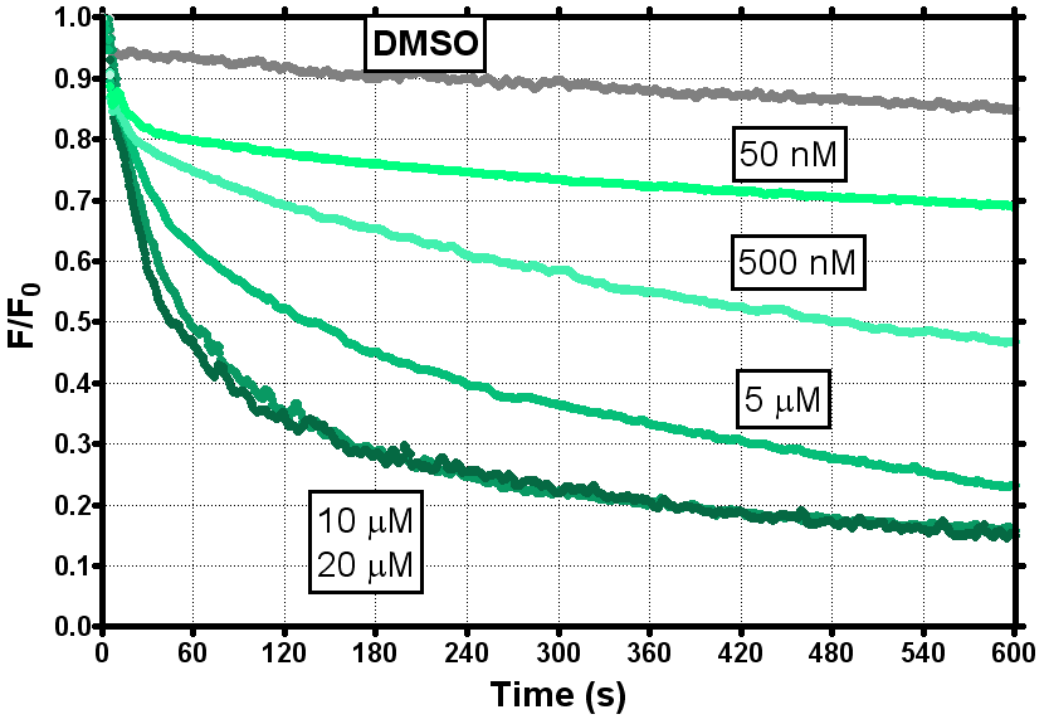

Figure 3.11. *The concentration dependence of the p-NO_2 dianilide,* ***4****, on chloride transport.*

Originally used in the study of enzyme kinetics, Hill plots are constructed to analyze the velocity of a measurable reaction or activity (in the present case, the initial rate of chloride transport) at different concentrations of enzyme or other agent (our chloride transporter). As these velocities are limited to some maximum value (Vmax) at a theoretically infinite concentration of activity-inducing agent, an asymptotic relationship is observed. The data are linearized by plotting on a log-log scale for the Hill plot with a line of slope 1 indicating a direct ideal linear relationship between activity-inducing agent and activity velocity. If the slope is greater than 1, a cooperative relationship is indicated, as

the activity velocity increases at a greater than linear rate. If the slope is less than 1, a competitive or non-cooperative relationship is indicated, as the presence of more activity-inducing agent leads to less activity per molecule of agent present.

$$\mathbf{F_0/F = 1 + K_D\,[Q]} \quad \textbf{(Eq. 2)}$$

Application of the Stern-Volmer equation (Eq. 2)[44] to the acquired fluorescence data yielded chloride concentrations for each half-second recording. Using the literature Stern-Volmer quenching constant for lucigenin with chloride (K_D = 390 M^{-1}) and the experimentally-determined F_0/F values (the inverse of the dependent values in Figure 3.10), intracellular chloride concentrations are derived for each observed point in time, ultimately yielding ion transport velocities.

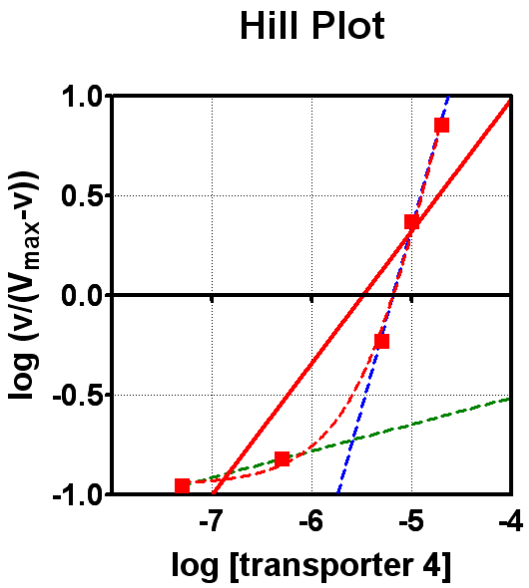

Figure 3.12. *A Hill plot derived from the data presented in Fig. 3.11 (variation of **[4]**) via application of the Stern-Volmer equation.*

Examination of the Hill plot seen in Figure 3.12 shows that when plotted on a log-log scale to linearize the transport velocity and concentration terms, a non-linear dependence is observed. If all 5 points were fit to a single straight line (full line), as

normally done with a Hill plot, a slope of 0.66 is the result, indicating a competitive concentration dependence. However, if the plot were divided into two parts, the first with the two lowest concentrations and the second with the three remaining, two straight lines result: the first half yielding a slope of 0.13 and the second a slope of 1.98, indicating a competitive and cooperative concentration dependence, respectively. Presumably, these two straight lines are a simplification, and a non-linear relationship is truly at work (dashed curve), but with only 5 data points, this is an assumption at this time.

However, while measuring membrane potential polarization rate in their work, Yang and co-workers also observe a non-linear concentration dependence with their α-aminooxyacid class of synthetic chloride transporters.[26b] These observations with other synthetic chloride transporters incapable of spanning a membrane may complement our own studies with similar compounds. The non-linear dependence may be based on a minimum concentration threshold that is required for these transporters to function as anion channels. At any given concentration, both the carrier and channel mechanism may be active, with more channel character present at higher concentrations.

Planar bilayer conductance

The planar bilayer conductance technique[45] (KCl, 0.45 M, pH 7.0, soybean asolectin) was used to probe for channel formation in experiments conducted by Saeedeh Negin. In this experiment, two potassium chloride buffer solutions (0.45M, pH 7.0) were separated by a phospholipid membrane (asolectin from soybean) painted onto a ~200 μm^2 aperture between the two buffer chambers. To this system, a DMSO solution of **4** was added to one buffer chamber (the cis chamber) yielding a final transporter concentration of 7 μM. A potential difference was then applied across the membrane and channel activity was observed by measurement of current in the trans buffer chamber. The distinctive open-

close behavior exhibited by the current measurements seen in Figure 3.13 is indicative of functional ion-channel formation in the bilayer.[45]

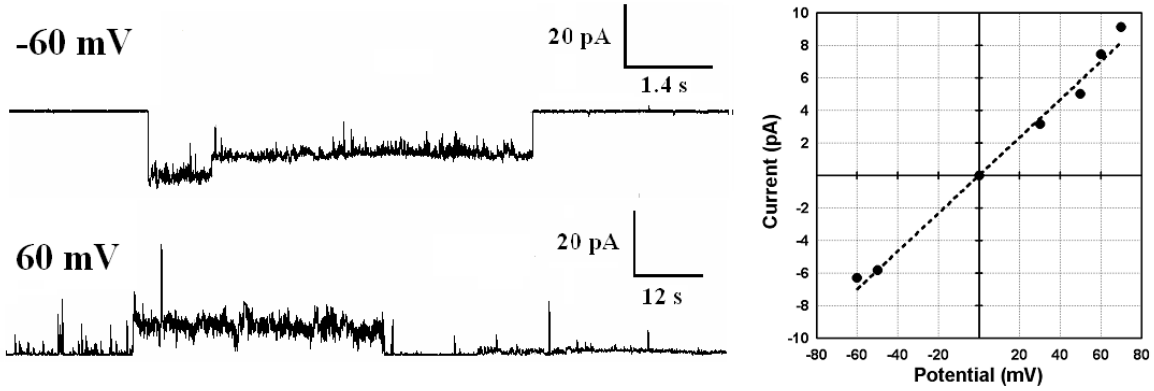

Figure 3.13. *(Left) The current observed at applied voltages of (Top) -60 mV and (Bottom) 60 mV elicited upon the addition of transporter* ***4*** *at 7 μM. (Right) I-V Plot, a plot of observed current vs. applied potential correlating to the major conductance state.*

When the experiments were conducted for durations as long as 3 hours after addition of transporter, a variety of "open" currents could be observed at the same voltage, meaning that multiple conductance states are present. Data for the major conductance state are shown in Figure 3.13. The conductance value determined from the graph in Figure 3.13 is 117 pS.

To estimate the pore diameter of this channel, Hille's equation[45] can be applied to the derived conductance value. A channel exhibiting a conductance of 117 pS in a 35Å thick bilayer has an estimated pore diameter of ~8Å. An unsolvated Cl^- ion with a 1.81Å van der Waals radius[46] ion would need a pore with a diameter of at least 3.6Å to transport ions and the calculated structures of the dipicolinamides show a binding cavity in a single receptor with a diameter of ~4.1Å. A pore of ~8Å would mean that at least two of these receptors would form the sides of the pore with their binding cavities directed inward. Unsolvated Cl^- has a diameter of ~3.6 Å[47] but fully aquated Cl^- is estimated to be ~6.5 Å,[48] which is close to the calculated pore size

Unsubstituted dipicolinamide, **2**, and isophthalamide, **5**, were also tested for channel functionality using the same procedure shown above. Tests were run for durations of 3 hours showing no conductance behavior for either of these compounds at a final transporter concentration of 7 μM.

Absorbance and fluorescence of the *p*-NO_2 derivative, 4

The formation of a transmembrane channel by **4** would require aggregation of the monomers. One possibility is that the triarenes self-assemble, stacking upon one another. To span the 30-35 Å insulator regime of a bilayer membrane, 8-10 molecules would be required to stack at the van der Waals distance of 3.4 Å. Such an arrangement would have a significant entropic cost in the bilayer but this type of stacking is apparent in the solid state structure.[31]

Inferential evidence for stacking was obtained from fluorescence studies. Nitro-substituted dipicolinamide (**4**) showed no fluorescence emission when excited at various wavelengths in DMSO solution. Compound **4** is soluble in DMSO but not in water. However, when a small amount of a concentrated DMSO solution of **4** is added to an aqueous solution (1% DMSO v/v), fluorescence is readily observed. The emission spectra seen in Figure 3.14 are from an excitation wavelength of 280 nm. The only peak observed at a receptor concentration of 50 μM was the peak having a maximum near 400 nm as seen in Figure 3.14. In subsequent studies varying the excitation wavelength (270-600 nm in 10 nm increments), it was determined that an excitation wavelength of 280 nm yielded the highest fluorescence intensity.

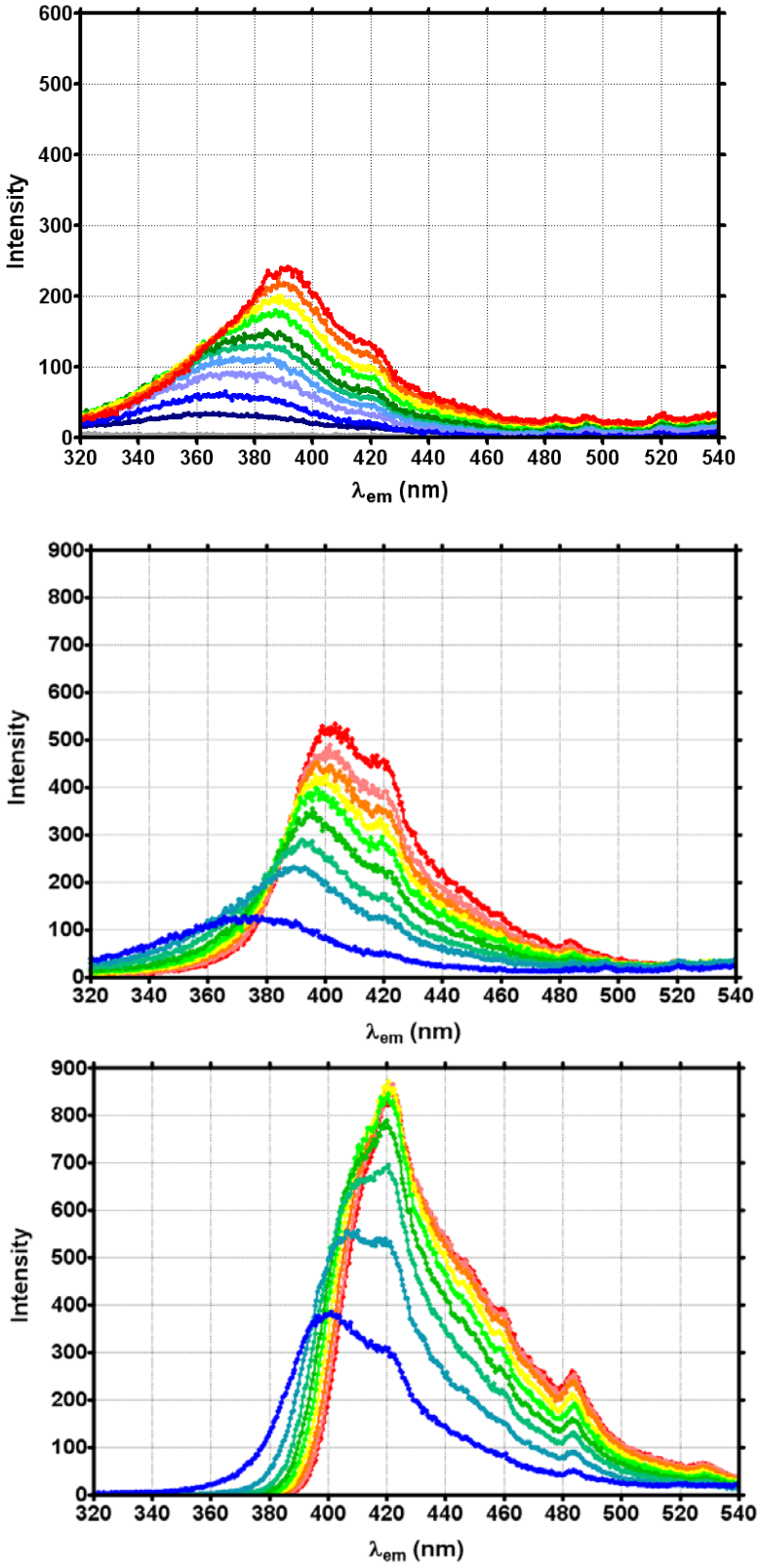

Figure 3.14. *Fluorescence in* ***4*** *in 1% DMSO / water at (Top) 2-20 μM host concentration (Center) 10-90 μM concentration and (Bottom) 10-90 μM with 0.17mM DOPC vesicles.*

The top panel of Figure 3.14 shows the fluorescence spectra obtained for **4** in 1% DMSO/H_2O over a concentration range of 2-20 μM, in 2 μM increments—concentrations relevant to eliciting chloride transport, from concentration dependence studies (Figure 3.11). Molecules of **4** aggregate under these conditions and the fluorescent emission is presumably due to the formation of excimers. Similar, but more intense spectra, were obtained at concentrations between 10-90 μM as shown in the middle panel of Figure 3.14. As the concentration increases, the peak intensifies while shifting from its first observable maximum of 372 nm to a final maximum of 403 nm.

The maximal emission intensity fluorescence excitation wavelength of 280 nm does not correlate with the maximal absorbance wavelength of 338 nm seen in Figure 3.15 (uppermost curve). However, when the same DMSO-water solution of **4** is titrated with a 10 equivalent mixture of NaCl and host **4**, an isosbestic point in the absorbance spectrum is observed near the aforementioned 280 nm wavelength.

The lower absorption at the longer wavelength (338 nm) upon addition of NaCl is most likely attributable to the disruption of the extended conjugated π-system of the planar receptor molecule. We speculate that with increasing NaCl concentration, the receptor anilide side-arms rotate to bind its Cl^- guest as seen previously in the calculated structure (Figure 3.15). While the absorbance at this higher wavelength is decreased, the absorbance intensity at 275 nm (and presumably lower wavelengths) increases proportionally. Unfortunately, the absorbance spectra below 275 nm is not able to be obtained due to instrumental limitations.

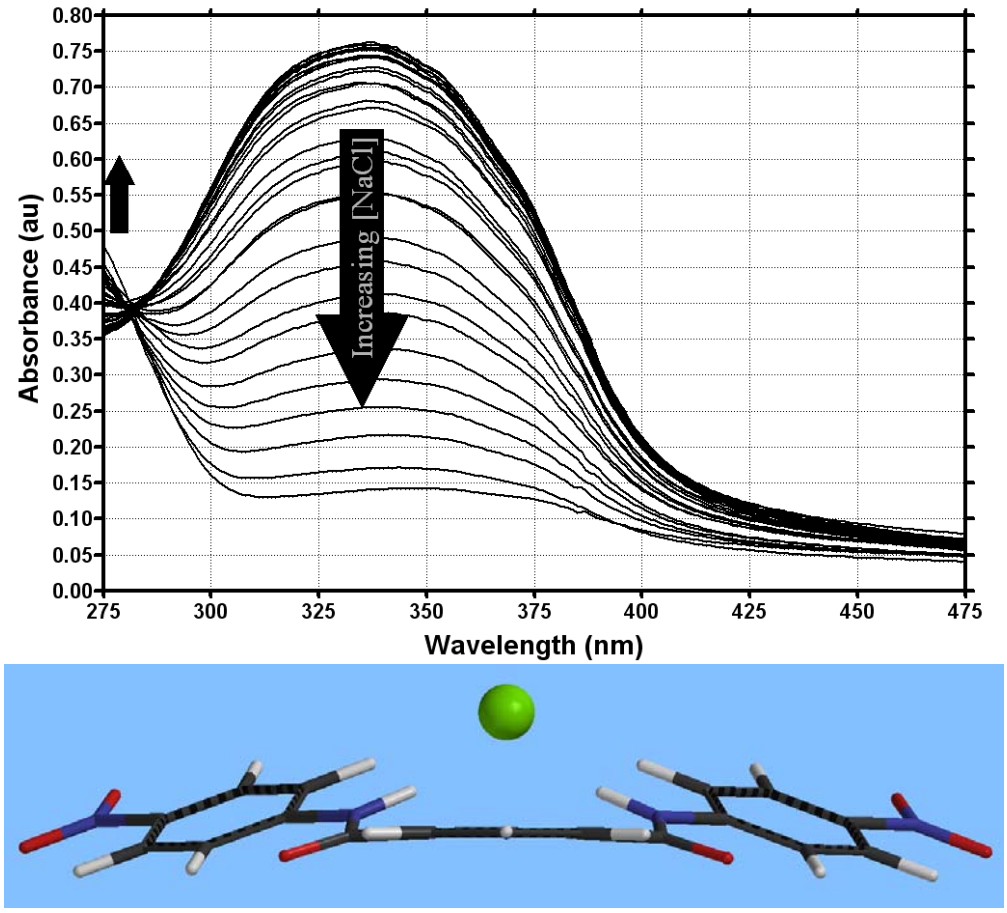

Figure 3.15. (Top) *Absorbance of host **4** in 1% DMSO/water at a concentration of 10mM. NaCl guest is added (0-70 equivalents) resulting in the lowered absorbance at the maximum at 338 nm and an increased absorbance for a species with a maximum below 275nm. (Bottom) The calculated geometry of a **4**·Cl⁻ complex. Presumably, the species absorbing at 338 nm is the planar host whereas the species absorbing at the shorter wavelength is a combination of the three discrete π-systems present in the complex.*

Conclusions

In this study, we have examined the chloride binding properties of hosts **1**-**4** using three independent methods—DFT-level gas-phase calculations, ^{1}H NMR binding constants in both polar DMSO- d_6 and non-polar CD_2Cl_2, and electrospray ionization MS in a polar methanol microenvironment. We observed the same general trend across the methods: the more electron-withdrawing *p*-NO_2 and *p*-CN dianilides (**4** and **3**, respectively) were better chloride binders than the unsubstituted and electron-donating *p*-CH_3 dianilides (**2** and **1**,

respectively). **3** and **4**'s chloride binding capabilities—even in polar environments—proved a boon in their ability to transport chloride across phospholipid membranes, an ability not displayed by their more weakly-binding counterparts. The rapid chloride transport evidenced by **4** was explored more fully, with its open-close behavior exhibited in planar-bilayer conductance tests proving its channel functionality.

The observation that compound **4** exhibits channel behavior may be surprising at first glance. While each molecule of **4** is at most 14.5 Å in length, the hydrophobic insulator regime of a bilayer is ~35 Å thick[49] meaning **4** and members of its structural family, **1-3**, would not span the bilayer in a typical unimolecular fashion as would natural ion channels[45] or many designed single-molecule synthetic channels.[50] Certainly, other channel modalities could be in play, such as a two-molecule, two-leaflet modality seen in gramicidin.[51] However, a vertically-stacked assembly of receptors such as seen in cartoon form in Figure 3.16 could be another possible mechanism. The formation of channels from stacked monomers has been proposed previously for cyclic peptides,[52] rosettes,[53] cyclic ureas[54] and for oligoamide macrocycles[55] even though π-π stacking has been the subject of controversy in recent years.[56]

Observation of the fluorescence of **4** in water leads us to believe that this stack is rapidly organized in the aqueous milieu by exclusion of water contacts at the hydrophobic arene faces. Examination of calculated gas-phase models argues that this pre-organized stack most likely organizes solvent water, binding the electronegative water oxygen. The exposed water protons in turn weakly (but dynamically) complex chloride in a water-and-ion filled pore.

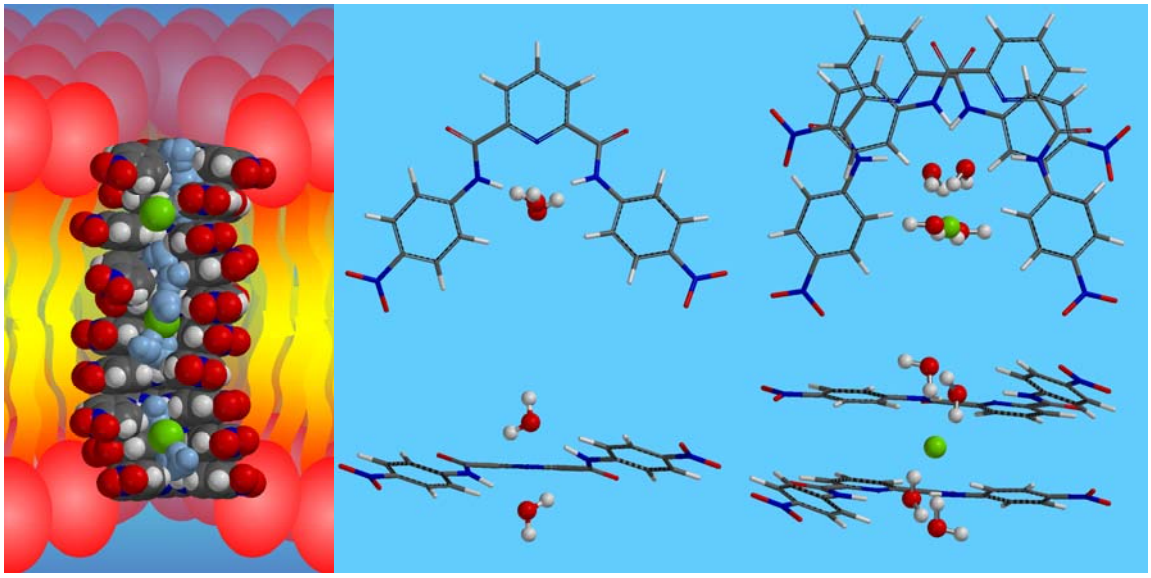

Figure 3.16. *(Left) CPK representation of a stack of molecules of receptor* ***4*** *with solvent water molecules in light blue and chloride ions in green. (Center) DFT-calculated structure of host* ***4*** *with two molecules of water. (Right) DFT-calculated structure of host* ***4*** *with four molecules of water and a chloride anion.*

The multiple conductance states seen in the planar-bilayer tests show that different channel sizes are possible. While a minimum of 8 to 10 transporters would be needed for a single stack, further lateral aggregation over time might form larger and larger pores leading to those of the size seen in the planar-bilayer conductance studies. The formation of channels by such small molecular species may have implications in the design of drugs, especially since the aminoxyisophthalamides described recently alter biological function.[26b]

The regulation of ion concentrations—maintaining gradients across ion-impermeable cellular membranes—is of paramount importance in living, functioning cells. Disruption of the regulation of the chloride ion gradient is implicated in the symptomatic manifestation of cystic fibrosis in humans,[57] a result of malfunctioning natural chloride channels.[58] While many commercially successful synthetic therapeutics are small, limiting the costs in an industrial process, they are tailored to interact with naturally-occurring

proteins, rarely affecting activity on their own. However, compounds such as transporters **3** and **4** that are small and easily made while independently eliciting a desired effect at a low concentration, could find many potential therapeutic uses.

Experimental

General.

All NMR spectra were recorded on a Bruker Avance 300 spectrometer at 300 MHz and all chemical shifts are reported in ppm (δ), calibrated to literature values for internal solvent in reference to TMS with integrated intensity (X H) and multiplicity (b = broad, s = singlet, d = doublet, t = triplet, q = quartet, bs = broad singlet, m = multiplet, etc.), and coupling constants in Hz. ^{13}C-NMR spectra were obtained at 75.4 MHz and calibrated to literature values for chemical shift in reference to TMS. Melting points were determined on a Thomas Hoover apparatus in open capillaries and are uncorrected. Reagents were the best (non-LC) grade commercially available and were distilled, recrystallized or used without further purification, as appropriate. CH_2Cl_2 was distilled from calcium hydride. Unless otherwise stated, all chemicals were purchased from Sigma-Aldrich (St. Louis, MO).

All Mass Spectrometry experiments were performed on a JEOL MStation, JMS-700, double focusing high-resolution instrument using either the fast-atom bombardment ionization technique in the positive ion detection mode at high resolution (FAB-MS), or the elesctrospray ionization technique in the negative ion detection mode (ESI-MS). All fluorescence spectra and fluorescence quenching data were recorded on a Perkin Elmer LS50B Luminescence Spectrometer. Planar bilayer conductance measurements were

performed with a Warner bilayer clamp instrument. All UV-Vis absorbance spectra were recorded on a Beckman Coulter DU 7400 Spectrophotometer. Calculations were run using the Spartan 2006 software package on a Dell Dimension DXP061 desktop with a 2.40GHz Intel® Core™2 Processor and 2.00GB of RAM.

Gas-phase binding calculations and molecular modeling.

A lowest energy conformation search was performed using the Monte-Carlo simulated annealing method with the MMFF force field to yield the ten lowest energy conformers for each host and complex modeled. The geometry of each of these conformers were optimized by the density-functional B3LYP method using the 6-31G* basis set. Single-point energy calculations were performed using the same method and basis set to determine the overall lowest energy conformer (LEC). Binding energies were determined for each complex by adding the calculated energies of the host LEC and guest then subtracting the calculated energy of the complex LEC.

Synthesis and characterization of hosts 1-12, general procedure.

All solvents used were freshly distilled and all reactions were performed under an inert nitrogen or argon atmosphere and vapor condenser.

The commercially-available diacid (2,6-pyridinedicarboxylic acid for **1-4**, isophthalic acid for **5** and **6**) was dissolved in acetonitrile or dichloromethane (~2mmol in 7mL) and added drop-wise to a stirring solution containing an excess of the appropriate aniline in the same solvent (~7mmol in 7mL in acetonitrile or dichloromethane) and triethylamine (3mL) held at 0°C in an ice bath. After addition, the mixture was returned to room temperature and then heated to reflux for 3h. After returning to room temperature,

the solid was filtered and washed with the reaction solvent (acetonitrile or dichloromethane) and dried under high vacuum yielding the final product.

2,6-Pyridinedicarbonyl dichloride

The commercially-available diacid, 2,6-pyridinedicarboxylic acid (4.00 g) was added to a stirring mixture of thionyl chloride (15.80 g) and 1,4-dioxane (24.0 mL) and heated to reflux for 4 hours. After cooling to room temperature, solvent, excess thionyl chloride and hydrogen chloride gas are removed *in vacuo*. Toluene (2 x 50 mL) is added to the concentrate and removed *in vacuo* to ensure removal of all traces of thionyl chloride and hydrogen chloride. The resulting brown solid (4.88 g, quantitative, mp = 61-62 °C, lit.[59] = 60 °C) is used immediately in the subsequent amide coupling reactions. ^{1}H-NMR (CD_2Cl_2): 8.18 (1H, dd, J_1 = 8.3 Hz, J_2 = 7.3 Hz Ar ***4-H***), 8.38 (2H, d, J = 7.8 Hz Ar ***3/5-H***), ^{13}C-NMR (CD_2Cl_2): 129.9, 140.3, 149.7, 169.8.

***N*^{2},*N*^{6}-*bis*(4-Methylphenyl)pyridine-2,6-dicarboxamide, 1**

This compound was made and reported previously. Spectral data and the melting point match literature values.[60] 2,6-Pyridinedicarbonyl dichloride (0.44 g, 2.2 mmol) was dissolved in acetonitrile (5.0 mL) and was added dropwise to a stirring solution of 4-toluidine (0.82 g, 7.7 mmol) and triethylamine (5.0 mL, 35.9 mmol) in acetonitrile (7.0 mL additional for 12.0 mL total) held at 0°C in an ice bath. Upon completion of the addition, the system was returned to room temperature and stirred for 24 hours. The resulting white suspension is filtered, resuspended with acetonitrile (2 x 25 mL) and diethyl ether (1 x 10 mL) and refiltered after each suspension before drying under high vacuum. The resulting white solid is retained as the pure product (0.33 g, 42%, mp = 223-224 °C, lit.[60] = 224 °C).

^{1}H-NMR (DMSO-d_6): 2.32 (6H, s, Anil-C***H*****$_3$**), 7.25 (4H, d, *J* = 8.4 Hz, Anil ***3/5-H***), 7.80 (4H, d, *J* = 8.4 Hz, Anil ***2/6-H***) 8.29 (1H, dd, J_1 = 8.6 Hz, J_2 = 6.9 Hz, Pyr ***4-H***), 8.38 (2H, d, *J* = 7.6 Hz Pyr ***3/5-H***), 11.03 (2H, s, C(O)N***H***-Anil). ^{13}C-NMR (DMSO-d_6): 20.6 (Anil-***C***H_3), 121.2, (Anil ***2/6-C***), 125.2 (Pyr ***3/5-C***), 129.1 (Anil ***3/5-C***), 133.4 (Anil ***4-C***), 140.2 (Pyr ***4-C***), 135.6 (Anil ***1-C***), 149.0 (Pyr ***2/6-C***), 161.5 (Pyr-***C***(O)NH). ESI-MS: m/z calc for $[M+Cl]^-$ 380, found: 380.

***N*^{2},*N*^{6}-*bis*(Phenyl)pyridine-2,6-dicarboxamide, 2**

This compound was made previously. Spectral data and the melting point match literature values.[61] 2,6-pyridinedicarbonyl dichloride (0.42 g, 2.1 mmol) was dissolved in acetonitrile (5.0 mL) and was added dropwise to a stirring solution of aniline (0.63 g, 6.8 mmol) and triethylamine (5.0 mL, 35.9 mmol) in acetonitrile (7.0 mL additional for 12.0 mL total) held at 0°C in an ice bath. Upon completion of the addition, the system was returned to room temperature and stirred for 24 hours. The resulting white suspension is filtered, resuspended with acetonitrile (2 x 25 mL) and diethyl ether (1 x 10 mL) and refiltered after each suspension before drying under high vacuum. The resulting white solid is retained as the pure product (0.56 g, 86%, mp = 277-278 °C, lit.[61] = 278 °C). ^{1}H-NMR (DMSO-d_6): 7.19 (2H, t, *J* = 7.4 Hz, Anil ***4-H***), 7.45 (4H, t, *J* = 7.9 Hz, Anil ***3/5-H***), 7.94 (4H, d, *J* = 7.5 Hz, Anil ***2/6-H***) 8.31 (1H, dd, J_1 = 8.7 Hz, J_2 = 6.6 Hz, Pyr ***4-H***), 8.41 (2H, d, *J* = 7.7 Hz Pyr ***3/5-H***), 11.09 (2H, s, C(O)N***H***-Anil). ^{13}C-NMR (DMSO-d_6): 121.1 (Anil ***2/6-C***), 124.4 (Anil ***4-C***), 125.3 (Pyr ***3/5-C***), 128.8 (Anil ***3/5-C***), 138.1 (Anil ***1-C***), 140.0 (Pyr ***4-C***), 148.9 (Pyr ***2/6-C***), 161.7 (Pyr-***C***(O)NH). ESI-MS: m/z calc for $[M-H]^-$ 316, found: 316; m/z calc for $[M+Cl]^-$ 352, found: 352.

***N*^{2},*N*^{6}-*bis*(4-Cyanophenyl)pyridine-2,6-dicarboxamide, 3**

This compound was made previously. Spectral data and the melting point match literature values.[62] 2,6-Pyridinedicarbonyl dichloride (0.42 g, 2.1 mmol) was dissolved in acetonitrile (5.0 mL) and was added dropwise to a stirring solution of 4-aminobenzonitrile (0.82g, 6.9 mmol) and triethylamine (5.0 mL, 35.9 mmol) in acetonitrile (7.0 mL additional for 12.0 mL total) held at 0 °C in an ice bath. Upon completion of the addition, the system was returned to room temperature and stirred for 24 hours. The resulting white suspension is filtered, resuspended with acetonitrile (2 x 25 mL) and diethyl ether (1 x 10 mL) and refiltered after each suspension before drying under high vacuum. The purified product is isolated as a white powder (0.26 g, 34%, mp = 304-306 °C, lit.[62] = 304-306 °C). ^{1}H-NMR (DMSO-d_6): 7.92 (4H, d, *J* = 8.6 Hz, Anil ***3/5-H***), 8.19 (4H, d, *J* = 8.6 Hz, Anil ***2/6-H***) 8.34 (1H, t, *J* = 7.7 Hz, Pyr ***4-H***), 8.43 (2H, d, *J* = 8.0Hz Pyr ***3/5-H***), 11.34 (2H, s, C(O)N***H***-Anil). ^{13}C-NMR (DMSO-d_6): 106.0 (Anil ***4-C***), 119.0 (Anil-***C***N), 120.7 (Anil ***2/6-C***), 126.0 (Pyr ***3/5-C***), 133.2 (Anil ***3/5-C***), 140.3 (Pyr ***4-C***), 142.3 (Anil ***1-C***), 148.3 (Pyr ***2/6-C***), 162.1 (Pyr-***C***(O)NH). ESI-MS: m/z calc for $[M-H]^-$ 366, found: 366; m/z calc for $[M+Cl]^-$ 402, found: 402.

***N*^{2},*N*^{6}-*bis*(4-nitrophenyl)pyridine-2,6-dicarboxamide, 4**

This compound was made previously. No spectral data were recorded, but the melting point matches the literature value.[63] 2,6-Pyridinedicarbonyl dichloride (1.65 g, 8.1 mmol) was dissolved in acetonitrile (20.0 mL) and was added dropwise to a stirring solution of 4-Nitroaniline (2.44g, 16.2 mmol) and triethylamine (9.0 mL, 64.6 mmol) in acetonitrile (25.0 mL additional for 45.0 mL total) held at 0 °C in an ice bath. Upon completion of the addition, the system was returned to room temperature and stirred for 24

hours. The resulting yellow-brown suspension is filtered, resuspended with acetonitrile (2 x 25 mL) and diethyl ether (1 x 10 mL) and refiltered after each suspension before drying under high vacuum. The resulting yellow-beige solid is retained as the pure product (1.70 g, 52%, mp > 330°C, lit.[63] >300°C). ^{1}H-NMR (DMSO-d_6): 8.13 (4H, d, J = 9.2 Hz, Anil ***3/5-H***), 8.24 (4H, d, J = 9.6 Hz, Anil ***2/6-H***) 8.23 (1H, [buried], Pyr ***4-H***), 8.34 (2H, d, J = 8.1 Hz Pyr ***3/5-H***), 11.48 (2H, s, C(O)N***H***-Anil).^{13}C-NMR (DMSO-d_6): 120.4, (Anil ***2/6-C***), 124.9 (Anil ***3/5-C***), 126.2 (Pyr ***3/5-C***), 140.4 (Pyr ***4-C***), 143.0 + 144.3 (Anil ***4-C*** +Anil ***1-C***), 148.2 (Pyr ***2/6-C***), 162.3 (Pyr-***C***(O)NH). ESI-MS: m/z calc for $[M-H]^-$ 406, found: 406; m/z calc for $[M+Cl]^-$ 442, found: 442.

***N*^{1},*N*^{3}-*bis*(phenyl)isophthalamide, 5**

This compound was made previously. Spectral data[64] and the melting point[65] match literature values. Isophthaloyl chloride (0.498 g, 2.45 mmol) was dissolved in acetonitrile (7.0 mL) and was added dropwise to a stirring solution of aniline (0.780 g, 8.38 mmol) and triethylamine (5.0 mL, 35.9 mmol) in acetonitrile (8.0 mL additional for 15.0 mL total) held at 0 °C in an ice bath. Upon completion of the addition, the system was returned to room temperature and stirred for 24 hours. The resulting white suspension is filtered, resuspended with acetonitrile (2 x 25 mL) and diethyl ether (1 x 10 mL) and refiltered after each suspension before drying under high vacuum. The resulting white solid is retained as the pure product (0.521 g, 67%, mp = 280-281 °C, lit.[65] = 279-281 °C). ^{1}H-NMR (DMSO-d_6): 7.13 (2H, t, J = 7.3 Hz, Anil ***4-H***), 7.38 (4H, t, J = 7.2 Hz, Anil ***3/5-H***), 7.70 (1H, t, J = 7.7 Hz, Isophth ***5-H***), 7.81 (4H, d, J = 8.1 Hz, Anil ***2/6-H***), 8.15 (2H, d, J = 7.7 Hz, Isophth ***4/6-H***), 8.54 (1H, s, Isophth ***2-H***), 10.44 (2H, s, C(O)N***H***-Anil). ^{13}C-NMR (DMSO-d_6): 120.4 (Anil ***2/6-C***), 123.8 (Anil ***4-C***), 127.0 (Isophth ***2-C***), 128.4

(Isophth ***5-C***), 128.7 (Anil ***3/5-C***), 130.6 (Isophth ***4/6-C***), 135.2 (Isophth ***1/3-C***), 139.1 (Anil ***1-C***), 165.1 (Isophth-***C***(O)NH). FAB-MS: m/z calc for $[M+H]^+$ 317.1290, found: 317.1285. ESI-MS: m/z calc for $[M+Cl]^-$ 351 found: 351.

N[1],*N*[3]-*bis*(4-Nitrophenyl)isophthalamide, 6

This compound was made previously. No spectral data were recorded, but the melting point agrees with the literature value.[66] Isophthaloyl chloride (1.199 g, 5.90 mmol) was dissolved in acetonitrile (15.0 mL) and was added dropwise to a stirring solution of 4-nitroaniline (2.478g, 17.94 mmol) and triethylamine (10.0 mL, 71.7 mmol) in acetonitrile (15.0 mL additional for 30.0 mL total) held at 0 °C in an ice bath. Upon completion of the addition, the system was returned to room temperature and stirred for 24 hours. The resulting brown-yellow suspension is filtered, resuspended with acetonitrile (2 x 25 mL) and diethyl ether (1 x 10 mL) and refiltered after each suspension before drying under high vacuum. A yellow-beige solid is isolated as the pure product (0.951 g, 40%, mp > 330°C, lit.[66] = 377°C). ^{1}H-NMR (DMSO-d_6): 7.76 (1H, t, *J* = 7.4 Hz, Isophth ***5-H***), 8.13 (4H, t, *J* = 7.7 Hz, Anil ***2/6-H***), 8.22 (2H, d, *J* = 7.8 Hz, Isophth ***4/6-H***), 8.30 (4H, d, *J* = 7.7 Hz, Anil ***3/5-H***), 8.67 (1H, s, Isophth ***2-H***), 11.22 (2H, s, C(O)N***H***-Anil). ^{13}C-NMR (DMSO-d_6): 119.9 (Anil ***2/6-C***), 124.8 (Anil ***3/5-C***), 127.8 (Isophth ***5-C***), 131.5 (Isophth ***4/6-C***), 134.4 (Isophth ***1/3-C***), 139.5 (Isophth ***2-C***), 142.6 (Anil ***4-C***), 145.3 (Anil ***1-C***), 165.6 (Isophth-***C***(O)NH). ESI-MS: m/z calc for $[M-H]^-$ 405, found: 405; m/z calc for $[M+Cl]^-$ 441, found: 441.

N[2],*N*[6]-*bis*(4-Aminoacetylphenyl)pyridine-2,6-dicarboxamide, 7

2,6-Pyridinedicarbonyl dichloride (1.10 g, 5.4 mmol) was dissolved in acetonitrile

(20.0 mL) and was added dropwise to a stirring solution of 4-aminoacetanilide (1.78 g, 11.9 mmol) and triethylamine (9.0 mL, 64.6 mmol) in acetonitrile (20.0 mL additional for 40.0 mL total) held at 0 °C in an ice bath. Upon completion of the addition, the system was returned to room temperature and stirred for 24 hours. The resulting white suspension is filtered, resuspended with acetonitrile (2 x 25 mL) and diethyl ether (1 x 10 mL) and refiltered after each suspension before drying under high vacuum. The resulting off-white (slight pink) solid is retained as the pure product (1.77 g, 76%, mp > 330°C). ^{1}H-NMR (DMSO-d_6): 1.49 (6H, s, C(O)C***H*****$_3$**), 7.08 (4H, d, *J* = 8.9 Hz, Anil ***3/5-H***), 7.25 (4H, d, *J* = 8.9 Hz, Anil ***2/6-H***) 7.73 (1H, dd, J_1 = 8.8 Hz, J_2 = 6.5 Hz, Pyr ***4-H***), 7.82 (2H, d, *J* = 7.5 Hz Pyr ***3/5-H***), 10.00 (2H, s, Anil-N***H***C(O)), 10.98 (2H, s, C(O)N***H***).^{13}C-NMR (DMSO-d_6): 24.0 (CO***C***H_3), 119.3 (Anil ***3/5-C***), 121.8, (Anil ***2/6-C***), 125.2 (Pyr ***3/5-C***), 133.08 (Anil ***1-C***), 136.0 (Anil ***4-C***), 139.4 (Pyr ***4-C***), 148.9 (Pyr ***2/6-C***), 161.5 (Pyr-***C***(O)NH-), 168.2 (NH***C***(O)CH_3). FAB-MS: m/z calc for $[M+H]^+$ 462.1665, found: 462.1658.

***N*^{2},*N*^{6}-*bis*(4-Acetylphenyl)pyridine-2,6-dicarboxamide, 8**

2,6-Pyridinedicarbonyl dichloride (0.44 g, 2.2 mmol) was dissolved in acetonitrile (7.0 mL) and was added dropwise to a stirring solution of 4'-aminoacetophenone (0.92 g, 6.8 mmol) and triethylamine (5.0 mL, 35.9 mmol) in acetonitrile (5.0 mL additional for 12.0 mL total) held at 0 °C in an ice bath. Upon completion of the addition, the system was returned to room temperature and stirred for 24 hours. The resulting white suspension is filtered, resuspended and refiltered with acetonitrile (2 x 25 mL) and diethyl ether (1 x 10 mL) before drying under high vacuum. The resulting off-white (slight pink) solid is retained as the pure product (0.63 g, 72%, mp = 195-196 °C). ^{1}H-NMR (DMSO-d_6): 2.58 (6H, s, C(O)C***H*****$_3$**), 8.04 (4H, d, *J* = 8.7 Hz, Anil ***3/5-H***), 8.18 (4H, d, *J* = 8.7 Hz, Anil ***2/6-***

H) 8.32 (1H, dd, J_1 = 8.6 Hz, J_2 = 6.7 Hz, Pyr ***4-H***), 8.42 (2H, d, J = 7.2 Hz Pyr ***3/5-H***), 11.33 (2H, s, C(O)N***H***).^{13}C-NMR (DMSO-d_6): 26.5 (CO***C***H_3), 120.2, (Anil ***2/6-C***), 125.8 (Pyr ***3/5-C***), 129.3 (Anil ***3/5-C***), 132.5 (Anil ***4-C***), 140.1 (Pyr ***4-C***), 142.6 (Anil ***1-C***), 148.7 (Pyr ***2/6-C***), 162.2 (Pyr-***C***(O)NH), 196.7 (Anil-***C***(O)CH_3). FAB-MS: m/z calc for $[M+H]^+$ 402.1454, found: 402.1448.

***N*^{2},*N*^{6}-*bis*(3-Methylphenyl)pyridine-2,6-dicarboxamide, 9**

2,6-Pyridinedicarbonyl dichloride (0.426 g, 2.09 mmol) was dissolved in dichloromethane (6.0 mL) and was added dropwise to a stirring solution of 3-toluidine (0.743 g, 6.93 mmol) and triethylamine (5.0 mL, 35.9 mmol) in dichloromethane (9.0 mL additional for 15.0 mL total) held at 0 °C in an ice bath. Upon completion of the addition, the system was returned to room temperature and stirred for 24 hours. The resulting white suspension is filtered, resuspended with acetonitrile (2 x 25 mL) and diethyl ether (1 x 10 mL) and refiltered after each suspension before drying under high vacuum. The resulting white solid is retained as the pure product (0.564 g, 78%, mp = 211-214 °C). ^{1}H-NMR (DMSO-d_6): 2.34 (6H, s, Anil-C***H*****$_3$**), 7.01 (2H, d, J = 7.5 Hz, Anil ***4-H***), 7.31 (2H, t, J = 7.8 Hz, Anil ***5-H***), 7.65 (2H, d, J = 8.0 Hz, Anil ***6-H***), 7.70 (2H, s, Anil ***2-H***), 8.28 (1H, dd, J_1 = 8.7 Hz, J_2 = 6.6 Hz, Pyr ***4-H***), 8.37 (2H, d, J = 7.3 Hz Pyr ***3/5-H***), 11.00 (2H, s, C(O)N***H***-Anil). ^{13}C-NMR (DMSO-d_6): 21.5 (Anil-***C***H_3), 118.9 (Anil ***6-C***), 122.2, (Anil ***2-C***), 125.2 +125.6 (Pyr ***3/5-C*** + Anil ***4-C***), 129.0 (Anil ***5-C***), 138.0 + 138.4 (Anil ***1-C*** + Anil ***3-C***), 143.5 (Pyr ***4-C***), 149.2 (Pyr ***2/6-C***), 162.1 (Pyr-***C***(O)NH). FAB-MS: m/z calc for $[M+H]^+$ 346.15555, found: 346.1555. ESI-MS: m/z calc for $[M+Cl]^-$ 380, found: 380.

***N*^{2},*N*^{6}-*bis*(3-Cyanophenyl)pyridine-2,6-dicarboxamide, 10**

2,6-Pyridinedicarbonyl dichloride (0.423 g, 2.07 mmol) was dissolved in acetonitrile (7.0 mL) and was added dropwise to a stirring solution of 3-aminobenzonitrile (0.785g, 6.64 mmol) and triethylamine (5.0 mL, 35.9 mmol) in acetonitrile (11.0 mL additional for 18.0 mL total) held at 0 °C in an ice bath. Upon completion of the addition, the system was returned to room temperature and stirred for 24 hours. The resulting white suspension is filtered, resuspended with acetonitrile (2 x 25 mL) and diethyl ether (1 x 10 mL) and refiltered after each suspension before drying under high vacuum. The resulting white solid is retained as the pure product (0.311 g, 41%, mp = 288-291 °C). ^{1}H-NMR (DMSO-d_6): 7.62-7.68 (4H, m, Anil ***4-H*** + Anil ***5-H***), 8.21 (2H, dt, J_1 = 6.5 Hz, J_2 = 2.5 Hz Anil ***5-H***), 8.32 (1H, dd, J_1 = 8.8 Hz, J_2 = 6.6 Hz, Pyr ***4-H***), 8.37 (2H, s, Anil ***2-H***), 8.42 (2H, d, J = 7.4 Hz Pyr ***3/5-H***), 11.31 (2H, s, C(O)N***H***-Anil). ^{13}C-NMR (DMSO-d_6): 111.9 (Anil ***3-C)***, 118.8 (Anil-***C***N), 124.1 (Anil ***2-C***), 126.1 + 126.2 (Anil ***6-C*** + Pyr ***3/5-C***), 128.3 (Anil ***4-C***), 130.6 (Anil ***5-C***), 139.2 (Anil ***1-C*** + Pyr ***4-C***), 148.6 (Pyr ***2/6-C***), 162.5 (Pyr-***C***(O)NH). FAB-MS: m/z calc for $[M+H]^+$ 368.1148, found: 346.1132. ESI-MS: m/z calc for $[M+Cl]^-$ 402, found: 402.

***N*^{2},*N*^{6}-*bis*(3-Trifluorophenyl)pyridine-2,6-dicarboxamide, 11**

2,6-Pyridinedicarbonyl dichloride (0.423 g, 2.07 mmol) was dissolved in acetonitrile (7.0 mL) and was added dropwise to a stirring solution of 3-trifluoromethylaniline (1.083 g, 6.72 mmol) and triethylamine (5.0 mL, 35.9 mmol) in acetonitrile (11.0 mL additional for 18.0 mL total) held at 0 °C in an ice bath. Upon completion of the addition, the system was returned to room temperature and stirred for 24 hours. The resulting white suspension is filtered, resuspended with acetonitrile (2 x 25

mL) and diethyl ether (1 x 10 mL) and refiltered after each suspension before drying under high vacuum. The resulting white solid is retained as the pure product (0.346 g, 37%, mp = 260-261 °C). ^{1}H-NMR (DMSO-d_6): 7.55 (2H, d, *J* = 7.7 Hz, Anil ***4-H***), 7.71 (2H, t, *J* = 7.8 Hz, Anil ***5-H***), 8.19 (2H, d, *J* = 7.9 Hz, Anil ***6-H***), 8.34 (1H, t, *J* = 7.9 Hz, Pyr ***4-H***), 8.44 (4H, m, Anil ***2-H*** + Pyr ***3/5-H***), 11.25 (2H, s, C(O)N***H***-Anil). ^{13}C-NMR (DMSO-d_6): 117.0 (Anil ***2-C***), 120.7 (Anil-***C***F_3), 124.6 (Anil ***4-C***), 125.7 (Anil ***6-C***), 129.3 (Pyr ***3/5-C***), 130.8 (Anil ***3-C*** + Anil ***5-C***), 138.9 (Anil ***1-C***), 140.3 (Pyr ***4-C***), 148.4 (Pyr ***2/6-C***), 162.1 (Pyr-***C***(O)NH). FAB-MS: m/z calc for $[M+H]^+$ 454.0990, found: 454.0995. ESI-MS: m/z calc for $[M+Cl]^-$ 488, found: 488.

***N*^{2},*N*^{6}-*bis*(3-Chlorophenyl)pyridine-2,6-dicarboxamide, 12**

2,6-Pyridinedicarbonyl dichloride (0.426 g, 2.09 mmol) was dissolved in acetonitrile (5.0 mL) and was added dropwise to a stirring solution of 3-chloroaniline (0.861 g, 6.75 mmol) and triethylamine (5.0 mL, 35.9 mmol) in acetonitrile (10.0 mL additional for 15.0 mL total) held at 0 °C in an ice bath. Upon completion of the addition, the system was returned to room temperature and stirred for 24 hours. The resulting white suspension is filtered, resuspended with acetonitrile (2 x 25 mL) and diethyl ether (1 x 10 mL) and refiltered after each suspension before drying under high vacuum. The resulting white solid is retained as the pure product (0.561 g, 70%, mp = 245-247 °C). ^{1}H-NMR (DMSO-d_6): 7.25 (2H, d, *J* = 7.9 Hz, Anil ***4-H***), 7.48 (2H, t, *J* = 8.1 Hz, Anil ***5-H***), 7.90 (2H, d, *J* = 7.9 Hz, Anil ***6-H***), 8.16 (2H, s, Anil ***2-H***), 8.31 (1H, t, *J* = 7.7 Hz, Pyr ***4-H***), 8.41 (2H, d, *J* = 8.2 Hz Pyr ***3/5-H***), 11.19 (2H, s, C(O)N***H***-Anil). ^{13}C-NMR (DMSO-d_6): 119.5 (Anil ***6-C***), 120.4 (Anil ***2-C***), 124.1 (Anil ***4-C***), 125.7 (Pyr ***3/5-C***), 130.5 (Anil ***5-C***), 133.0 (Anil ***3-C***), 139.6 (Anil ***1-C***), 140.1 (Pyr ***4-C***), 148.6 (Pyr ***2/6-C***), 161.9 (Pyr-

C(O)NH). FAB-MS: m/z calc for $[M+H]^+$ 386.0463, found: 386.0463. ESI-MS: m/z calc for $[M+Cl]^-$ 420, found: 420.

Chloride binding constants from ^{1}H-NMR titrations.

Solutions of the receptor molecule in DMSO-d_6 or CD_2Cl_2 were prepared at a concentration of 1.8 mM. A 1 mL solution thus prepared was transferred to a glass NMR tube and titrated with a solution containing both 1.8 mM of host and 18 mM solutions (10 equiv.) of $NBu_4^+Cl^-$. The chemical shifts of the NH protons were monitored as a function of the anion concentration until saturation was reached. Using data accrued from a minimum of three independent determinations, the association constants were calculated using a nonlinear regression analysis (GraphPad) with a curve fit for 1:1 binding originally used by Kavallieratos *et al*.[17b]

Competitive chloride binding assayed by electrospray mass spectrometry, as performed by I. Alexandru Carasel, Joseph Kramer and Dr. Rudolph Winter.

In each experiment, competing hosts were present in equimolar concentrations (50 μM) and chloride (as NBu_4Cl salt) was kept sub-stoichiometric (5 μM) so that competition for the guest would be obvious. The excess neutral host molecules are not observed unless complexed by Cl^-, so excess host could be ignored. The ratios shown in Table 3.2 were calculated from the total integration of relevant m/z peaks for host-Cl^- adducts. Five charged adducts were observed at significant abundances: $[host^A \bullet Cl]^-$, $[host^B \bullet Cl]^-$, $[(host^A)_2 \bullet Cl]^-$, $[(host^B)_2 \bullet Cl]^-$, and $[host^A \bullet host^B \bullet Cl]^-$, and total relative abundances were calculated for both hosts. In every case, the total relative abundance of the unsubstituted isophthalamide, **5**, was normalized to 1, with a value established for the competing

compound. Errors are the calculated standard deviations of ratios from at least three independent experiments.

Preparation of phospholipid vesicles.

3.6 mL of a 25 mg mL^{-1} chloroform solution of dioleoylphosphatidylcholine (DOPC, from Avanti Polar Lipids; Alabaster, AL), was distributed equally to 6 test tubes before evaporating the solvent *in vacuo* for 4 hours to yield dry films of 15 mg each. For each vesicle preparation, a dry film sample was dissolved in a mixture of Et_2O (375 μL) and aqueous 1 mM lucigenin – 225mM $NaNO_3$ (375 μL). The combined mixture was sonicated for 30 s yielding a yellow suspension. The diethyl ether was removed under low vacuum at 30 °C for 2 to 2.5 hours. The resulting mixed micellar, vesicular, and aggregate aqueous suspension was extruded through a 200 nm pore-size membrane filter 5 times. The filtered suspension was passed through a Sephadex G25 size exclusion column that was previously equilibrated with a 225 mm $NaNO_3$ external buffer, collecting the first translucent fractions. This process effectively eliminated undesired extra-vesicular lucigenin as well as micelles and vesicles of a smaller-than-desired size. The size of the resulting purified vesicles was confirmed by light-scattering analysis, and the sample was diluted to the appropriate concentration using the 225 mm $NaNO_3$ external buffer.

Lucigenin quenching assay.

A 1900 μL aliquot of 0.31 mM vesicles in external buffer was placed in a quartz cuvette to be used for the lucigenin quenching experiment. The excitation wavelength was set to 368 nm and the emission wavelength to 506 nm, with both slits set to 5 nm. After a brief initial equilibration phase, 100 μL of a 4 M NaCl solution were added in order to

create a chloride gradient between the outside (190 μM) and the inside (0 μM) of the vesicles. When the fluorescence intensity stabilized, 2 μL of the desired compound at the appropriate concentration (10 mM stock solution for studies with 10 μM concentrations) in DMSO were added. At the end of each experiment the vesicles were lysed with 100 μL of a 2% Triton X-100 solution to establish the level of baseline fluorescence. The traces shown are an average of at least 3 independent trials.

Planar bilayer conductance as performed by Saeedeh Negin.

Membranes were formed by painting lipid solutions (asolectin from soybean dissolved in *n*-decane, 25mg mL^{-1}, from Avanti Polar Lipids; Alabaster, AL) over a 200 μm aperture separating two chambers containing 3.000 mL buffer solutions (450 mM KCl, 10 mM HEPES, pH = 7.00). 21μL of a DMSO solution of the appropriate transporter was then added into the *cis* chamber (the side of the membrane that hosts the input electrode) to yield a final concentration of 7 μM. Working in a Faraday cage (Warner Instruments) at room temperature, specific potentials were applied between two electrodes immersed in the two buffer solutions. The resulting currents were amplified (amplifier BC-525 D, from Warner Instruments), filtered with a 4-pole Bessel filter at 1 kHz, digitized by Digitizer (Digidata 1322A from Axon Instruments), sampled at 100 Hz amplifier filter frequency and collected using Clampex 9.2 (Axon Instruments). The data were analyzed later using Clampfit 9.2 (Axon Instruments).

Fluorescence of compound 4.

Fluorescence emission intensity was found to be maximal for all wavelengths with λ_{ex} = 280 nm when both slits were set to 5 nm. The fluorescence emission spectrum was

recorded while titrating a solution of host in 1% DMSO/Water into a solution of either 1% DMSO/Water or 1% DMSO/Water with 0.31 mM DOPC vesicles. In all cases, the recorded spectra are the average of 10 scans per concentration per trial with a minimum of three independent trials totaling a minimum of 30 scans.

1 Yamnitz, C. R.; Negin, S.; Carasel, I. A.; Winter, R. K.; Gokel, G. W. *Chem. Commun.* **2010**, *46*, 2838-2840.

2 Gokel, G. W.; Barkey, N. *New J. Chem.*, 2009, **31**, 947-963.

3 Stark, G.; Ketterer, B.; Benz, R.; Lauger, P. *Biophys. J.* **1971**, *11*, 981-994.

4 Läuger, P. *Biochim. Biophys. Acta* **1973**, *311*, 423-441.

5 Buck, R. P. *J. Phys. Chem.* **1987**, *91*, 2347-2350.

6 (a) Bianchi, A.; Bowman-James, K.; Garcia-Espana, E., Ed. *Anion Receptor Chemistry*; Wiley-VCH: New York, **1997.** (b) Sessler, J. L.; Gale, P.; Cho, W.-S. *Anion Receptor Chemistry*; Royal Society of Chemistry: Cambridge, **2006**.

7 (a) Pressman, B. C. *Fed. Proc.* **1973**, *32*, 1698-1703. (b) Andreu, C.; Galán, A.; Kobiro, K.; de Mendoza, J.; Park, T. K.; Rebek Jr., J.; Salmerón, A.; Usman, N. *J. Am. Chem. Soc.* **1994**, *116*, 5501-5502.

8 (a) Yamnitz, C. R.; Gokel, G. W. *Chem. Biodivers.* **2007,** *4*, 1395-1412. (b) Gokel, G. W.; Carasel, I. A. *Chem. Soc. Rev.* **2007,** *36*, 378-389.

9 Lehn, J.-M. *Supramolecular Chemistry*; Wiley-VCH: Weinheim, **1995**.

10 Park, C. H.; Simmons, H. E. *J. Am. Chem. Soc.* **1968**, *90*, 2431-2432.

11 Schmidtchen, F. P *Angew. Chem.* **1977**, *89*, 751-752.

12 Graf, E.; Lehn, J. M. *J. Am. Chem. Soc.* **1975**, *97*, 5022-5024.

13 Echavarren, A.; Galan, A.; De Mendoza, J.; Salmeron, A.; Lehn, J. M. *Helv. Chim. Acta* **1988**, *71*, 685-693.

14 Newcomb, M.; Blanda, M. T. *Tetrahedron Lett.* **1988**, *29*, 4261-4264.

15 (a) Gale, P. A. *Coord. Chem. Rev.* **2000**, *199*, 181-233. (b) Sessler, J. L.; Camiolo, S.; Gale, P. A. *Coord. Chem. Rev.* **2003**, *240*, 17-55. (c) Kubik, S.; Reyheller, C.; Stuwe, S. *J. Inclusion Phenom. Macrocyclic Chem.* **2005**, *52*, 137-187.

16 (a) Sakai, N.; Brennan, K. C.; Weiss, L. A.; Matile, S. *J. Am. Chem. Soc.* **1997**, *119,* 8276. (b) Otto, S.; Osifchin, M.; Regen, S. L. *J. Am. Chem. Soc.* **1999**, *121*, 7276-7277. (c) Koulov, A. V.; Lambert, T. N.; Shukla, R.; Jain, M.; Boon, J. M.; Smith, B. D.; Li, H.; Sheppard, D. N.; Joos, J.-B.; Clare, J. P.; Davis, A. P. *Angew. Chem. Int. Ed.* **2003**, *42*, 4931-4933. (d) Ferdani, R.; Li, R.; Pajewski, R.; Pajewska, J.; Winter, R. K.; Gokel, G. W. *Org. Biomol. Chem.* **2007**, *5*, 2423-2432. (e) Santacroce, P. V.; Davis, J. T.; Light, M. E.; Gale, P. A.; Iglesias-Sanchez, J. C.; Prados, P.; Quesada, R. *J. Am. Chem. Soc.* **2007**, *129*, 1886-1887. (f) McNally, B. A.; O'Neil, E. J.; Nguyen,

A.; Smith, B. D. *J. Am. Chem. Soc.* **2008**, *130*, 17274-17275. (g) Berezin, S. K.; Davis, J. T. *J. Am. Chem. Soc.* **2009,** *131*, 2458-2459.

17 (a) Kavallieratos, K.; de Gala, S. R.; Austin, D. J.; Crabtree, R. H. *J. Am. Chem. Soc.* **1997**, *119*, 2325-2326. (b) Kavallieratos, K.; Bertao, C. M.; Crabtree, R. H. *J. Org. Chem.* **1999**, *64*, 1675-1683.

18 (a) Gale, P. A. *Acc. Chem. Res.* **2006**, *39*, 465-475. (b) Bates, G. W.; Gale, P. A.; Light, M. E. *Chem. Commun.* **2007**, 2121-2123.

19 Koulov, A. V.; Mahoney, J. M.; Smith, B. D. *Org. Biomol. Chem.* **2003**, *1*, 27-29.

20 (a) Bates, G. W.; Gale, P. A.; Light, M. E. *Chem. Commun.* **2007**, 2121-2123. (b) Zielinski, T.; Dydio, P.; Jurczak, J. *Tetrahedron* **2008**, *64*, 568-574.

21 Lizarraga, E.; Zabaleta, C.; Palop, J. A. *J. Thermal Anal. Colorim.* **2007**, *89*, 783-792.

22 Berl, V.; Huc, I.; Khoury, R. G.; Lehn, J.-M., *Chem. Eur. J.* **2001**, *7*, 2798-2809.

23 Bisson, A. P.; Lynch, V. M.; Monahan, M.-K. C.; Anslyn, E. V. *Angew. Chem. Int. Ed. Engl.* **1997**, *36*, 2340-2342.

24 Sakai, N.; Kamikawa, Y.; Nishii, M.; Matsuoka, T.; Kato, T.; Matile, S. *J. Am. Chem. Soc.* **2006**, *128*, 2218-2219.

25 (a) Schlesinger, P.H.; Ferdani, R.; Liu, J.; Pajewska, J.; Pajewski, R.; Saito, M.; Shabany, H.; Gokel, G. W. *J. Am. Chem. Soc*. **2002**, *124*, 1848-1849. (b) Sidorov, V.; Kotch, F. W.; Abdrakhmanova, G.; Mizani, R.; Fettinger, J. C.; Davis, J. T. *J. Am. Chem. Soc.* **2002**, *124*, 2267-2278. (c) Broughman, J. R.; Brandt, R.; Hastings, C.; Iwamoto, T.; Tomich, J. M.; Schultz, B. D. *Cell Physiol*. **2004**, *286*, C1312-1323. (d) Sakai, N.; Kamikawa, Y.; Nishii, M.; Matsuoka, T.; Kato, T.; Matile, S. *J. Am. Chem. Soc.* **2006**, *128*, 2218-2219.

26 (a) Li, X.; Shen, B.; Yao, X.-Q.; Yang, D. *J. Am. Chem. Soc.* **2007**, *129*, 7264-7265. (b) Li, X.; Shen, B.; Yao, X.-Q.; Yang, D. *J. Am. Chem. Soc.* **2009**, *131*, 13676–13680.

27 (a) Leonard, J. P.; Jensen, P.; McCabe, T.; O'Brien, J. E.; Peacock, R. D.; Kruger, P. E.; Gunnlaugsson, T. *J. Am. Chem. Soc.* **2007**, *129*, 10986-10987; (b) Malone, J. F.; Murray, C. M.; Dolan, G. M. *Chem. Mater.* **1997**, *9*, 2983-2989.

28 Ben-Haida, A.; Hodge, P. *Macromol.* **2005**, *38*, 722-729.

29 Nimmanpipug, P.; Tashiro, K.; Maeda, Y.; Rangsiman, O. *J. Phys. Chem. B* **2002**, 106, 6842-6848.

30 Qi, J. Y.; Yang, Q. Y.; Lam, K. H.; Zhou, Z. Y.; Chan, A. S. C. *Acta Cryst.* **2003**,

E59, o415-o416.

31 Yin, Z.; Li, Z.; Yang, W.-Z.; He, J.; Cheng, J.-P. *Struct. Chem.* **2005**, 641-647.
32 Coles, S. J.; Frey, J. G.; Gale, P. A.; Hursthouse, M. B.; Light, M. E.; Korakot, Navakhun; Thomas, G. L. *Chem. Commun.* **2003**, 568-569.

33 Light, M. E.; Gale, P. A.; Navakhun, K. *Acta Cryst.* **2006**, *E62*, o1097-o1098

34 (a) Anslyn, E. V.; Dougherty, D. A. *Modern Physical Organic Chemistry*; University Science Books: Sausalito, CA, **2006**; pp.14. (b) Cramer, C.J. *Essentials of Computational Chemistry*; John Wiley & Sons: New York, **2004** (2nd ed., 2005); pp. 308-309

35 Ritchie, C. D.; Sager, W. F. *Prog. Phys. Org. Chem*. **1964**, *2*, 323.

36 Lee, C.; Yang, W.; Parr, R. G. *Phys. Rev. B* **1988**, *37*, 785-789.

37 Hammett, L. P. *J. Am. Chem. Soc.* **1937**, *59*, 96-103.

38 Connors, K. A. *Binding Constants*, 1st ed.; John Wiley & Sons: New York, **1987**, 189-215.

39 Fenn, J. B.; Mann, M.; Meng, C. K.; Wong, S. F.; Whitehouse, C. M. *Science* **1989**, *246*, 64-71.

40 Ferdani, R.; Li, R.; Pajewski, R.; J. Pajewska, J.; Winter, R. K.; Gokel, G. W. *Org. Biomol. Chem.,* **2007**, *5,* 2423-2432.

41 Seganish, J. L.; Fettinger, J. C.; Davis, J. T. *Supramol. Chem.* **2006**, *18*, 257-264.

42 Legg, K. D.; Hercules, D. M. *J. Phys. Chem.* **1970**, *74*, 2114-2121.

43 Segel, I. *Enzyme Kinetics. Behavior and Analysis of Rapid Equilibrium and Steady-State Enzyme Systems.* John Wiley & Sons: New York, **1975** (Wiley Classics Edition, 1993); pp 371-375.

44 Lakowicz, J. R. *Principles of Fluorescence Spectroscopy.* Springer Science: New York, **1983** (3rd ed., 2006); pp 278-297.

45 Hille, B. *Ionic pores of Excitable Membranes*, 3rd ed.; Sinauer: Sunderland, MA, **2001**.

46 Pauling, L. *The Nature of the Chemical Bond and the Structure of Molecules and Crystals; an Introduction to Modern Structural Chemistry*, 3rd ed., Cornell University Press: Ithaca, NY, **1960**.

47 Shannon, R. D. *Acta Crystallogr. A* 1976, **A32**, 751.

48 Zhou, J.; Lu, X.; Wang, Y.; Shi, J. *Fluid Phase Equilibria* **2002**, *194-197*, 257-270.

49 Wiener, M. C.; White, S. H. *Biophys. J.,* **1992**, *61*, 434.

50 (a) Gokel, G. W. *Chem. Commun.* **2000**, 1-9. (b) Djedovic, N.; Ferdani, R.; Harder, E.; Pajewska, J.; Pajewski, R.; Weber, M. E.; Schlesinger, P. H.; Gokel, G. W. *New J. Chem.* **2005**, *29*, 291-305.

51 Miloshevsky, G. V.; Jordan, P. C. *Structure* **2006**, *14*, 1241-1249.

52 Clark, T. D; Buehler, L. K.; Ghadiri M. R. *J. Am. Chem. Soc.* **1998**, *120*, 651-656.

53 Bhosale, S.; Sisson, A. L.; Sakai, N.; Matile, S. *Org. Biomol. Chem.,* **2006**, *4*, 3031-3039.

54 Yang, J.; Dewal, M. B.; Sobransingh, D.; Smith, M. D.; Xu, Y.; Shimizu, L. S. *J. Org. Chem.* **2009**, *74*, 102.

55 Helsel, A. J.; Brown, A. L.; Yamato, K.; Feng, W.; Yuan, L.; Clements, A. J.; Harding, S. V.; Szabo, G.; Shao, Z.; Gong, B. *J. Am. Chem. Soc.* **2008**, *130*, 15784.

56 Grimme, S. *Angew. Chem. Int. Ed.* **2008**, *47*, 3430-3434.

57 Collins, F. S. *Science* **1992**, *256*, 774-779.

58 Wagner, J. A.; Cozens, A. L.; Schulman, H.; Gruenert, D. C.; Stryer, L.; Gardner, P. *Nature* **1991**, *349*, 793-796.

59 Biniecki, S.; Modrzejewska, W.; Rogala-Zawadzka, G. *Acta Pol. Pharm.* **1985**, *42*, 1-3.

60 Horino, H.; Sakaba, H.; Arai, M. *Synthesis* **1989**, 715-718.

61 Kirsanov, A. V. *Zhurn. Obsh. Khim.* **1953**, *23*, 1920-1922.

62 Donkor, I. A.; Huang, T. L.; Tao, B.; *et al.*; *J. Med. Chem.* **2003**, *46*, 1041-1048.

63 Lizarraga, E.; Zabaleta, C.; Palop, J. A. *J. Thermal Anal. Colorim.* **2007**, *89*, 783-792.

64 Khanna, Y. P.; Pearce, E. M.; Forman, B. D.; Bini, D. A. *J. Polym. Sci. Polym. Chem. Ed.* **1981**, *19*, 2799.

65 Grimmel, H. W.; Guenther, A.. US Patent 2508860; **1950**.

66 Ben-Haida, A.; Hodge, P. *Macromol.* **2005**, *38*, 722-729.

CHAPTER 4

Solvent Dependence of Solid-State and Nanoscale Structures of Branched-Chain Pyrogallol[4]arenes

Summary and Contributions to this Work

The work presented in this chapter focuses on the solid-state and nanoscale morphologies of pyrogallol[4]arene macrocycles with branched sidechains. These compounds were analyzed for solid-state or "Angstrom-scale" geometry and morphology by X-ray crystallography and analyzed for nanoscale geometry and morphology by cryogenic transmission electron microscopy (cryo-TEM).

Solid-state structures show that within a family of branched-chain pyrogallol[4]arenes, one in particular self-assembles into unique hexameric nanotubes. Further analysis reveals that while the phenolic "head-group" is identical for all pyrogallol[4]arenes, sidechain-sidechain interactions dominate the self-assembly, and a unique intermolecular hydrogen bonding motif exists.

Both the crystallizations and electron microscopy sample preparations were performed in various solvent conditions—polar, non-polar, protic, aprotic—and in mixed solvents. While crystallizations were unsuccessful in many cases, EM sample preparations by slow evaporation generally yielded usable specimens. These specimens reveal that nanoscale aggregates self-assemble in polar media. Under 50000x magnification, these aggregates are shown to be formed from bundles of what appear to be short nanotubes of a diameter congruent with measurements taken from X-ray crystal structures.

The solid-state X-ray crystal structures of these compounds were solved at the University of Missouri – St. Louis by Dr. Nigam Rath using crystals grown by Dr. Kulikov. My contributions to the solid-state work are confined to the analysis of the structures and the associated DFT-level calculations.

With the exception of the first set of specimens examined (seen in Figure 4.8, below), I prepared samples of compound **2** for analysis by transmission electron microscopy, which was performed with the assistance of Dr. Dan Zhou and David Osborn at the University of Missouri – St. Louis.

A portion of this work is included in a paper[1] published in *Chemical Communications* in 2009.

Introduction

While covalent and ionic bonds are the strongest of interatomic forces and are thus key factors in the formation of structures on the nanometer scale, weaker forces such as hydrogen bonding, dipole-dipole, and van der Waals' (or London dispersion) forces can play prominent roles as well. Solid-state and nanoscale morphologies are of utmost importance when considering the activity of a compound in a biological membrane. Aggregates visible on the nanoscale using techniques such as transmission electron microscopy (TEM) may be indicative of a propensity for a compound to self-aggregate. Self-aggregation may preclude membrane insertion in some cases or may lead to unexpected characteristics in other cases. This paradox is seen in the two synthetic chloride channels that have been developed in our lab—the peptidic SAT transporters and the dipicolinic dianilide triarenes detailed in Chapter 3.

With the SAT molecules, self-aggregation of those family members with long alkyl chains at either the N- or C-terminus anchors leads to a decrease in chloride transport activity at a given applied concentration.[2] A large proportion of these specific SAT molecules form large, stable aggregates in the aqueous media. As a result, the effective concentration—the fraction of the total concentration that inserts into the membrane and transports chloride—is decreased. Generally, with increasing alkyl chain length and, by extension, hydrophobic character, the effective concentration decreases and overall chloride transport activity decreases.

Hydrophobic character was designed into the amphiphilic SAT system, as it was believed that it was necessary for membrane insertion. Indeed, it is true that for SAT molecules with alkyl chains that are too short, chloride transport rate is significantly diminished due to lack of membrane insertion and a lowered effective concentration. Thus, the hydrophobic character of a potential ion transporter must be balanced to both allow membrane insertion and minimize unwanted self-aggregation.

With dipicolinic dianilides, however, self-aggregation in aqueous solution leads to increased chloride transport activity as, with higher concentration, more aggregation occurs. A stacked aggregate is capable of spanning the phospholipid bilayer and transporting chloride via a channel mechanism.[3] This aggregation is explored in full detail in Chapter 3 of this work.

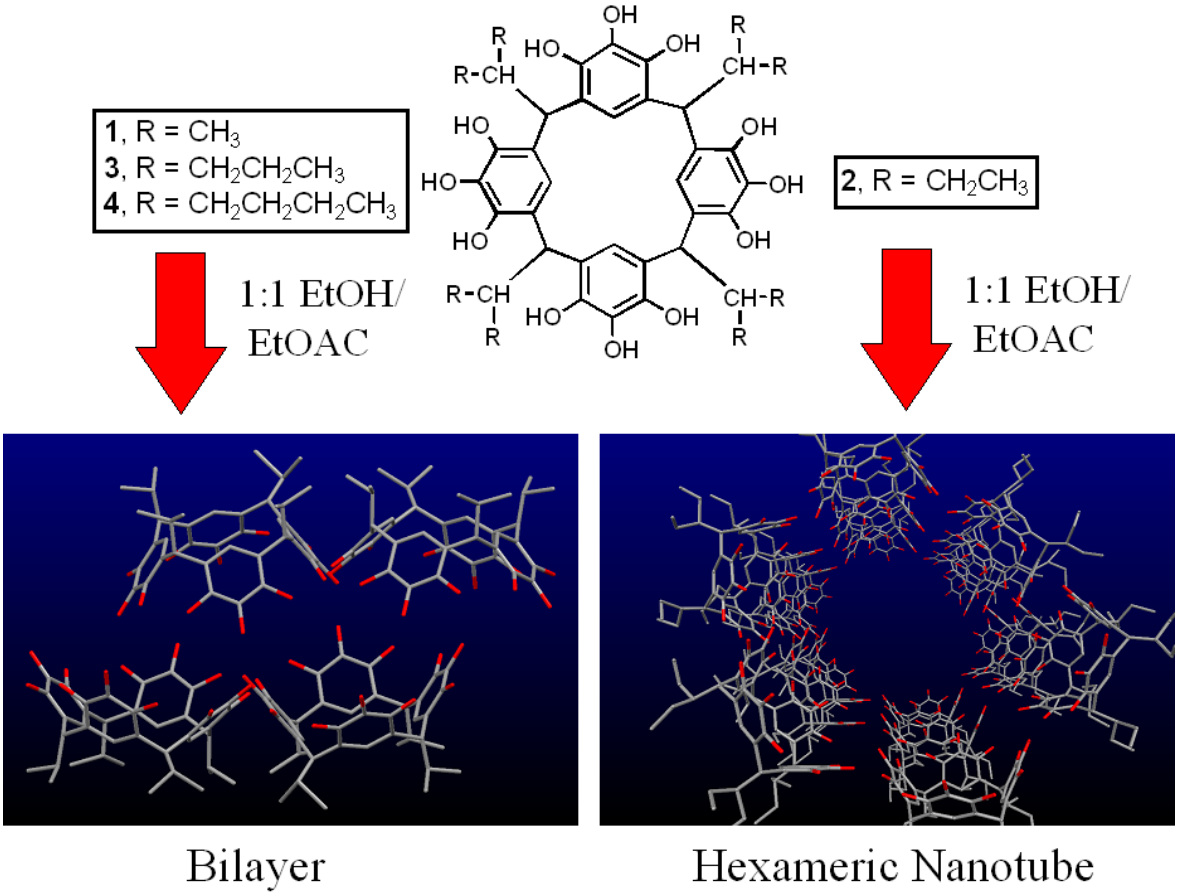

Figure 4.1. *Structures of branched-chain pyrogallol[4]arenes **1-4**, investigated in this work. As variation is present only in the aldehyde-derived side chains, they can be distinguished in future reference as 2-propyl (compound **1**), 3-pentyl (**2**), 4-heptyl (**3**) and 5-nonyl (**4**). In the same crystallization conditions, **1**, **3** and **4** form the bilayer (example in bottom left panel) while **3** forms a unique hexameric nanotube (bottom right).*

Another family of compounds known as pyrogallol[4]arenes have been made and characterized by a colleague in our research group, Oleg Kulikov. The hydroxyl-rich tetrarenes are formed from the 4+4 condensation of pyrogallol (1,2,3-trihydroxybenzene) and an aldehyde under acidic conditions.[4] The reaction proceeds through an electrophilic aromatic substitution at the 4 and 6 positions of the arene, ultimately resulting in cyclization. Variation of the aldehyde used in the condensation allows for modification of the four "legs" or "sidechains" of the macrocycle. Pyrogallol[4]arenes with sufficiently lipophilic sidechains are amphiphilic in nature, owing to the hydroxyl-rich "upper rim" of

the macrocycle seen in Figure 4.2. Work performed by another colleague, Megan Daschbach, indicates that this amphiphilic behavior extends to pyrogallol[4]arenes with sidechains as short as three carbons.[5]

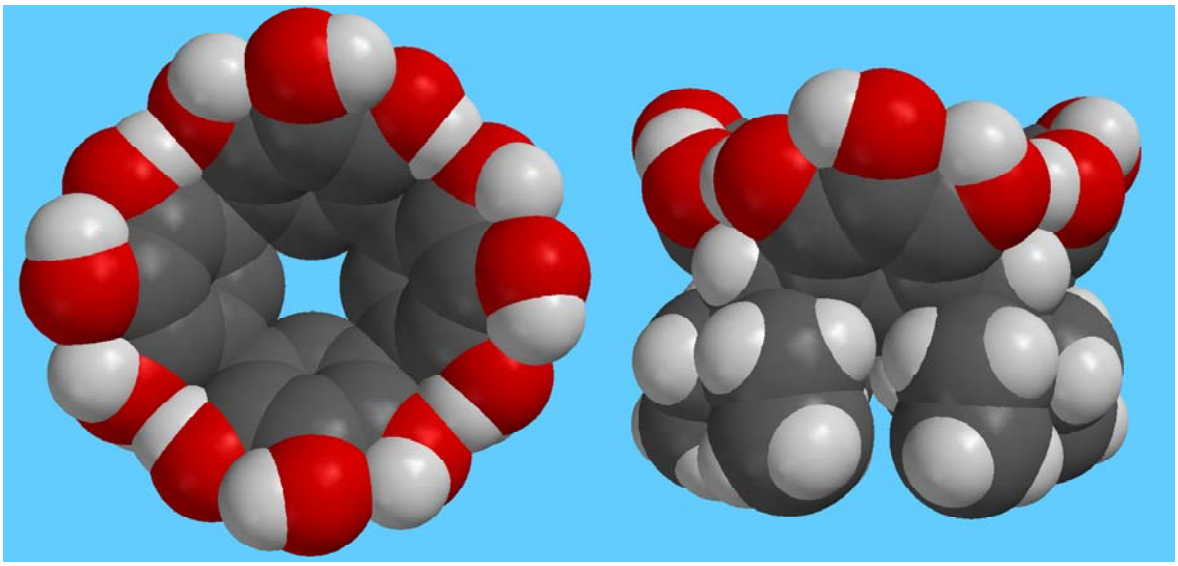

Figure 4.2. *Orthogonal perspectives of the calculated lowest energy gas-phase conformation of the 3-pentyl branched chain pyrogallol[4]arene,* ***2***.

The pioneering work of Atwood and collaborators with these pyrogallol[4]arenes has explored a wide variety of straight-chain alkane and alkene sidechains, among others.[4,6] While many of the solid-state structures of these macrocycles exhibit a bilayer morphology that is typical of amphiphiles,[7] a number of these compounds have been shown to self-assemble under the proper solvent conditions to form hydrogen-bonded dimeric[8] and hexameric[9] nanocapsules. Additionally, one pyrogallol[4]arene has been shown to assemble, in the presence of an ancillary molecule, into a solid-state nanotube formed from stacks of hydrogen-bonded rings of four macrocycles each.[6b]

In the present work, Dr. Kulikov was able to isolate crystals of compounds **1**-**4** grown from the polar solvent systems 1:1 ethanol to ethyl acetate and 1:1 acetonitrile to

ethyl acetate. These crystals were characterized by X-ray analysis and the resulting structures were studied further to elaborate structural detail and solid-state geometry.

One pyrogallol[4]arene, the 3-pentyl compound, **2**, was found to form nanotube structures in the solid state, while the remainder form a typical bilayer morphology. The nanotubes formed by **2** appear to pack tightly with one another, leaving open the possibility of forming nanostructures, which are shown to form on a carbon coated copper grid after slow evaporation of solvent.

The nanoscale characterization is extended in the current work to investigate the variation in nanoscale morphologies based on the evaporation of solvent, as well as to determine the presence of and analytically compare the crystallinity and order in the solvent-evaporated specimen. If different solvents yield different nanoscale morphologies, and if diffraction patterns are present, a comparison of patterns can be made. If the same diffraction pattern and lattice spacings arise from different nanoscale morphologies, it supports the argument that both morphologies form from the same supramolecular structure—the nanotube, for example. If the diffraction patterns are different, it lends credence to the argument that different nanoscale morphologies arise from different supramolecular structures.

Diffraction patterns of soft materials—most notably carbon nanotubes[10]—have been acquired and used to differentiate varying molecular structures from similar or nearly-identical nanostructure morphologies. In another previous study, calix[4]arenes, which are similar in structure to the pyrogallol[4]arenes used in this study, were deposited on a particular face of a gold crystal, self-organizing into a flat crystalline overlayer.[11] This supramolecular organization was determined by the combined use of scanning tunneling microscopy and low-energy electron diffraction. In both of these previous studies, low

energy-electron diffraction (LEED) was used to garner structural information on the molecular level—a strategy that may be used with normal energy electron diffraction to simply reveal differences in molecular/supramolecular structure, if not the structures themselves. Unfortunately, these techniques were not available for our efforts, so TEM visualization of nanostructures and analysis of polycrystalline diffraction rings are the techniques used to garner as much information as possible herein.

Results and Discussion

Solid-state structure of branched-chain pyrogallol[4]arenes

The synthetic efforts of Dr. Kulikov, further characterized as presented here, were targeted at understanding the effects of branched sidechains on the self-assembly of pyrogallol[4]arenes in solution and in the solid-state. Four branched-chain pyrogallol[4]arenes were prepared for the present study. The acid-catalyzed reaction of pyrogallol with isobutyraldehyde, 2-ethylpropanal, 2-propylbutanal, or 2-butylpentanal gave, respectively, pyrogallol[4]arenes **1**, **2**, **3** and **4** shown in Figure 4.1. With one of these sidechain variations, macrocycle **2**, a self-assembled hydrogen-bonded nanotube has been shown to form in the solid-state. The nanotube consists of an infinite stack of rings of six hydrogen-bonded macrocycles. Conversely, under identical crystallization conditions, pyrogallol[4]arenes **1**, **3**, and **4** crystallize in the more common bilayer morphology.

Samples suitable for X-ray crystal structure determination were obtained for compounds **1**, **2**, **3**, and **4** by crystallization from 20:19:1 (v/v/v) EtOAc:EtOH:H_2O. Solid-state structural analysis confirmed the bilayer structures for **1**, **3**, and **4**. In all three cases,

the pyrogallol[4]arene molecules align face-to-face with the phenolic hydroxyls participating in a significant amount of intermolecular and interfacial hydrogen bonding. Simultaneously, the branched hydrocarbon sidechains align tail-to-tail, maximizing polar solvent exclusion and minimizing void space. Although none of these bilayer structures had been previously described, the observed bilayer organization is similar to that reported for related compounds with straight alkyl chains.

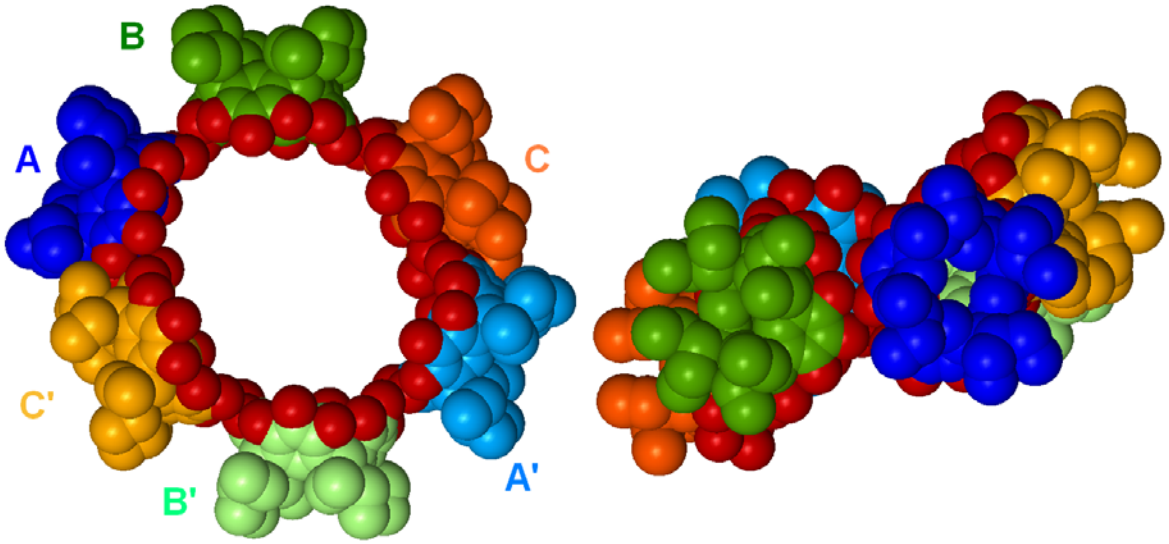

Figure 4.3. *Orthogonal perspectives of a single hydrogen-bonded hexameric ring of molecules of compound **2** formed in a 20:19:1 (v/v/v) EtOAc:EtOH:H_2O solvent mixture. Molecules directly opposite one another in the ring are related by C_i symmetry, with the inversion point located on the tube axis. Solvent molecules and side-chains are omitted for clarity.*

In contrast, when 3-pentylpyrogallol[4]arene, **2**, was crystallized, either from 20:19:1 (v/v/v) EtOAc:EtOH:H_2O ("form A") or 1:1 (v/v) EtOAc:MeCN ("form B"), identical structures of the hexameric nanotube morphology were obtained. The organization of a single hexameric ring is shown in Figure 4.3 as a cross-section of the solid-state structure obtained from the ethanol-ethyl acetate solvent system.

Form A, which crystallized from 20:19:1 (v/v/v) EtOAc:EtOH:H_2O, has an empirical formula $C_{152}H_{238}O_{52}$ and a molecular weight of 2897.4 g/mol that is consistent

with half of a hexameric ring (*i.e.*, a trimeric "half-ring"). This corresponds to 3 pyrogallol[4]arene subunits, 4 EtOH, and 12 H_2O molecules. This repeating structure comprises one half of a hexameric nanotube ring, with the other half-ring related by reflection through a single inversion point that lies on the nanotube axis (C_i symmetry). A full ring is held together by two direct hydrogen bonds between each neighboring subunit and direct solvent-bridging interactions involving 2 EtOH and 6 H_2O molecules. Rings are linked by 18 subunit-to-subunit hydrogen bonds — 2 per subunit plus 6 additional H-bonds between specific subunits. These interactions are shown in Figure 4.4. Note that no solvent molecules participate in direct ring-to-ring bridging, and no organized ethyl acetate molecules are present.

Form B of **2**, crystallized from 1:1 (v/v) EtOAc:MeCN and has the empirical formula $C_{162}H_{229}N_5O_{43}$ (mw 2934.5 g/mol). The molecular weight corresponds to 3 units of **2**, 3 EtOAc, 5 MeCN, and 3 H_2O molecules. As in form A, this comprises half of the hexameric ring. The internal and external dimensions of Forms A and B are not identical but differ by less than 1 Å in any direction. The direct subunit-to-subunit hydrogen bond network is identical in Forms A and B, although additional interactions occur with either EtOH (Form A) or EtOAc (Form B).

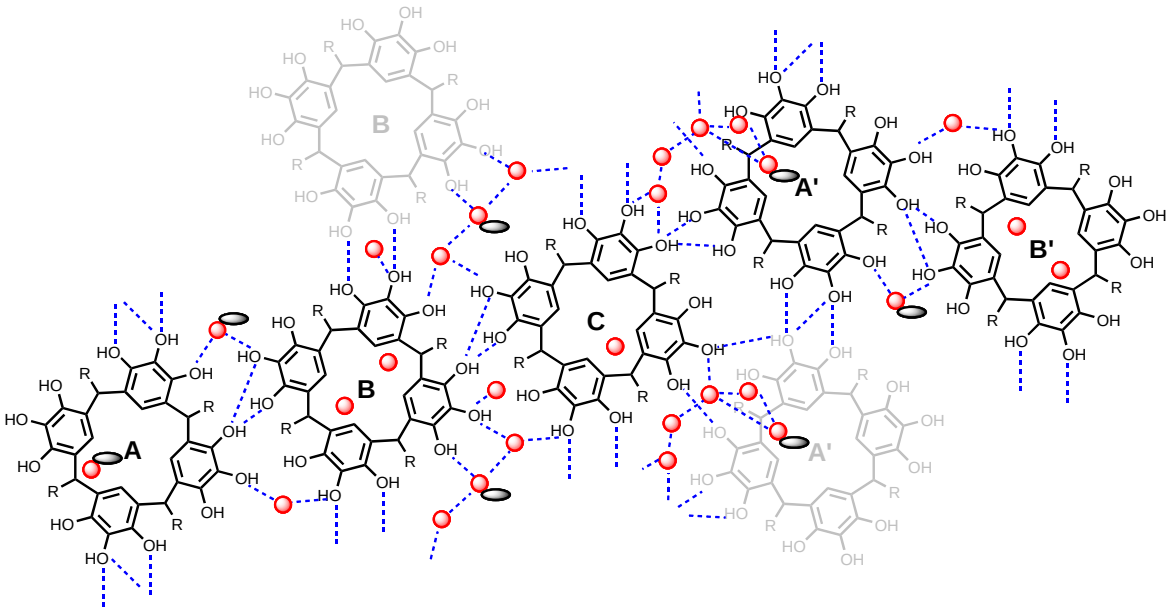

Figure 4.4. *A depiction of the supramolecular interactions involved in a hexameric ring derived from the ethanol-ethyl acetate system (Form A). The depiction is a "Mercator-like" projection from the outside of the tube looking towards the tube axis running vertically and is not drawn to scale. The sixth subunit (C') is not shown as its interactions are identical to those between the C subunit and its neighbors B and A'. The A' subunit of the ring below and the B subunit of the ring above are shown for clarification of inter-ring interactions. Bridging waters are shown as red spheres while bridging ethanol molecules are shown as red spheres connected to black ellipses. Relevant hydrogen bonds are depicted as blue dashed lines.*

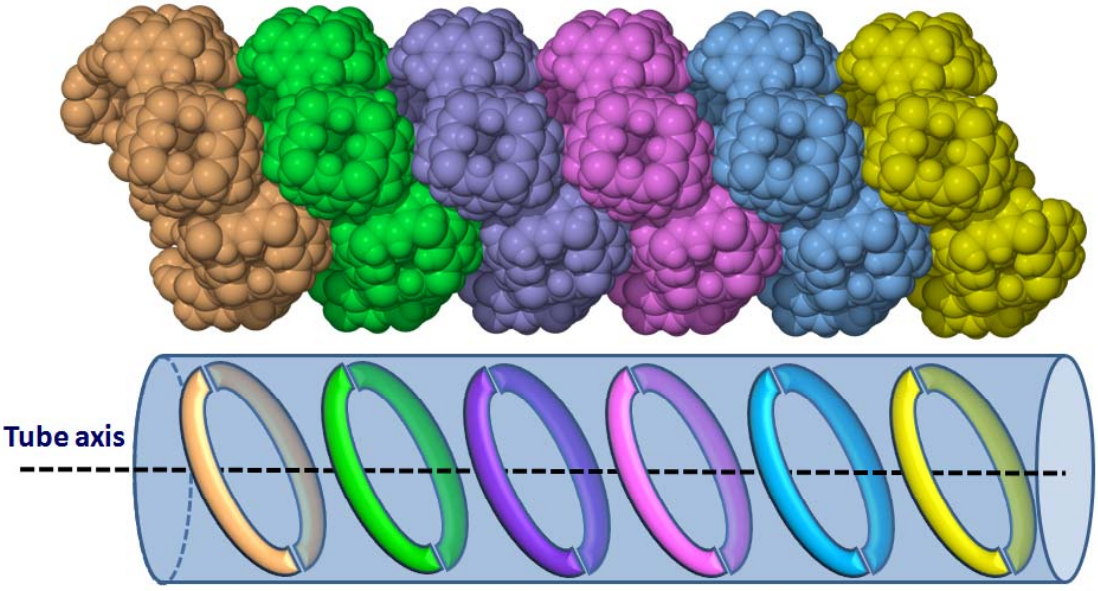

Figure 4.5. *(Top) Side view of a stack of six hexameric rings composed of pyrogallol[4]arene* ***2****. For clarity, the 3-Pentyl side chains and solvent molecules are not depicted. (Bottom) A cartoon representation of tube formed by the stacked rings, showing the tube axis and the cylinder formed. The dimensions of the elliptical tube are measured within the plane that is normal to the tube axis.*

Analysis of Form A shows that the hexameric rings that form the nanotubes are elliptical and tilted by about 30° with respect to the tube axis normal, as presented in Figure 4.5. Using measurements of atoms that are coplanar with the tube axis normal, the nanotubes themselves are shown also to be elliptical with short and long axis internal dimensions of 16 Å x 22 Å between hydroxyl oxygen atoms and external dimensions of 26 Å x 33 Å measured between distal side-chain carbon atoms.

The nanotube formed in this structure is much larger than related predecessors. Approximately 60% of the crystal's volume is an intra-annular, solvent-filled void. This compares with previously reported internal volumes of 38% for Atwood's pyrogallol[4]arene tetrameric ring nanotubes,[6b] and 6% for the resorcin[4]arene inverted hexameric ring nanotube characterized by Rissanen and co-workers.[12] The larger void volume in the present case may explain the higher *R*-factor (R_1) of 16.5% (form A) and 18.2% (form B) compared to R_1 values of 9.4%,[6b] 11.8%,[6b] and 9.0%[12] for the previously reported nanotubes. These void volumes are compared visually in Figure 4.6.

In the previous cases of nanotube formation from resorcin[4]arene or pyrogallol[4]arene, a compound such as pyrene, 1-bromopyrene,[6b] or a diammonium salt[12] was present as an ancillary to the nanotube. In the current work, ordered solvent molecules appear in the crystal lattice, but the H-bond network does not appear to require them. In contrast to the previous nanotubes and the other branched-chain solid-state structures, the 3-pentyl sidechains appear to interlock like the teeth (or cogs) of gears to tightly join adjacent nanotubes and exclude solvent from the interannular domain. This interaction and the excellence of the fit are apparent in the top panel of Figure 4.7, which shows a top-down view of three closely packed nanotubes.

Intertube side-chain carbon-carbon distances are often between 3.5Å and 4.5Å – at or near the sum of the van der Waals radii. These contacts have been measured and enumerated for all four of the solid-state structures derived from branched chain molecules crystallized from 20:19:1 (v/v/v) EtOAc:EtOH:H_2O. When normalized to the unit cell composition (crystals of **1**, **3** and **4** have two pyrogallol[4]arenes present in the unit cell, while **2** has three monomers), a direct comparison of contact distances can be made. The counts are portrayed in relation to carbon-carbon distances, with values binned to maximum cut-off points (0.05 Å, 5 pm). The data binning is cumulative, meaning that a contact of 3.71 Å would be included in the 3.75Å count and counts for all higher values (3.80Å, 3.85Å, etc.).

The number of close contacts present in these solid state structures suggests that the unique hexameric nanotube morphology formed by **2** is energetically advantageous. The high number of close contacts (< 3.75 Å) formed in the solid-state as well as the high number of total contacts less than 4.10 Å is a manifestation of this energetic advantage, underscoring the possibility that these structures form spontaneously in polar environments.

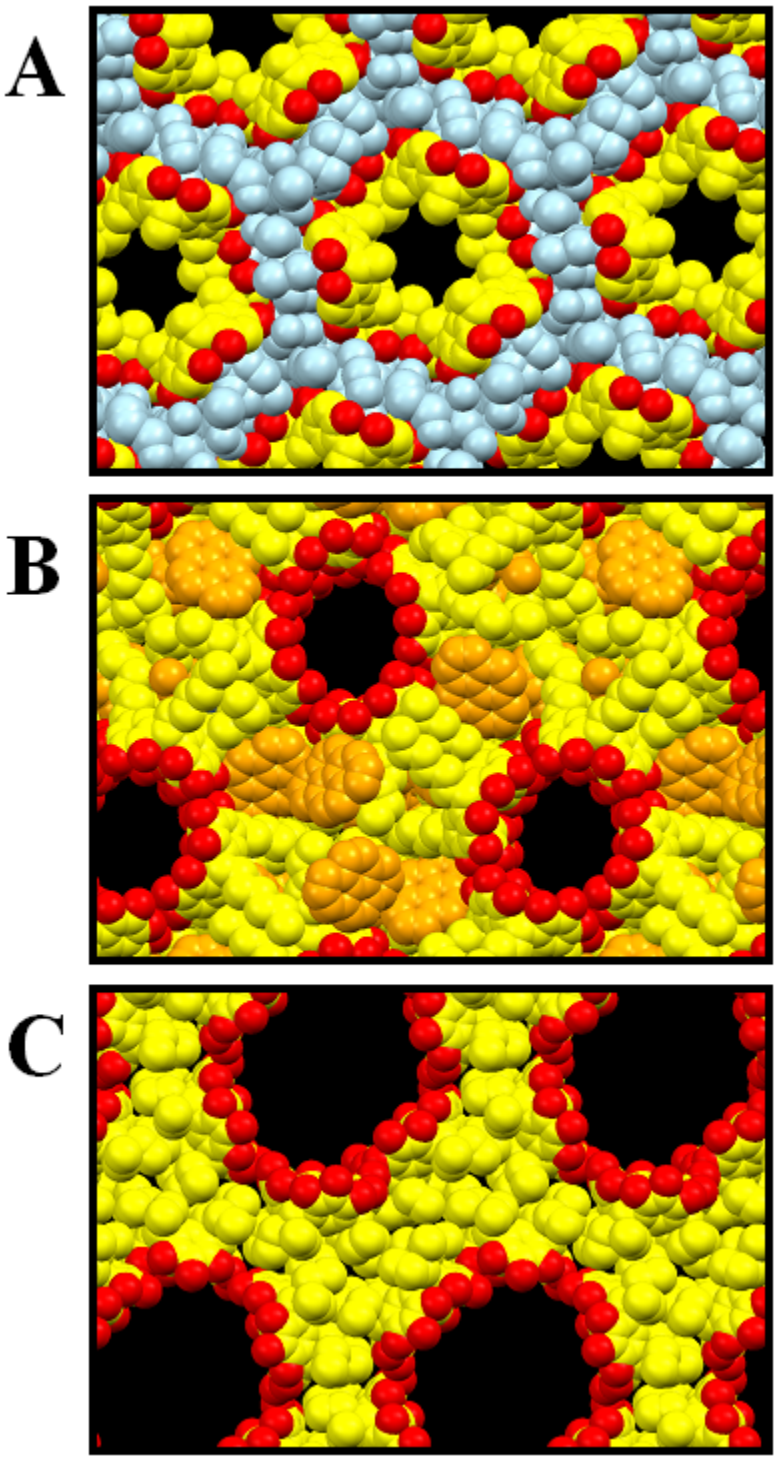

Figure 4.6. *Comparison of tube size and volume of Rissanen's trimeric ring resorcin[4]arene tube (Panel A), Atwood's tetrameric ring pyrogallol[4]arene tube (Panel B), and the current hexameric ring pyrogallol[4]arene tube (Panel C). All projections are along the tube axis, and no ordered intraannular solvent molecules are shown. Polar interannular solvent molecules (present only in the resorcinarene nanotube, Panel A) are depicted in blue, macrocycle oxygen atoms are depicted in red, macrocycle carbon atoms in yellow, and lipophilic solvent molecules/co-crystallents shown in orange.*

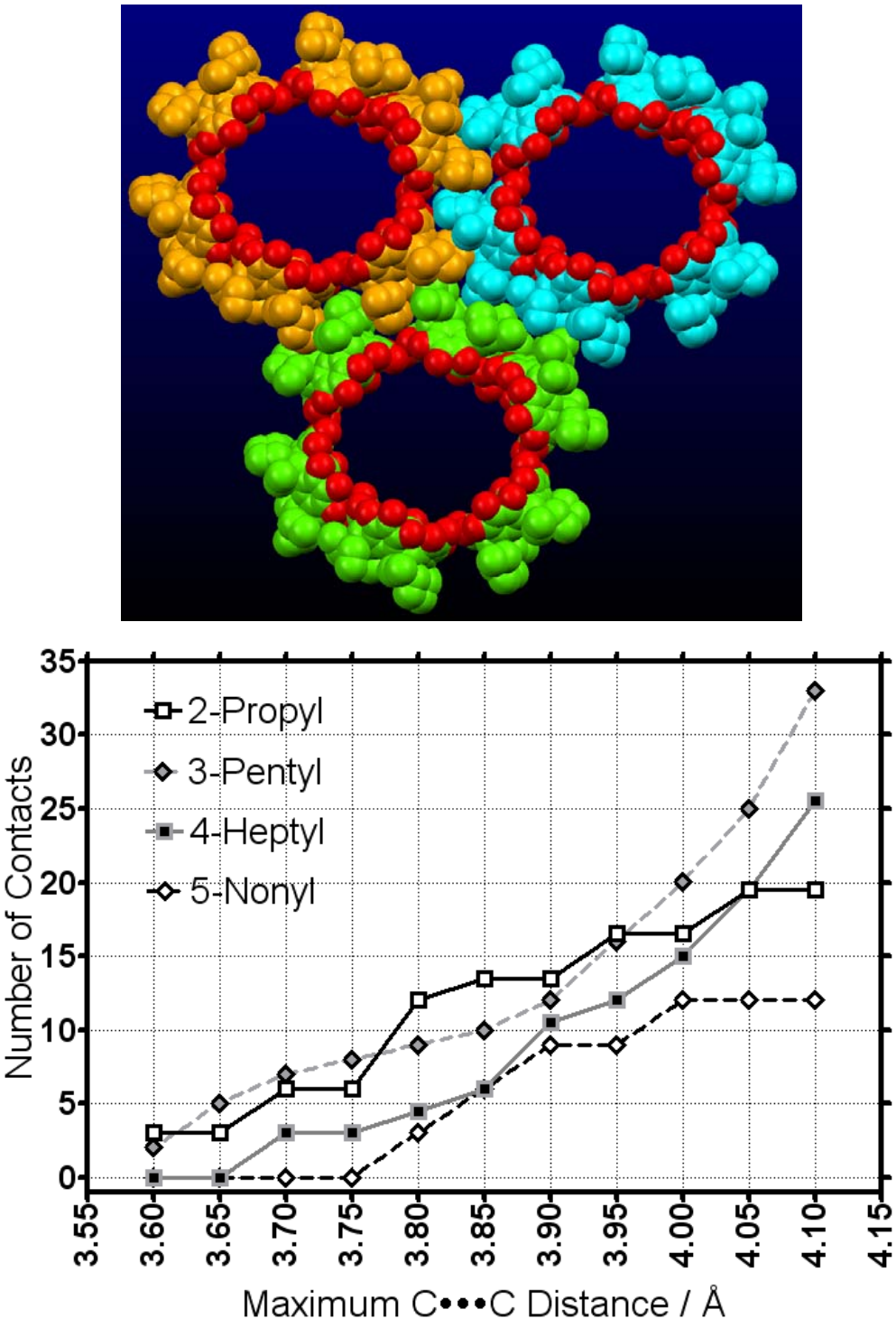

Figure 4.7. *(Top) End-on perspective of three rings of three adjacent nanotubes (carbon atoms in green, blue or orange for each ring) showing the cogged or interlocked nature of the branched side chains in the interannular space. (Bottom) Cumulating histogram of interannular carbon-carbon contacts binned to the maximum contact distance.*

Nanoscale morphologies of 3-pentyl pyrogallol[4]arene, 2

The tight interlocking of pyrogallol[4]arene sidechains between nanotubes provides a mechanism for bundling of nanotubes and formation of discrete identifiable nanostructures. Previous transmission electron microscopy (TEM) work by Oleg Kulikov shows that when specimens are prepared by evaporation of solutions or sonicated suspensions of these pyrogallol[4]arenes, nanoscale morphologies are evident. His specimen was taken from a sample of **2** that had crystallized as form A and was resuspended in 20:19:1 (v/v) EtOAc:EtOH:H_2O. When this mixture was evaporated on a copper-continuous carbon support, nanowires composed of what are presumably bundles of tens to thousands of nanotubes are seen by transmission electron microscopy. The specimen, as seen in Figure 4.8, exhibits small bundles forming in amorphous areas of the sample and larger bundles in the more ordered areas of the sample. As the solvent evaporates, the nanotube bundles could form more quickly or thoroughly in one area versus another.

Detailed examination of TEM images acquired for the sample of compound **2** revealed that the smallest dark lines typically have a width of 9-10 nm. The thinnest lines that are visible have a width of 6-7 nm. If the microfiber bundles are exclusively nanotubes, then each individual nanotube is a cylinder of approximate dimension 30 Å. Four coaxial tubes would have an external dimension of 60-70 Å (6-7 nm).

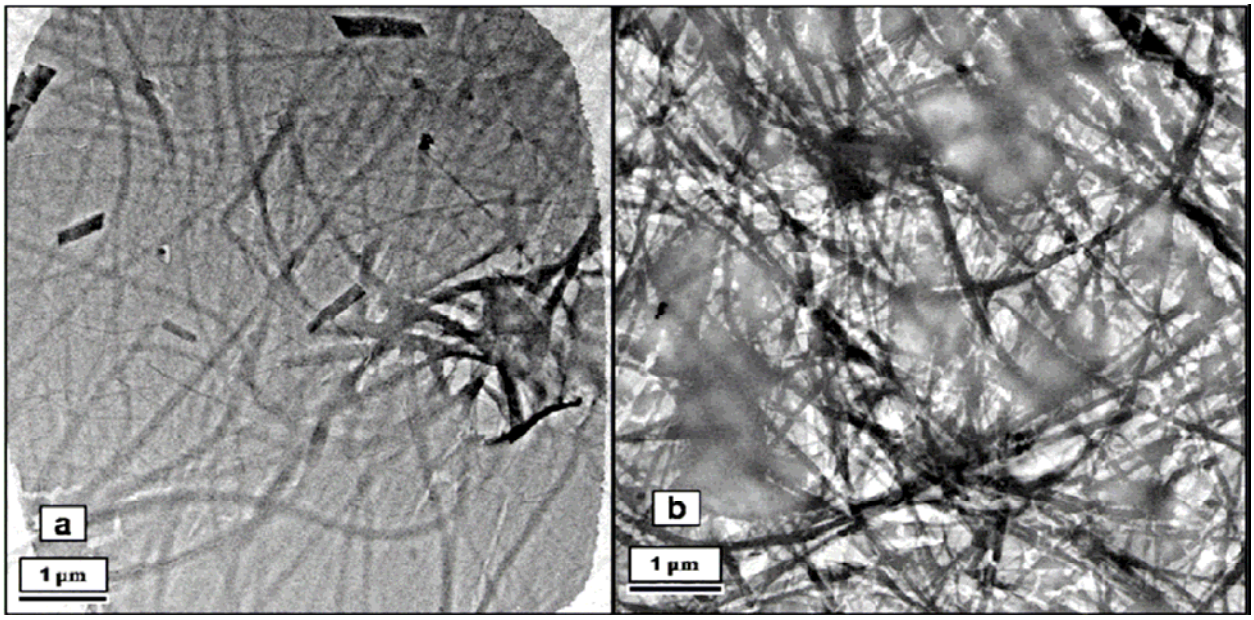

Figure 4.8*: Bright-field images of a single specimen prepared by Dr. Oleg Kulikov from the evaporation of a solution of pyrogallol[4]arene in a 1:1 mixture of ethyl acetate and acetonitrile. Images are taken at a magnification of 2500x. Larger, thicker rhomboidal cylinders with diameters between 270 nm and 13 nm are seen in panel A in a more amorphous, thicker "field" of presumably disordered pyrogallol[4]arene. Panel B shows a more extensive and numerous "web" of nanotube bundles with fewer areas of amorphous "fields."*

Dr. Kulikov's work has proven that these compounds can form nanostructures when evaporated from solution. However, only one solvent system—a 1:1 mixture of ethyl acetate and acetonitrile has been used to form nanostructures. Variation of the solvent systems used to prepare the specimen may yield different nanostructures.

Four solvent systems were investigated for the current work—the original 1:1 ethyl acetate to acetonitrile mixture, a 1:1 ethyl acetate to ethanol mixture, a 99:1 water to ethanol mixture, and a pure ethanol mixture. The 99:1 water to ethanol mixture yielded the most interesting results and will be discussed at length. Nanostructures derived from the other solutions were all varied, and comparisons will be made following the discussion on the specimen prepared from the 99:1 water to ethanol suspension.

Particle size analysis of the post-sonication 99:1 water to ethanol suspension by dynamic light scattering showed that aggregates were non-spherical, with a wide distribution of average diameters. Using the TEM at 2500x magnification, large particles of what appeared to be crystalline powder were seen, as shown in Figure 4.9. However, under higher magnification (10000 x) the large aggregates appeared as large cylinders of diameters varying from 900 nm to 150 nm. These large cylinders displayed ordered texture, spaced at about 25 to 26 nm, running the length of the cylinder, as seen in Figure 4.10. Also evident at this magnification were smaller nanowire-like structures that appeared to emanate from the surface of the larger cylinders, as seen in Figure 4.11. These also varied in diameter with a range of about 80 nm to 20 nm, and may have been deposited by solvent in an ordered manner at the cylinder surfaces during the evaporation process. As thickness cannot be easily judged using phase-contrast imaging, it is unknown whether these structures are 3-D nanowires or 2-D nanobelts. Presumably, a large proportion of the pyrogallol[4]arene monomers in the sonicated solution remained as the large cylindrical aggregates that form, immediately. However, a smaller proportion becomes solvated in the sonication process and the solvated monomers deposited at the ordered cylinder surfaces.

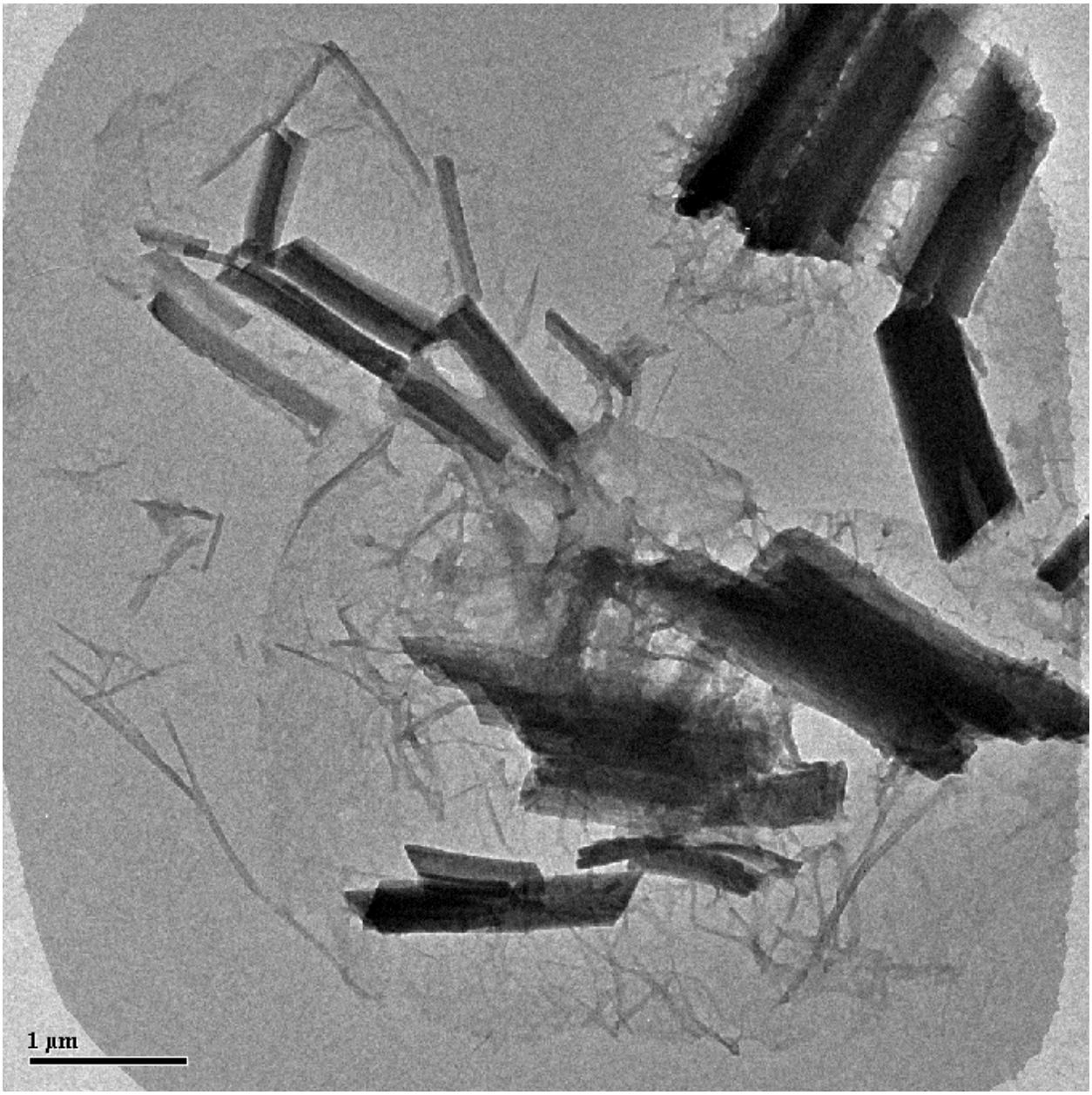

Figure 4.9*: Phase contrast image (2500x magnification) of the specimen, taken from an evaporated, sonicated solution of pyrogallol[4]arene in 99:1 water to ethanol. The larger, thicker cylinders are between 900 nm and 150 nm in diameter, while the smaller nanowires are between 80 nm and 20 nm in diameter.*

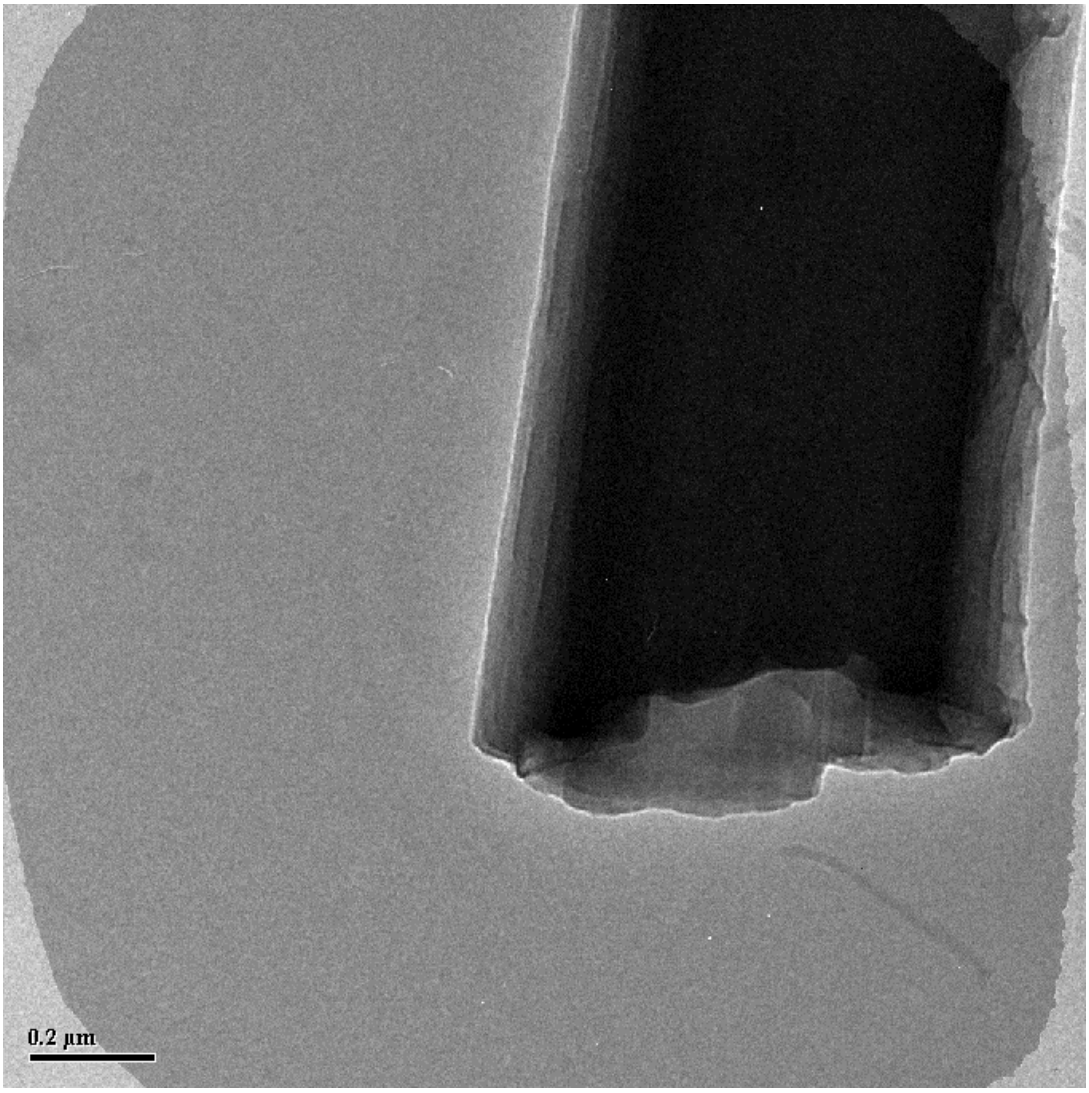

Figure 4.10*: Phase contrast image of a large cylindrical aggregate taken at 10000x magnification. Ordered texture is seen running the length of the cylindrical aggregate, with thickness, and thus transmission loss, increasing near the center of the cylinder.*

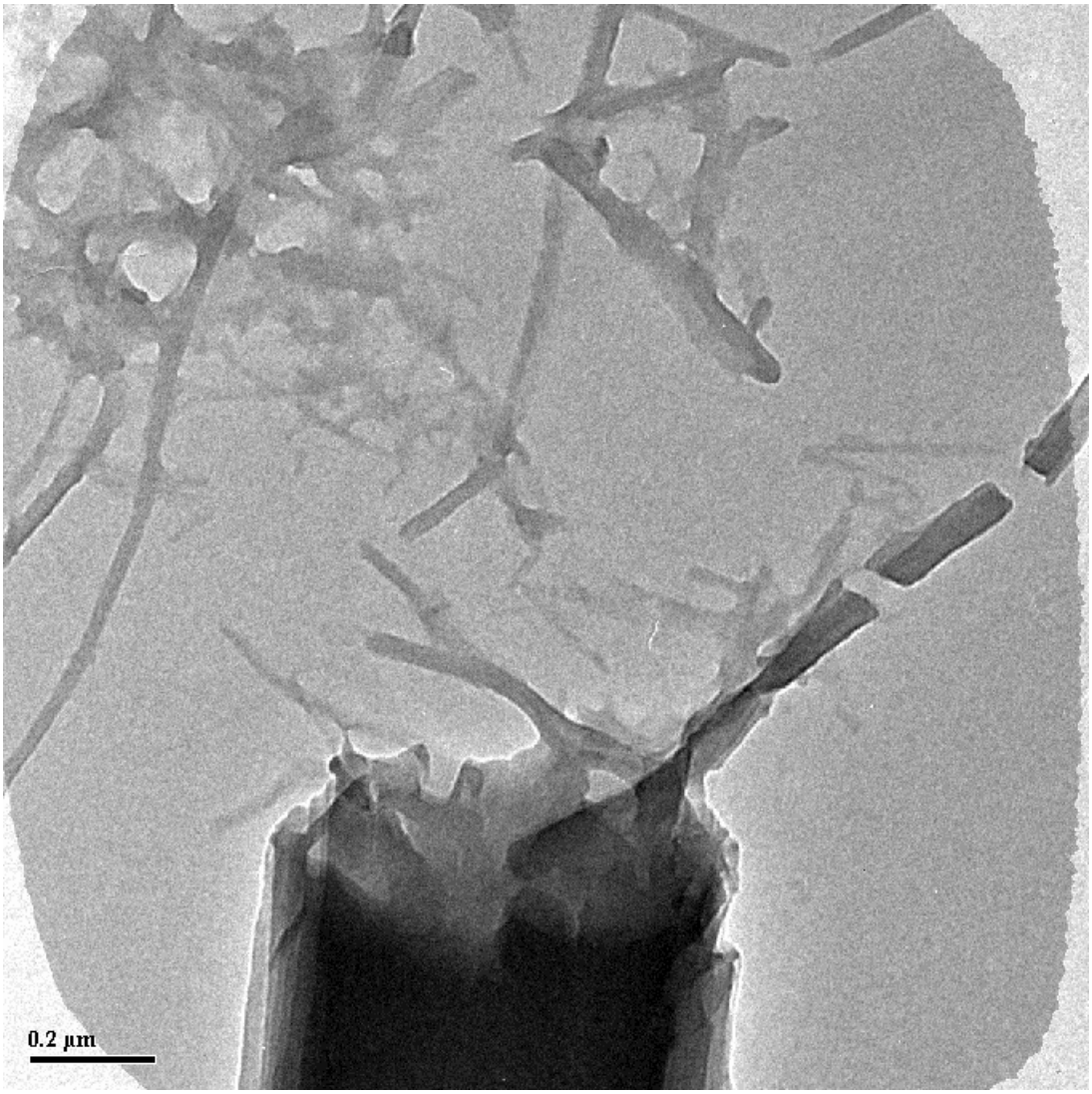

Figure 4.11*: Phase contrast image (10000x magnification) of the same cylindrical aggregate seen in Figure 4.10. Bundles of nanotubes (8-20 nm diameter) are seen radiating from the circular edge, or "top," of the cylinder. This phenomenon is seen throughout the specimen.*

This ethanol-water post-sonication specimen was investigated further for possible crystallinity and order. When a large cylindrical aggregate is isolated by the selective-area aperture, a polycrystalline-like diffraction ring is seen, but the wide bands indicate that the nanostructure is too amorphous to be considered polycrystalline. Polycrystalline can be differentiated from crystalline in that the latter is organized into a single crystal lattice (or relatively few crystal lattices) while the former consists of crystallites that can be of

various sizes and different orientations. Rings are formed in the diffraction patterns of polycrystalline materials due to their random orientations, while crystalline materials diffract at distinct points.

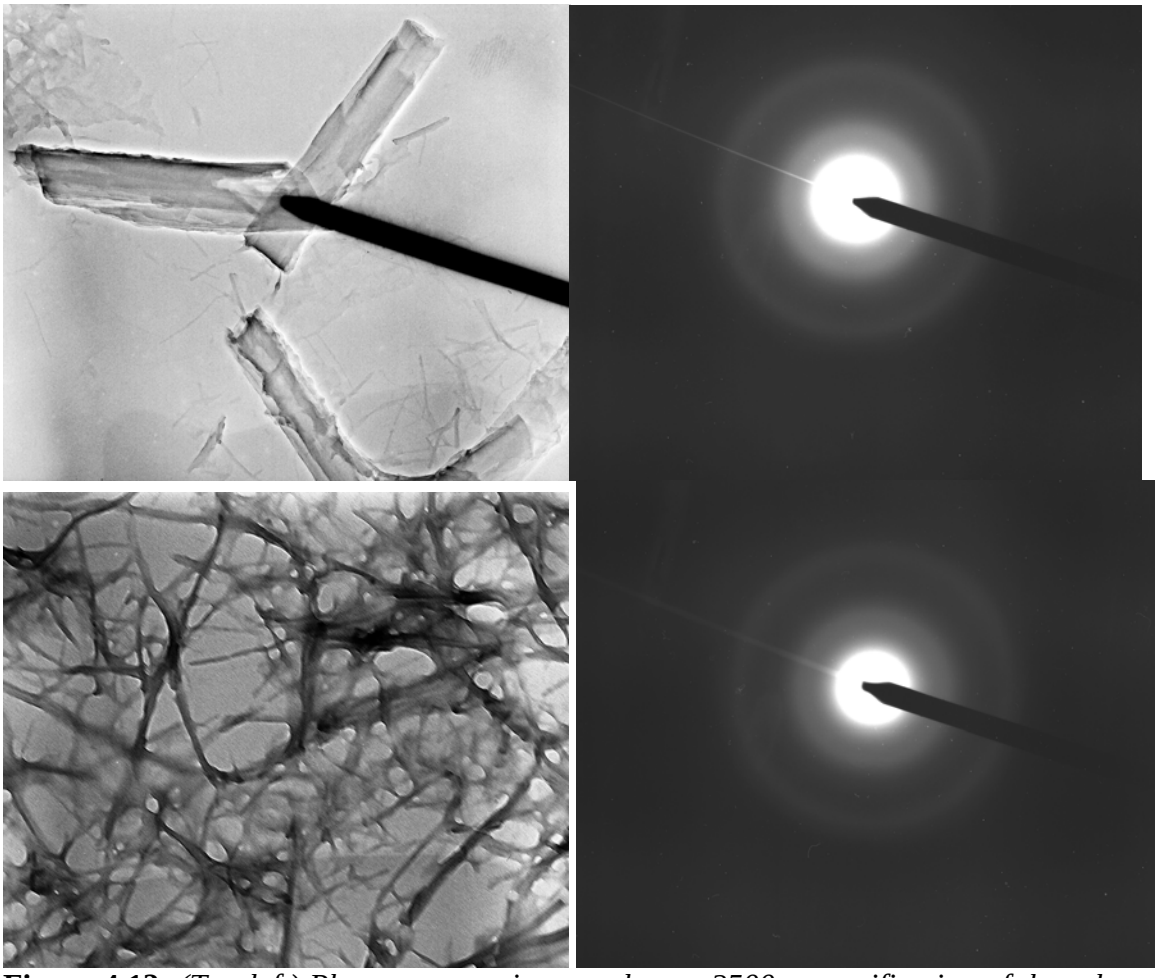

Figure 4.12*: (Top left) Phase contrast image taken at 2500x magnification of three larger cylindrical aggregates. The area of the image under the beam-stop tip is selected for using the SAD aperture to produce the diffraction rings (top right). Image (bottom left) and the derived ring pattern (bottom right) of a "web" of smaller bundles of nanotubes not associated with a large aggregate.*

The aggregate examined and the resulting diffraction pattern can be seen in the upper left and upper right panels of Figure 4.12, respectively. The observed ring pattern is the same when examining a "web" of smaller bundles of nanotubes as seen in lower left panel of Figure 4.12. A direct comparison can be made between the rightmost panels.

Nanostructures formed from the evaporation of the other three solvents were dramatically different. The 1:1 ethyl acetate to acetonitrile solution originally used to prepare the specimen seen in Figure 4.8 was used once again, nearly three months later, to determine if the nanostructures morphology remains stable over time. The more recent transmission electron micrograph, seen in Figure 4.13, is dramatically different. The sample exhibits the same "fields" of presumably amorphous disordered pyrogallol[4]arene, yet the visible nanostructures formed are spherical outcroppings, or "buds," from the amorphous fields. Attempts to examine fine structure at higher magnification showed that no fine structure was apparent (Figure 4.13, Right)

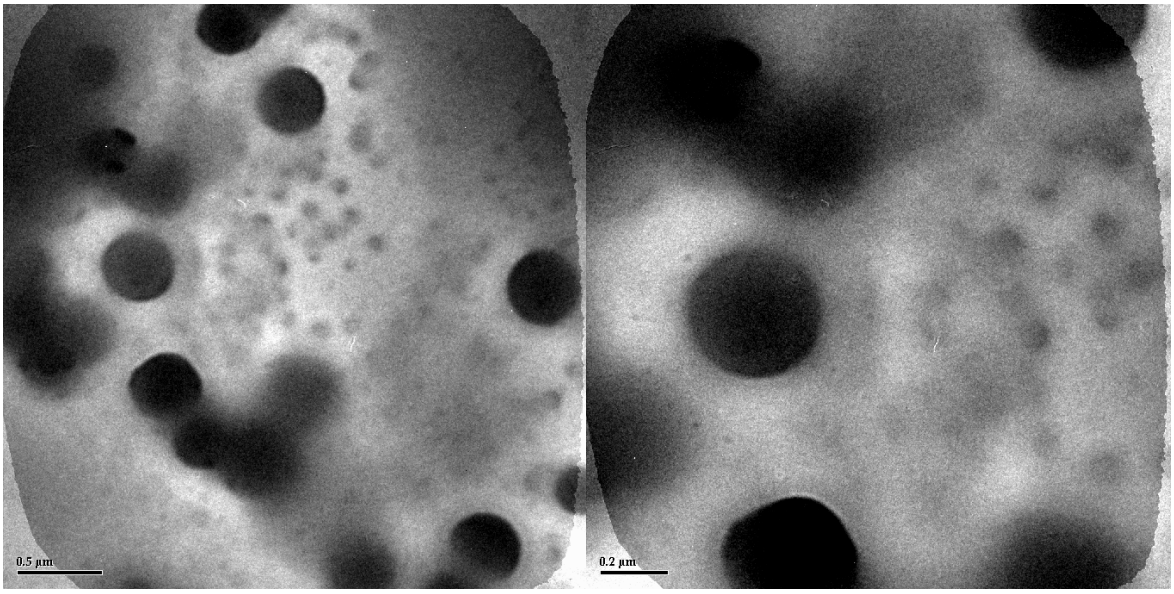

Figure 4.13*: (Left) Phase contrast image (5000x) magnification of spherical "buds" or outcroppings from the amorphous pyrogallol[4]arene fields present in this specimen, prepared from evaporation of a solution of monomer in 1:1 ethyl acetate to acetonitrile. (Right) An image (10000x) magnification revealing no additional insights into fine structure or nanostructure order.*

The nanostructures seen in the specimens prepared from evaporation of absolute ethanol and 1:1 ethyl acetate to ethanol possessed the most similar nanostructure morphologies. Side-by-side comparison of the two—seen on the left and right panels, respectively—was made at 25000x magnification (Figure 4.14) and 50000x magnification

(Figure 4.15). The similarities were striking at both magnifications, particularly at 50000x, and one can reasonably assume that these solvent systems form the same nanostructures upon evaporation. This observation, coupled with the observation that crystallization of this pyrogallol[4]arene from 1:1 ethyl acetate to ethanol shows no ordered ethyl acetate molecules in the solid-state crystal structure, supports the argument that even though there is a difference in polarity between the two solvents, ethyl acetate has no effect in both supramolecular and nanoscale structure formation when ethanol is involved.

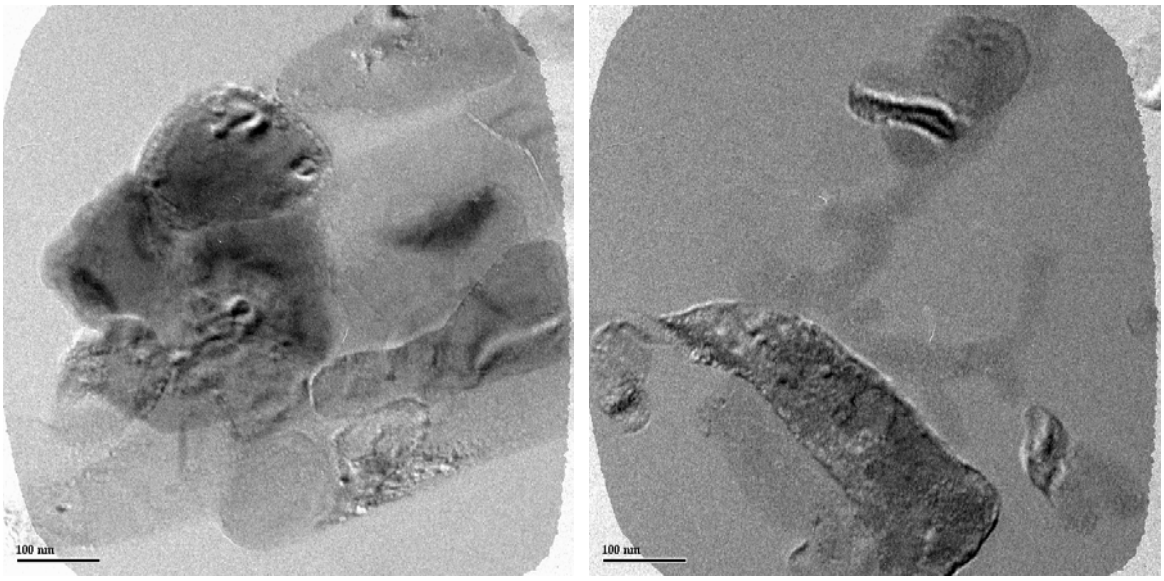

Figure 4.14*: (Left) Phase contrast image (25000x magnification) of a specimen prepared from evaporation of a solution of monomer in 1:1 EtOAc to EtOH. (Right) An image (25000x magnification) of a specimen prepared from absolute EtOH.*

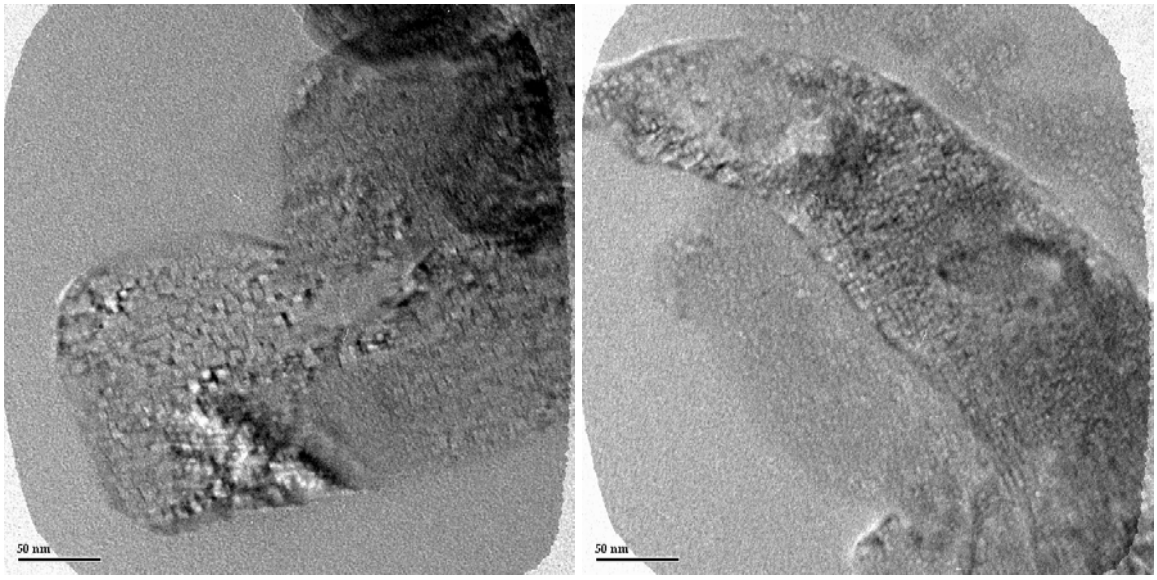

Figure 4.15*: (Left) Phase contrast image (50000x magnification) of the same 1:1 ethyl acetate to ethanol specimen seen in the left panel of Figure 4.14. (Right) An image (50000x magnification) of the absolute ethanol specimen seen in the right panel of Figure 4.14.*

Evident at the higher magnification (50000x) seen in Figure 4.15, are distinct rectangular and ordered "tiles" measuring about 25 to 35 Å in diameter. This is roughly the size of a single nanotube in the solid state structures. These "tiles" are closely packed in 2-D space, as one sees in the solid-state crystal structure. These nanostructures could perhaps be large aggregates or bundles of short nanotubes, but the amorphous environment of the surrounding material and the difficulty in studying a given particle at high magnification for long periods of time makes this statement a supposition.

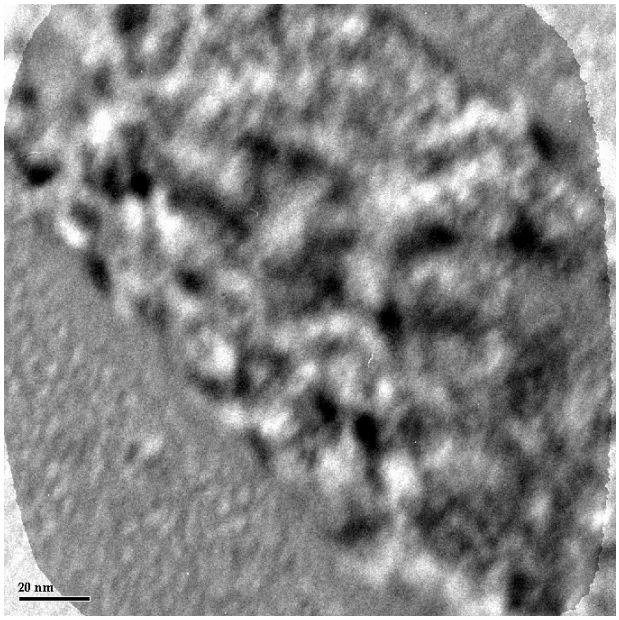

Figure 4.16*: (Left) Phase contrast image taken at 100000x magnification of the same absolute EtOH specimen seen in the right panels of Figure 4.14 and 4.15.*

Attempts to image the material at high magnification were made, but were futile. As seen in Figure 4.16, specimen drift and degradation of the sample prevented the capture of a high-resolution image, and no additional information could be gleaned. Unfortunately, at high magnifications (>50000x), specimen degradation and shift is significant in all of the studied samples.

Conclusions

The formation of the hexameric nanotube morphology by compound **2** is surprising. No ancillary or solvent molecules are present to aid in ordering the sidechains or filling void space in the hydrophobic domain of the crystal. Enthalpically, the only energetically favorable supramolecular interactions exist at the interfaces of the

hydrophilic phenolic regions of the macrocycle. As the pyrogallol[4]arenes are structurally identical in this region, one would expect the supramolecular interactions to also be identical in solution and the solid-state. As with the "hydrophobic interactions" mentioned previously, the variation in solid-state morphology is derived from the geometry that minimizes supramolecular hydrophobic-hydrophilic contacts and increases solvent entropy.

This entropy is easily exemplified in the void space that is present in the crystal. The *inter*annular portion of the crystal is roughly 60% of the crystal lattice by volume. A layer of polar protic solvent molecules (water and ethanol) are organized by the phenolic hydroxyls lining the nanotube interior (or pore). However, significant disorganization of the space between this first layer of solvation signifies that a favorable solvent entropic situation exists.

The tight interlocking between the 3-pentyl sidechains of pyrogallol[4]arene **2** appears to be the dominant force in the crystal lattice. This "gearing" interaction completely excludes water or other solvent molecules from the hydrophobic region of the crystal and perfectly minimizes void space in this *intra*annular domain. The larger branched-chain pyrogallol[4]arenes **3** and **4**, have 12 and 24 extra methylenes per macrocycle, respectively. In an extended geometry, the extra carbon atoms expand the radius of the hydrophobic domain beyond the radius encompassed by the phenolic upper rim of the macrocycle. With too much steric bulk to accommodate between the rings, the cogged, hexameric ring geometry of **2** is not the entropically-preferred morphology and a bilayer is formed. Presumably, the shorter-chained pyrogallol[4]arene **1** would yield too much void space in the cogged nanotube morphology, as the steric bulk of 12 methylenes per macrocycle would be absent. While studies at the air-water interface[1,5] suggest that

some entropically-favored interaction occurs between macrocycle monomers, only the bilayer morphology is observed in the solid state.

Specimens prepared by evaporation of pyrogallol[4]arenes in four different solvent systems were studied and imaged by transmission electron microscopy. The nanostructures morphologies were different for each solvent system, indicating that the solid-state crystallized nanotubes of compound **2** can form different nanostructures out of different solutions. However, all nanostructures appear to be spontaneously-formed in polar solution, with the 1% ethanol in water solution yielding the only structures formed from evaporation.

The specimens formed from solutions of pyrogallol[4]arene 2 in ethanol or 1:1 ethanol to ethyl acetate show ordered aggregates that exhibit fine structure. At 50000x magnification, these aggregates are shown to be composed of structures approximately 25 to 35 Å in diameter, the same dimensions as the nanotube observed in the solid state. This observation confirms the nanotube supramolecular morphology. In this solvent system, however, the rings do not form into infinite stacks—a trait which may only be present in the sonicated 1% ethanol in water specimens.

Experimental

Compounds Studied

Compounds 1-4

These compounds were synthesized by Dr. Oleg Kulikov and were used as received. Synthetic details are reported in the literature.[1]

X-Ray Analysis

Crystallographic data for compound **2** crystallized from the mixture 20:19:1 (v/v/v) EtOAc:EtOH:H_2O in nano-tubular motif (form A). $C_{152}H_{238}O_{52}$, M = 2897.42, triclinic, a = 12.5581(17), b = 29.097(5), c = 30.504(7) Å, U = 9743(3) $Å^3$, μ = 0.074 mm^{-1}, T = 100(2) K, space group P-1, Z = 2, GOF = 1.129, final R-indices (R_1 = 0.1645, wR_2 = 0.3740), 103521 reflections collected, 33806 unique (R_{int} = 0.186), CCDC 729499.

Crystallographic data for compound **2** crystallized from the mixture 1:1 (v/v)EtOAc:MeCN in nano-tubular motif (form B). $C_{162}H_{229}N_5O_{43}$, M = 2934.50, triclinic, a = 12.546(2), b = 29.291(6), c = 29.804(5) Å, U = 9564(3) $Å^3$, μ = 0.073 mm^{-1}, T = 100(2) K, space group P-1, Z = 2, GOF = 1.619, final R-indices (R_1 = 0.1820, wR_2 = 0.4672), 155193 reflections collected, 32525 unique (R_{int} = 0.1644), CCDC 729498.

Data for both crystal structures were collected on a Bruker Kappa Apex II CCD detector single crystal X-ray diffractometer.

Transmission Electron Microscopy

Four solvent systems were investigated for this study—the original 1:1 ethyl acetate to acetonitrile mixture, a 1:1 ethyl acetate to ethanol mixture, a 99:1 water to ethanol mixture, and a pure ethanol mixture. The 99:1 water to ethanol specimen yielded large extended aggregates that were easily visible with the naked eye and thus too large for TEM work. This mixture was sonicated for 15 minutes to give a stable suspension usable for specimen preparation. In all cases, a copper/continuous carbon support grid was

dipped in a given pyrogallol[4]arene solution with a concentration of 600μM and left to air dry for 30 minutes.

Specimens were examined and imaged primarily with the JEOL 2000 FX microscope with an electron acceleration voltage of 120kV. CryoTEM conditions are achieved using a suitable specimen holder that cools the specimen using liquid nitrogen. A digital CCD camera was used to capture all images with this microscope. However, for the images and associated diffraction patterns shown in Figure 4.12, the more powerful Phillips EM 430 microscope (acceleration voltage of 300kV) was used with a film camera for image/pattern collection. The film negatives were developed and digitized by David Osborn.

Images were taken primarily at 25000 x magnification or lower, as the nanostructures of interest were easily visible at these magnifications. However, in a few cases, images were taken at 50000 x and 100000 x magnifications in an attempt to investigate the fine structure of nanostructures. In many cases, specimen degradation and drift under the electron beam rendered images of low clarity and resolution, though these are examined.

1 Kulikov, O. V.; Daschbach, M. M.; Yamnitz, C. R.; Rath, N.; Gokel, G. W. *Chem. Commun.* **2009**, 7497-7499.

2 Elliott, E. K.; Daschbach, M. M.; Gokel, G. W. *Chem. Eur. J.* **2008**, *14*, 5871-5879.

3 Yamnitz, C. R.; Negin, S.; Carasel, I. A.; Winter, R. K.; Gokel, G. W. *Chem. Commun.* **2010**, *46*, 2838-2840.

4 (a) Atwood, J. L.; Barbour, L. J.; Jerga, A. *Chem. Commun.* **2001**, 2376-2377. (b) Antesberger, J.; Cave, G. W.; Ferrarelli, M. C.; Heaven, M. W.; Raston, C. L.; Atwood, J. L. *Chem. Commun.* **2005**, 892-894.

5 Daschbach M. M.; Unpublished work.

6 (a) Cave, G. W.; Ferrarelli, M. C.; Atwood, J. L. *Chem. Commun.* **2005**, 2787-2789. (b) Dalgarno, S. J.; Cave, G. W.; Atwood, J. L *Angew. Chem. Int. Ed. Engl.* **2006**, *45*, 570-574. (c) Dalgarno, S. J.; Power, N. P.; Atwood, J. L *Coord. Chem. Rev.* **2008**, *252*, 825-841.

7 Gerkensmeier, T.; Iwanek, W.; Agena, C.; Frölich, R.; Kotila, S.; Näther, C.; Mattay, J. *Eur. J. Org. Chem.* **1999**, 2257-2262.

8 Shivanyuk, A.; Friese, J. C.; Doring, S.; Rebek Jr., J. *J. Org. Chem.* **2003**, *68*, 6489-6496.

9 MacGillivray, L. R.; Atwood, J. L. *Nature* **1997**, *389*, 469-472.

10 Qin, L.C. *Rep. Prog. Phys.* **2006**, *69*, 2761-2821.

11 Langlais, V. A.; Gauthier, Y.; Belkhir, H.; Maresca, O. *Phys. Rev. B.* **2005**, *72*, 085444.

12 Mansikkamaki, H.; Nissinen, M.; Rissanen, K. *Angew. Chem. Int. Ed. Engl.* **2004**, *43*, 1243-1246.

CHAPTER 5

Antimicrobial Activity and the Development of Antimicrobial Resistance to Synthetic Ion Carriers and Channels in Bacteria

Summary and Contributions to this Work

The work presented in this chapter focuses on the characterization of antimicrobial activity of novel compounds as well as an investigation into the development of antimicrobial resistance to a known novel synthetic cation channel in *Escherichia coli*. 27 compounds were tested for their activity in Gram negative *E. coli,* revealing that only cation transporters of the known hydraphile family of compounds[1] are active in the bacterium. The other compounds studied, including known cation and anion transporters, did not elicit growth inhibition in *E. coli*.

Growth curve measurements of Gram-positive *Staphylococcus epidermidis* were used to study the effects of co-application of a diaza-18-crown-6 antimicrobial cation transporter with one of two dipicolinic dianilide (Chapter 3) anion transporters. The activity of the diaza-crown was monitored at both lethal and sub-lethal concentrations. While alone, the diaza-18-crown-6 that is studied affects antimicrobial activity, when co-applied with a dipicolinic dianilide chloride transporter the effects are completely negated.

The third and final project explored the development of antimicrobial resistance in *E. coli* to synthetic cation channel with known antimicrobial activity. The antimicrobial resistance was studied with regular application of sub-lethal concentrations of the

hydraphile cation channel over 12 days. While resistance did develop over the time period, it plateaued after 6 days of growth, developing no further resistance.

Compounds **1-12** (structures below) were made and chemically characterized by Dr. Wei Wang, a former collaborator. Compounds **13** and **14** were made and chemically characterized by Dr. Lei You, compounds **15-17** were made and chemically characterized by Dr. Oleg Kulikov, and compounds **18-27** were made and chemically characterized by me, as outlined in Chapters 2 and 3. The 24-hour growth curves were measured for the last 6 hours by an undergraduate researcher, Jason Atkins. Otherwise, I performed all of the sample preparation, specimen storage, and microbiological assays reported here.

A portion of this work is included in a paper published in *Heterocycles* in 2007.[2]

Introduction

The development of resistance to first-, second-, and even third-line antibiotics is an alarming upward trend, prevalent in both the developing and developed world.[3] Overuse and misuse of antibiotics—antibacterial soaps for the general population, prophylactic antibiotic use in livestock, doctors wrongly prescribing antibiotics for the flu, patients not completing their prescribed regimen after they feel healthy—can all further the development of resistance.[4] Application of antibiotics at sub-lethal concentrations—an end result of scenarios such as these—inevitably kills the weakest, least resistant phenotypes of a given bacterial strain, while the strongest and most resistant survive.[5] This acceleration of evolution, coupled with the twenty minute average generation time for *E. coli*, exacerbates a problem (from a human perspective) that arises naturally, without antibiotics.[6]

Resistance to antibiotics can develop for many different reasons and through many different mechanisms.[7] Eons before the pharmaceutical industry existed, a molecular arms race began between organisms small and large, simple and complex. Over the millennia, multi-cell eukaryotic organisms have developed a myriad of defenses against their distant prokaryotic relatives. Whereas humans have their own immune systems to fight off infection, other organisms have developed their own methods and molecules to do the same.

At the same time, the prokaryotes have developed ways to circumvent these eukaryotic defenses, as well as put themselves at an advantage against other prokaryotes. As evolution continues, the organisms that can exploit their genetic advantages will go on to procreate and multiply—while those that cannot go by the wayside.

While modern science has allowed us to isolate, characterize, improve, and use what antibiotic defenses nature has provided, we are only now beginning to see the effects of harnessing and improving nature on the organisms that we target for elimination. Many of these natural molecules and synthetic analogues, such as the β-lactam antimicrobial agents, that have been cornerstones in antibiotic regimens, have been showing a marked increased of tolerance in pathogenic organisms.[8] Only in the past few decades have we come to understand the many mechanisms and modes of antibiotic resistance.[9] Once we are able to fully elucidate all of these mechanisms, efforts to target antibiotics in order to circumvent these prokaryotic defenses can come about at full steam.

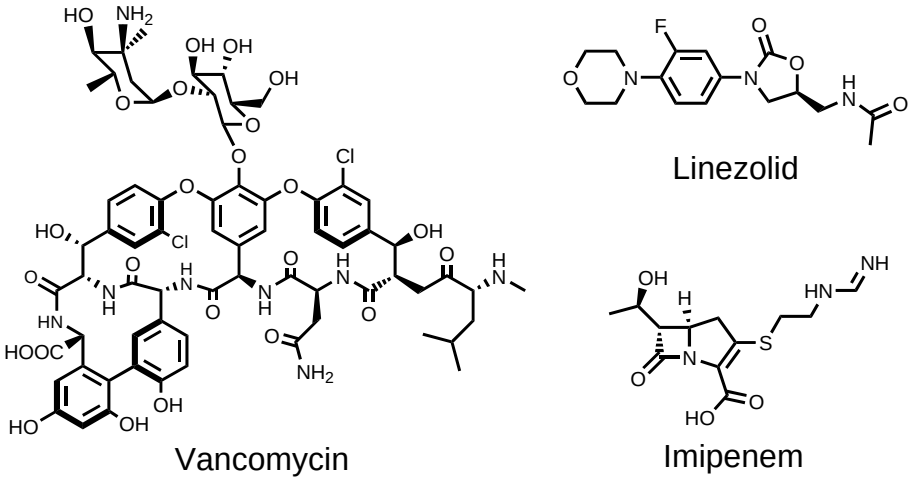

Figure 5.1 *Common drugs of "last resort" include the glycopeptide, vancomycin, the first oxazolidinone, linezolid, and the broad-spectrum beta lactam, imipenem.*

The third-line of antibiotic defense, or "drugs of last resort," include antibiotics such as vancomycin, imipenem, and linezolid that are prohibitively expensive, broad-spectrum (adversely affecting ones natural gastric flora), relatively toxic to the host, or some combination of the three.[10] While these have been used quite successfully against bacterial strains such as methicillin-resistant *Staphylococcus aureus* (MRSA)[11] that are resistant to older drugs, some of these newer antibiotics are inciting resistance themselves, as evidenced by the appearance of vancomycin-resistant *S. aureus* (VRSA).[12]

At some point in the future, medical practitioners facing an outbreak of bacterial infections resistant to multiple antibiotics may have to release these drugs of last resort for broad use. If this nightmare scenario comes to pass time and time again, our existing stockpile of novel antibiotics may run out. To circumvent this future problem, an obvious solution is better handling and use of the antibiotics already in the field. However, it might also be wise to find a proverbial über-drug—an antibiotic that is not only active against drug-resistant strains, but is immune to the development of resistance in bacteria. [13]

This über-drug may be found in the realm of novel synthetic molecules that have no significant structural basis in natural materials and do not interact directly with enzyme active sites or genetic material—areas where mutations could quickly lead to the development of resistance.[14] Compounds derived from abiotic materials may be less likely to be metabolized by either the host or the target organisms. "Foreign" structures and uncommon chemical moieties may have no "molecular predators"—enzymes with active sites that can bind with and break down the molecule. Such a substance has a two-fold therapeutic advantage *in vivo*: (1) molecules that have diffused to the infection site will be broken down only slowly by the bacterial colonies, if at all and (2) bioavailability, or the proportion of the original dosage available where needed, is higher if the host cannot metabolize the substance. This second advantage could be a drawback if the host cannot eliminate the foreign substance, inevitably becoming toxic if a build-up occurs. Such considerations must be weighed during pre-clinical *in vivo* testing with mammals, but this is beyond the scope of knowledge gleaned in a chemical biology laboratory.

The application of sub-lethal concentrations of antimicrobial agents has been employed previously to understand what fraction of the total may survive contact with the agent, and what changes may take place.[15] However, it is now well known that the presence of sub-lethal concentrations of antimicrobial agents leads to multi-drug resistance, [16] specifically in nosocomial infections where both different strains of bacteria and different antimicrobial agents are present.

Our group's studies in the biological realm consist primarily of assaying functionality in both natural and biological model systems. In this regard, we have developed a number of membrane-active ion transporters, many of which display channel functionality. Earlier work with diaza-18-crown-6 synthetic cation carriers showed that

channel functionality is not a requirement for antimicrobial activity.[17] Therefore, a broad range of ion transporters—anion or cation transporters with carrier or channel mechanisms—have been assayed for antimicrobial activity in the present work.

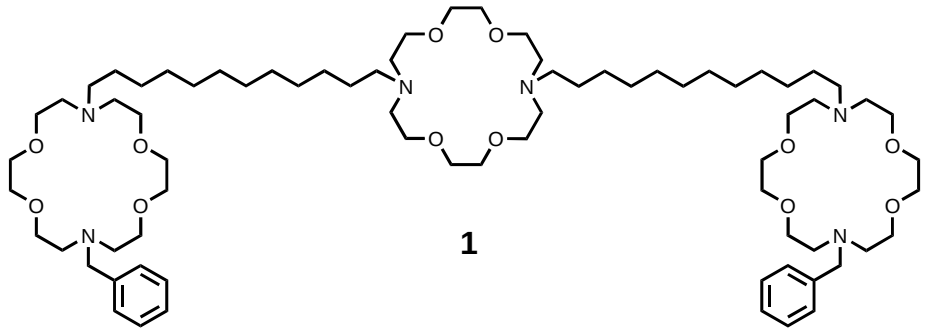

1

Previous work in our laboratory group has yielded a well-studied membrane-spanning, ion-conducting family of compounds known as hydraphiles.[18] Aside from showing ion channel activity, many of the hydraphiles have exhibited antimicrobial activity, with efficacy against Gram negative *Escherichia coli*, Gram positive *Bacillus subtilis*, and eukaryotic *Saccharomyces cerevisiae*.[17] The best characterized, and one of the most biologically-active members of this family is the C_{12} benzyl channel hydraphile, compound **1**, used for a further study into the development of antibiotic resistance in *E. coli*.

Results and Discussion

Antimicrobial activity of novel compounds

Drawn from various research projects carried out in our group, a collection of known, membrane-active ion transporters and suspected transport agents was gathered and assayed for antimicrobial activity.

Minimum inhibitory concentration (MIC) assays are performed in liquid culture

with bacteria grown over time in a liquid nutrient-rich growth media. A set of cultures with varied concentrations of the compound of interest is grown in an incubator-shaker at 37°C for 24 h. Cultures with low enough concentrations of an antimicrobial compound show growth in the form of visual turbidity. Cultures in the presence of high enough concentrations of an antimicrobial compound show no visual turbidity and thus no growth. The lowest concentration at which no growth is seen is the MIC. More active antimicrobial agents would therefore have a lower MIC. This method yields quick quantitative results that are sufficient for this broad-range study.

For the sake of comparison, many common antimicrobial agents, such as penicillin and erythromycin, are active at concentrations less than 20 μM.[19] Novel compounds that prove to be inactive in a bacterial species at concentrations of 100 μM or lower are deemed inactive and in most cases not worthy of further study in the use against the respective organism.

The first set of compounds tested for antimicrobial activity was a subset of the previously mentioned hydraphile family of synthetic cation channels. This subset was synthesized and chemically characterized by a collaborator, Wei Wang, and is unique in that they feature amide moieties at specific diazacrown-alkyl chain interfaces (outlined in Figure 5.2) rather than tertiary amines which are typical for the hydraphile family. Due to the predicted variation of nitrogen basicity and molecular geometry in tertiary amides and tertiary amines, it was believed that pH could play a determining role in the cation transport effectiveness and antimicrobial activity of the hydraphile channels.

Dr. Wang's work with the compounds focused on the cation transport activity of the hydraphiles in phospholipid vesicles, while my portion of the project entailed characterizing variations in antimicrobial activity in *E. coli* at various pH conditions.

Under normal circumstances, the pH of the unadulterated growth media is around 7.0. When used for all microbiological tests, the pH of the media is maintained using HEPES (4-(2-hydroxyethyl)-1-piperazineethanesulfonic acid), a common, biologically-inert buffer. For the more acidic growth cultures, malonic acid was added until a pH of 6.5 was indicated by a pH meter.

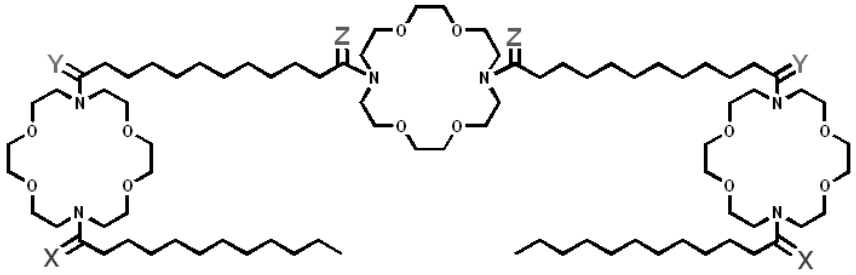

Compound	X =	Y =	Z =	MIC (μM) at pH 7	MIC (μM) at pH 6.5
2	H_2	H_2	H_2	4	1
3	H_2	H_2	O	>32	4
4	H_2	O	H_2	32	2
5	O	H_2	H_2	>32	16
6	O	O	H_2	>32	>32
7	O	H_2	O	>32	>32
8	H_2	O	O	>32	>32
9	O	O	O	>32	>32

Figure 5.2 *Amide hydraphile channels tested for microbial activity at pH 7 and 6.5. Compounds **3-9** containing amide moieties have a gray shaded box at the appropriate position, highlighting the presence of the carbonyl moiety.*

Hydraphiles **2-9** were dissolved in ethanol and serially-diluted in two-fold steps to yield a range of concentrations from 32 to 0.5 μM. While ideally ranges up to 100 μM are desired, solubility issues prevented exploration of activity at these higher concentrations. Therefore, as seen in Figure 5.2, where an MIC is reported as >32, no activity is seen in the culture with the highest concentration of hydraphile present. Note that this is distinct from a reported MIC of 32 μM (Compound **4** at pH 7).

A second set of compounds that were made and characterized by Wei Wang, called aplosspan or "simple span," were found to elicit sodium transport and channel activity in biological membranes. As with hydraphiles, these compounds, seen in Figure 5.3, were thought to be able to exhibit antimicrobial activity and were thus tested for this characteristic. The limited solubility of these aplosspans in ethanol led to the use of dimethyl sulfoxide as a solvent. As with ethanol, all assays using test compounds were compared to cultures grown in the presence of solvent alone. The solutions were prepared to yield a high end 64 μM concentration in-culture, with dilutions down to 1 μM. Limited solubility precluded the preparation of a 128 μM in-culture concentration for any of the compounds.

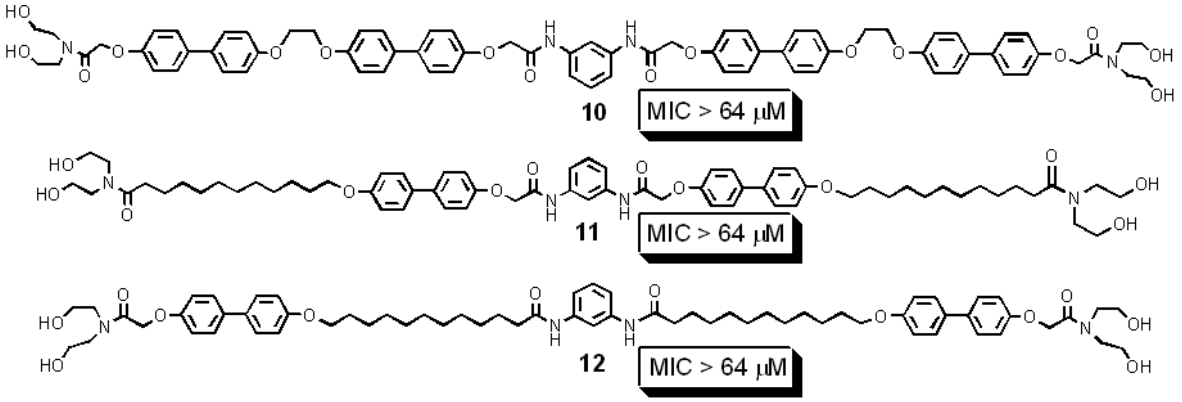

Figure 5.3 *Aplosspan molecules tested with antimicrobial activity in* E. coli *shown.*

Unfortunately, none of the aplosspans effected growth inhibition in *E. coli*. To confirm the negative results, the experiment was repeated using compound **1** as a positive control, with the same conditions used in the assay. Additionally, the optical density at 600 nm (OD_{600}, discussed in greater detail below) was measured for each of the cultures to ensure that no degree of growth inhibition occurred at the higher end of the concentration range. If growth is present in a culture, any differences in the amount of growth are

indiscernible to the naked eye, so visible light spectroscopy is necessary to ensure that no antimicrobial activity is observed. With the exception of the first set of compounds (**2-9**), which includes the known internal positive control compound, **2**, this confirmation procedure is used for all of the antimicrobial assays performed.

While **10-12**, like hydraphiles, have cation transport and channel functionality, the lack of antimicrobial activity can be attributed to the inherent solubility issues. Unaided, the compounds may not be able to pass both of the bilayer membranes present in *E. coli*. If they are able to insert into both the cell wall and plasma membrane, they may not be present in concentrations significant enough to exhibit cation transport activity due to self-aggregation in solution.

A series of synthetic anion channels was investigated for their antimicrobial activity. Heptapeptides **13** and **14**, seen in Figure 5.4, are members of the well-characterized class of compounds known as Synthetic Anion Transporter (SATs). Whereas compound **13** has established chloride transport ability and channel functionality,[20] compound **14** is cationic. Cationic peptides such as Polymyxin B[21] and synthetic lipopeptides characterized by Shai *et al*.[22] have shown antimicrobial activity due to membrane disruption and cell necrosis. These compounds selectively target membranes that are rich in anionic phospholipids—a characteristic common to both Gram positive and Gram negative bacteria,[23] as well as a number of fungi,[24] but is atypical of mammalian cells.

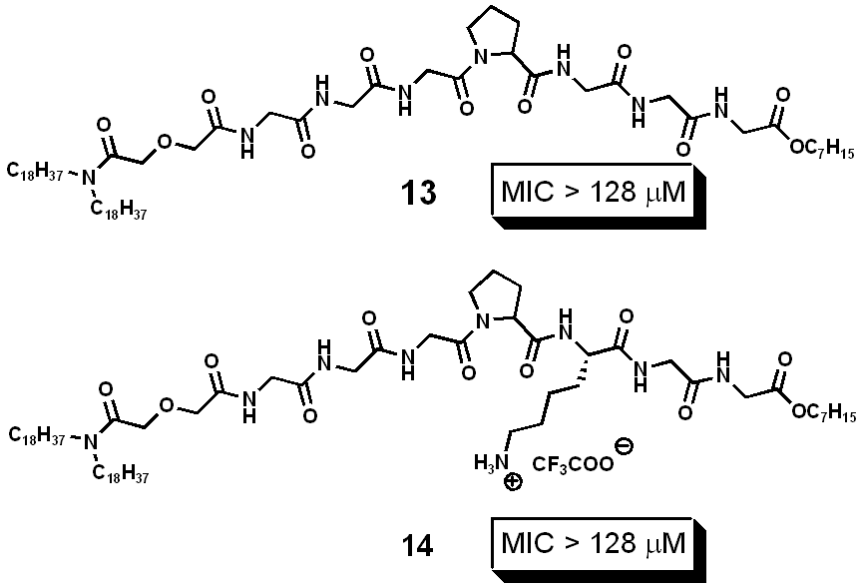

Figure 5.4 *Heptapeptide synthetic anion transporters (SATs)* ***13*** *and* ***14*** *investigated for antimicrobial activity in* E. coli.

As with the aplosspans discussed above, no antimicrobial activity is observed for compounds **13** and **14** in *E. coli*. The anion channel functionality of these compounds in biological model systems suggest that ion homeostasis can be disrupted in natural systems. Previous studies with airway epithelial cells confirm that they are, in fact, active in natural systems.[25] However, the composition of bacterial membranes—particularly the higher proportion of anionic phospholipids—may preclude membrane activity in *E. coli*. Complexation with anionic phospholipid head-groups would presumably lower chloride transport rate. Although membrane disruption, such as seen with the previously-mentioned Polymyxin B and lipopeptides, could occur, this does not appear to be the case, even with the cationic heptapeptide **14**. Finally, the heptapeptide sequence, unlike the antimicrobially-active hydraphile structure, is biotic in nature, and metabolism may occur *in situ*, effectively destroying the applied transporter molecule. In an effort to circumvent this latter drawback in using the heptapeptide SATs, only abiotic synthetic compounds were tested for the remainder of the survey.

The next three compounds studied for antimicrobial activity are members of the pyrogallol[4]arene family of compounds detailed in Chapter 4—branched chain 2-propyl (**15**) and 3-pentyl (**16**), as well as straight chain 1-undecyl (**17**), which has been shown to exhibit channel functionality in asolectin black lipid membranes.[26] These compounds, as seen in Figure 5.5, do not exhibit antimicrobial activity when applied as either ethanolic or DMSO solutions to inoculated growth cultures. Compound **16** precipitates from ethanol at concentrations greater than 32 μM. The same holds true for compounds **15** and **17** at a final concentration higher than 64 μM.

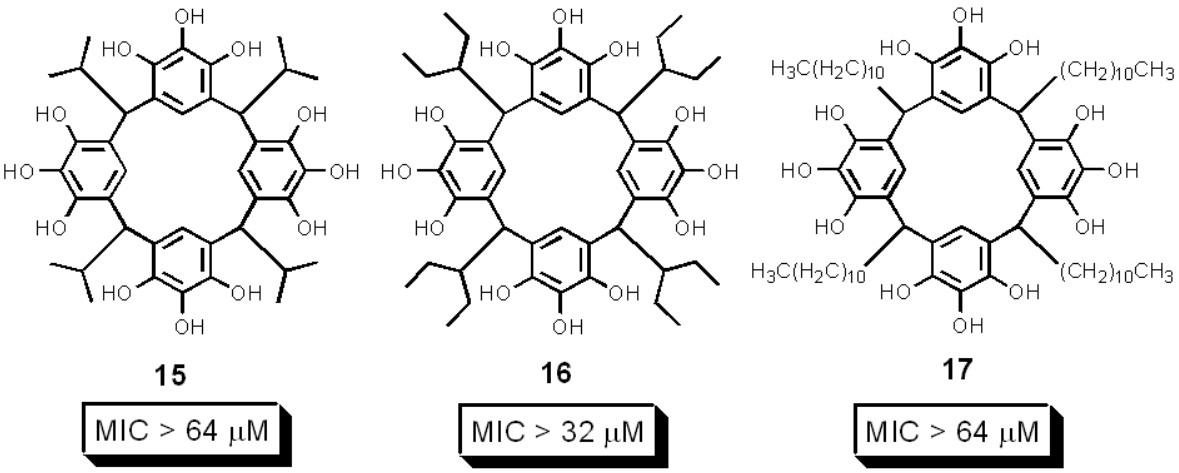

Figure 5.5 *Pyrogallol[4]arenes **15-17** tested for antimicrobial activity in* E. coli.

The potential for these compounds to act as antimicrobial agents seemed greater due to the known channel functionality of **17** and their abiotic structural motif. However, the limited solubility of the compounds in aqueous solution, particularly of 3-pentyl compound **16**, precluded membrane insertion rather than assisted in the process, as with the dipicolinic dianilides. Chronologically, these studies were performed before those in Chapter 4, so the understanding of the aggregation of **16** was not yet complete. In

retrospect, the strong intermolecular cogging interactions observed in the solid state, expanded in the nanoscale, would prevent any significant interaction with membranes.

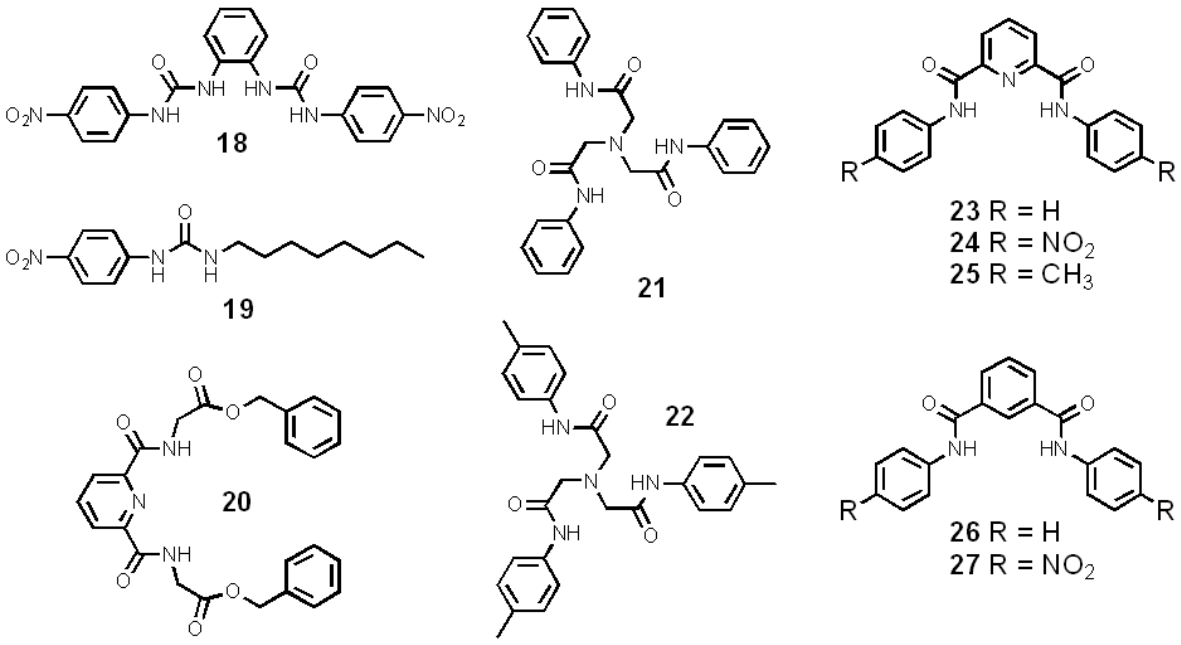

Compound	Solvent	MIC	Compound	Solvent	MIC
18	DMSO	>16 μM	**23**	DMSO	>128 μM
19	DMSO	>128 μM	**24**	DMSO	>128 μM
20	EtOH	>128 μM	**25**	DMSO	>128 μM
21	DMSO	>128 μM	**26**	DMSO	>128 μM
22	DMSO	>128 μM	**27**	DMSO	>128 μM

Figure 5.6 *Synthetic anion receptors **18-27** detailed previously in Chapters 2 and 3 and tested here for antimicrobial activity in* E. coli*. All of these compounds were applied to growing cultures of bacteria using dimethyl sulfoxide as solvent. The solubility of these compounds varied, though all were inactive at the highest concentrations that could be tested.*

A final set of compounds tested for antimicrobial activity includes the anion receptors modeled, synthesized, and characterized in Chapters 2 and 3 of this work. The anion-binding character of these compounds, seen in Figure 5.6, is similar to that of SATs **13** and **14**. However, the abiotic composition of the compounds (excepting compound **20** with two glycine residues) suggests that they may be resistant to microbial metabolism.

As the observations show, however, these anion receptors, like the heptapeptide SATs, elicit no antimicrobial activity. As before, the anionic character of bacterial

membranes may impede anion transport and preclude disruption of ion homeostasis, lending no significant growth inhibition.

Growth curves of *S. epidermidis* in the presence of ion transporters

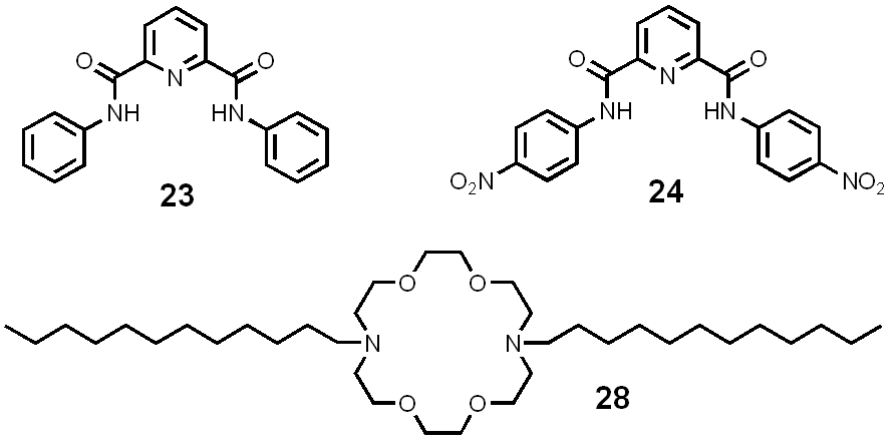

Figure 5.7 *Synthetic anion receptors **23** and **24** detailed previously in Chapter 3 and cation transporter **28** shown previously to elicit antimicrobial activity in Gram positive bacteria.*[17]

N,N'-Didodecyl-4,13-diaza-18-crown-6, compound **28**, has been shown to have antimicrobial activity against the Gram positive bacterium *Bacillus subtilis*. Presumably, this activity results from the disruption of ion homeostasis due to transmembrane sodium transport that is observed in phospholipid vesicles.[17]

With diaza-crown **28** being a known sodium transporter and **24** being a proven chloride transporter,[27] co-application of the two species may produce synergistic or deleterious effects. Compound **24** itself, as shown above, displays no antimicrobial activity in Gram negative *E. coli*, but this study tests its effects on *Staphylococcus epidermidis*, a Gram positive bacterium with significant differences in cell wall composition and architecture. *S. epidermidis* is used as the target organism as it has not been previously assessed for antimicrobial activity in our research group. Additionally, *S.*

epidermidis is in the same genus as *Staphylococcus aureus*, a microbe known for developing resistance to antibiotics. Antibiotic-resistant *S. aureus* infects an estimated 100,000 people, killing nearly 20,000 in the United States, annually.[28]

With a co-application of an anion and cation transporter, three results can be expected:

1. Transporters of both chloride and sodium working in tandem would elicit a synergistic effect that increases the antimicrobial activity of **28** alone. This can be due to a more rapid disruption of ion homeostasis
2. Transport of sodium and chloride in tandem elicits a deleterious effect wherein the antimicrobial activity of **28** is decreased.
3. The presence of a chloride transporter would not have any impact in bacterial growth rates

Whereas the third result would show that no activity is implicated in this particular biological system, either of the first two results would be a positive indication of activity in biological systems. The lack of antimicrobial activity by **23** and **24** in the first section of this chapter

To monitor the effects of the co-application of transporters, bacterial growth curves were measured using spectrophotometric means (OD_{600}) over a 24 hour growth period with recordings made every 30 minutes. While the minimum inhibitory concentration (MIC) and IC_{50} (or the concentration required for the inhibition of 50% of bacterial) can yield quantitative results, they are determined at only one given time point and give no sense of dynamic characteristics. Growth curves measure the optical density of cultures at regular intervals—yielding an understanding of bacteriostatic activity that is present for a certain

time frame. They can also give a better understanding of the interaction of two compounds in a bacterial culture as more data is recorded over the time frame, providing more than the "snapshot" afforded by antimicrobial assays.[29]

The MIC of **28** was determined using the methods outlined above, showing a lethal concentration of 16 μM. The growth curves of the three compounds alone are shown in Figure 5.8 with **28** applied at a lethal concentration and **23** and **24** applied at 50 μM. The growth curve of both **23** and **24** nearly overlap with the control, indicating that they elicit no antimicrobial activity when applied alone.

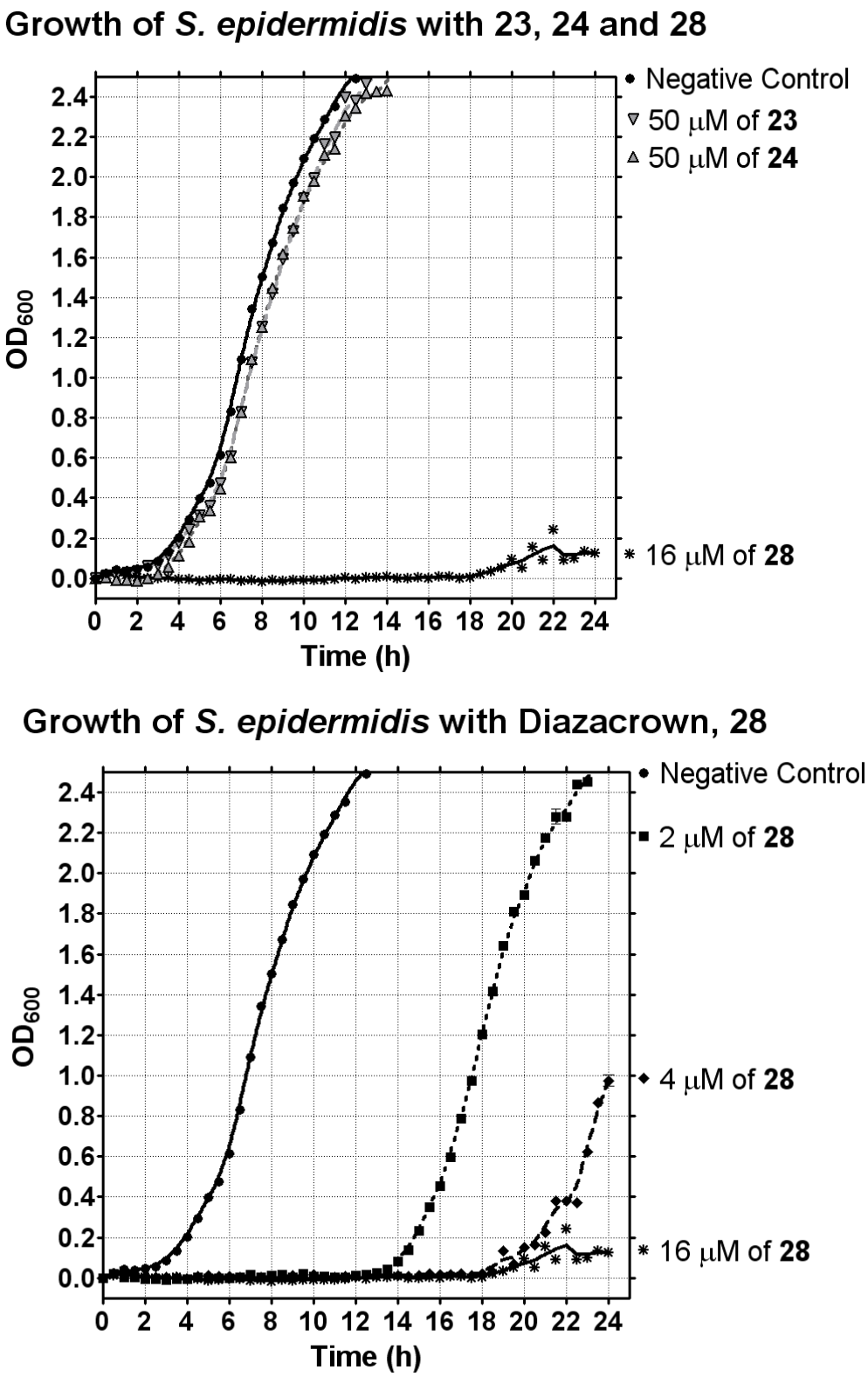

Figure 5.8 *(Top) Growth curves of* S. epidermidis *grown with either* ***23***, ***24*** *and* ***28*** *compared to the control. (Bottom) Growth curves of* ***28*** *grown at a lethal concentration (16 μM) and sub-lethal concentrations (2 and 4 μM) compared to the control.*

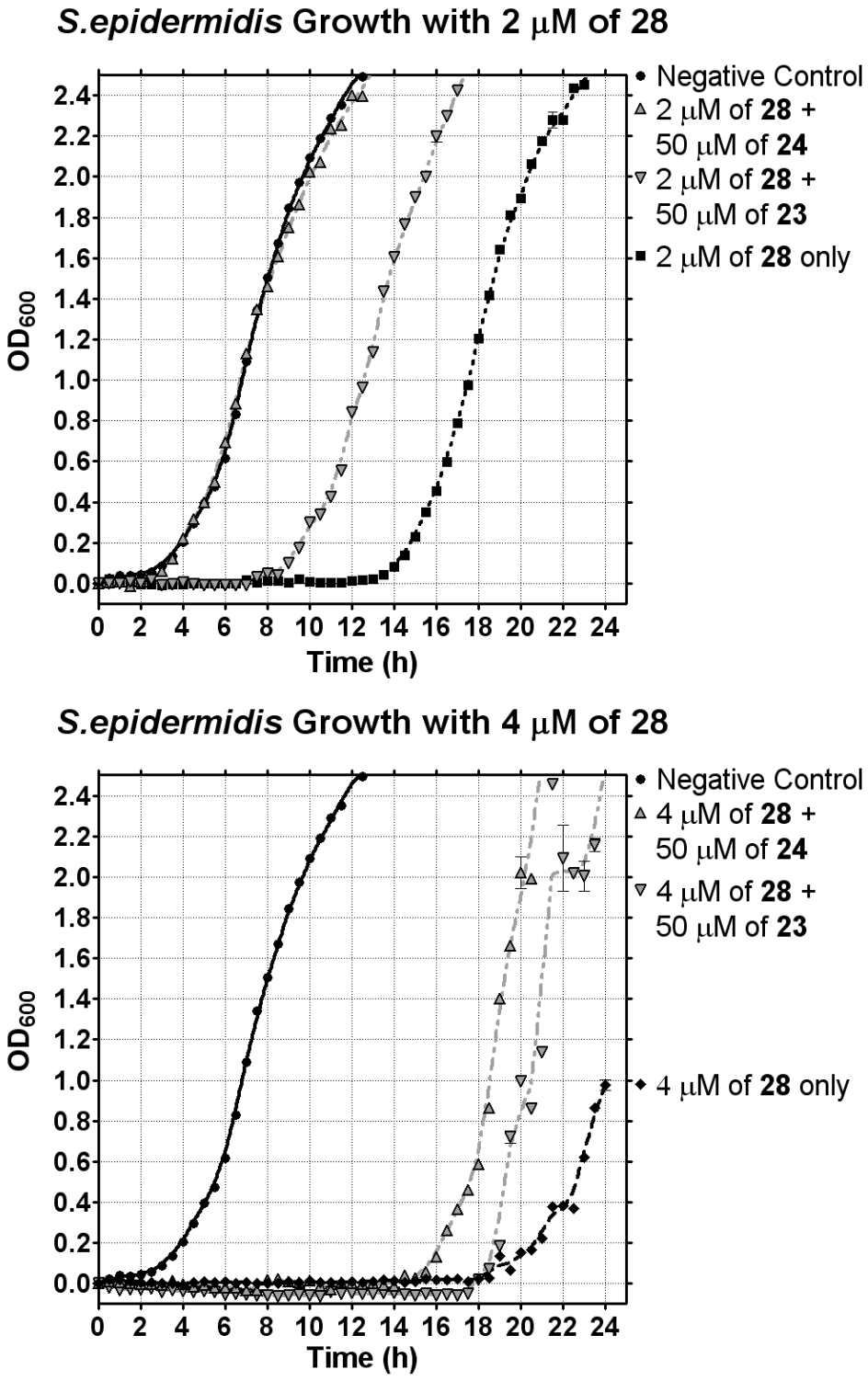

Figure 5.9 *(Top) Growth curves of* S. epidermidis *grown with 2 μM of* ***28*** *applied alone (dark boxes), with 50 μM of* ***23*** *(light down triangles) or with 50 μM of* ***24*** *(light up triangles) compared to the control. (Bottom) Growth curves with co-application using 4 μM.*

One important facet of this dynamic study is the length of lag time before the cultures began to undergo mitosis and proliferate. The addition of stressors or beneficial compounds can alter these lag times as the bacteria "mature" more slowly or more rapidly, respectively.[30] A summary of these results, focusing on the lag phase of the growth cultures are seen in Table 5.1.

Anion Transporter	Concentration (μM)	Cation Transporter	Concentration (μM)	Lag Phase (hours)	Final OD_{600}
None	0	*None*	0	3.0	>2.5
23	50	*None*	0	3.0	>2.5
24	50	*None*	0	3.0	>2.5
None	0	**28**	16	19.0[a]	0.1
None	0	**28**	4	19.0	1.0
23	50	**28**	4	17.5	>2.5
24	50	**28**	4	15.0	>2.5
None	0	**28**	2	13.5	>2.5
23	50	**28**	2	8.5	>2.5
24	50	**28**	2	3.0	>2.5

Table 5.1 *Summary of the lag phase and final optical density after 24 hours of growth. A higher OD_{600} signifies more growth at a given time while a shorter lag phase signifies quicker growth.* [a]*Deviation from the baseline occurs at this time, but exponential growth does not follow.*

The co-application with the synthetic anion transporter, *p*-nitro substituted dicipicolinic dianilide **24**, with a cation transporter, C_{12} diazacrown **28**, shows that a significant deleterious effect is imposed on the antimicrobial activity of the latter. As shown in Figure 5.9, the growth curve of this culture nearly overlaps with the control culture, indicating that the antimicrobial activity of **28** is completely negated. When **28** is

co-applied with the unsubstituted dianilide, **23**, the lag phase of bacterial growth is roughly 5 hours shorter indicating that while **23** does not efficiently transport chloride in phospholipid vesicles, and exhibits weaker chloride binding interactions, mitigation of the antimicrobial activity of **28** is still seen. At the 4 μM concentration of **28**, this mitigating effect is still seen, but the presence of **24** does not completely negate the activity of **28**, and the difference in lag phase between co-application of **23** versus **24** is not as significant**.**

Development of antimicrobial resistance in *E. coli* to hydraphile, 1

The initial step in the antimicrobial resistance study was the confirmation of the previously determined minimum inhibitory concentration (MIC) of hydraphile, **1**, when applied to *E. coli*. Four iterations of the assay yielded an average MIC of 10 μM—a value that agrees with the established value of 9.4 μM.[31] The superficial difference arises from the fact that the previous studies produced dilution series by a mass to volume ratio, whereas the current study factored in the molecular weight of the compound, resulting in exact micromolar values.

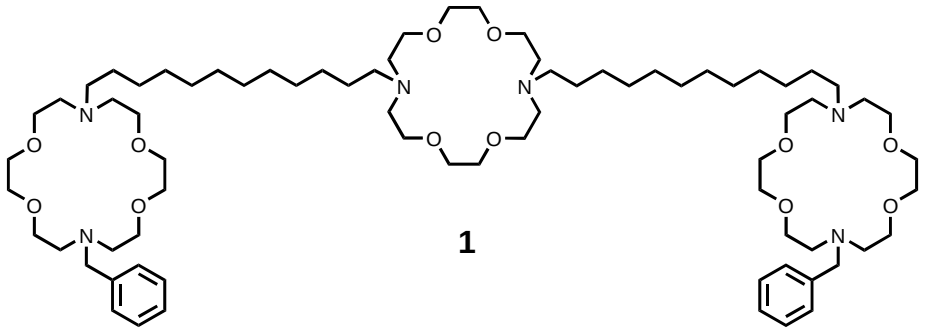

1

From this initial MIC determination, a sub-MIC (*i.e.* "sub-lethal") concentration of 8 μM (4/5 of the MIC) of **1**, in ethanolic solution, as well as an ethanol blank, is applied to stock *E. coli* in successive 24 hour growth periods, transferring a portion of the last growth culture into fresh growth media, complete with the given concentration of **1**. The non-

transferred portion of each growth culture is then frozen and preserved for later assays. This process is repeated in this study eleven additional times to yield 288 hours of growth and 12 testable samples for both the control and sub-lethal application of **1**.

The development of antibiotic resistance in the test organism is gauged using two methods, the minimum inhibitory concentration assay[32] and the spectrophotometric assay of growth,[33] both outlined previously. The former is a quick and easy estimation of antibiotic activity, while the latter can yield more sensitive results by compiling and using data from growth at all concentrations of antibiotic. The data garnered from spectrophotometric assays can be mathematically fit to a sigmoidal curve on a logarithmic concentration scale to determine the IC_{50}, or the concentration required for 50% inhibition through interpolation.[1]

The studies detailed below have determined the MIC and IC_{50} for *E. coli* cultures grown at both 8 μM and at 0 μM (blank) for up to 288 hours at each 24 hour interval, with each assay performed in at least three and up to five replications at each relevant concentration. For each iteration of spectrophotometric assays, results were normalized in the following fashion: (1) The absorbance values for all spectrophotometric readings were first adjusted by subtracting out the blank absorbance value—the optical density of uninoculated culture in the presence of only ethanol (which is normalized to 0% survival). (2) These results were then normalized by dividing by the adjusted optical density of inoculated culture with only ethanol added (which is normalized to 100% survival) to yield a percentage value. These adjusted, normalized, and averaged values were plotted against their concentrations on a logarithmic scale. A sigmoidal curve was fit to the data, and the concentration at which 50% inhibition of growth results can be interpolated from the resulting equation as shown in Figure 5.10.

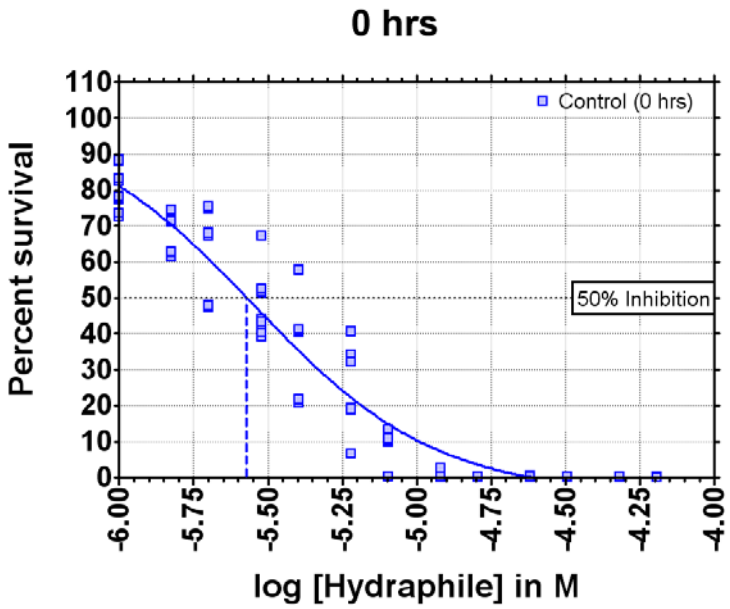

Figure 5.10 *Sigmoidal curve fit of the percent growth readings for the original stock culture. The results for all replications are shown. A 50% survival (50% inhibition) line is added to show the interpolative determination of the IC_{50} value from the curve. A second dashed line intersecting the 50% growth line is added to show the approximate IC_{50} concentration. The actual value is derived from the calculated equation.*

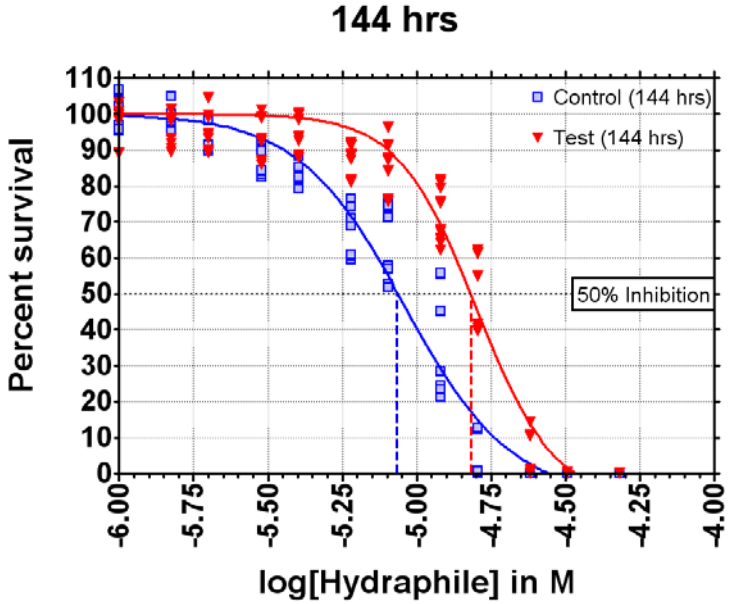

Figure 5.11 *Sigmoidal curve fit of the percent growth readings for the culture grown continuously for 144 hrs in 8 μM of* ***1*** *and 1% ethanol (Test, down triangles) and with 1% ethanol only (Control, open boxes). The results for all replications are shown. Vertical dashed lines show the concentration differences in the IC_{50} values of the test and control. The effective concentration of* ***1*** *at this time recording is the difference between the two concentrations.*

	MIC			IC_{50}		
Hours	Control	Test	**Difference**	Control	Test	**Difference**
0	10.0	10.0	**0.0**	3.2	3.2	**0.0**
24	12.0	13.0	**1.0**	5.0	5.9	**0.9**
48	14.0	20.0	**6.0**	7.2	10.5	**3.3**
72	15.2	22.4	**7.2**	8.8	12.1	**3.3**
96	16.0	24.0	**8.0**	8.7	13.3	**4.6**
120	18.7	26.7	**8.0**	9.5	14.7	**5.1**
144	17.6	27.2	**9.6**	9.4	16.0	**6.6**
168	17.3	26.7	**9.3**	8.9	16.6	**7.7**
192	16.0	24.0	**8.0**	9.9	16.2	**6.3**
216	17.6	27.2	**9.6**	10.5	17.4	**6.9**
240	18.7	26.7	**8.0**	10.7	15.9	**5.3**
264	16.0	26.7	**10.7**	9.8	17.9	**8.1**
288	17.6	27.2	**9.6**	9.3	16.2	**7.0**

Table 5.2 *Average MICs of at least three independent trials for both control and test cultures. IC_{50} values are interpolated from a curve fit to the normalized growth percentages of the same trials used for determining MIC values.*

These same methods and mathematical relationships can be applied to the other samples taken from each culture. This has been done with cultures grown for every 24 h interval up to 288 h. These results can all be compared to the original results from the stock culture of *E. coli*, and a time-dependent trend can be established. To describe this trend, the effects of the hydraphile alone must be differentiated from the effects of adding ethanol to the growing cultures. Thus, the activity values of the blank samples are subtracted from the activity values of the test growth cultures to yield the effect of the presence of hydraphile at the given concentration. MIC values can be subtracted from one another to yield these results, and the differences in the interpolated values from the IC_{50} curves can be used for the effective activity. An example of this is shown in Figure 5.11

with dashed lines showing where on the concentration coordinate the IC_{50} value for the test and control cultures fall. The tests, blanks, and final results for both methods are summarized in Table 5.2, IC_{50} curves fit to normalized measurements can be seen in Appendix A and the final results are graphically represented in Figure 5.12.

The results show that while the concentration required to effect antimicrobial activity increases with constant exposure to hydraphile, some portion of this increase can be attributed to growth in the presence of 1% ethanol. After about 6 days, or 144 hours of growth, this change in effective concentration plateaus, for both the test and control cultures.

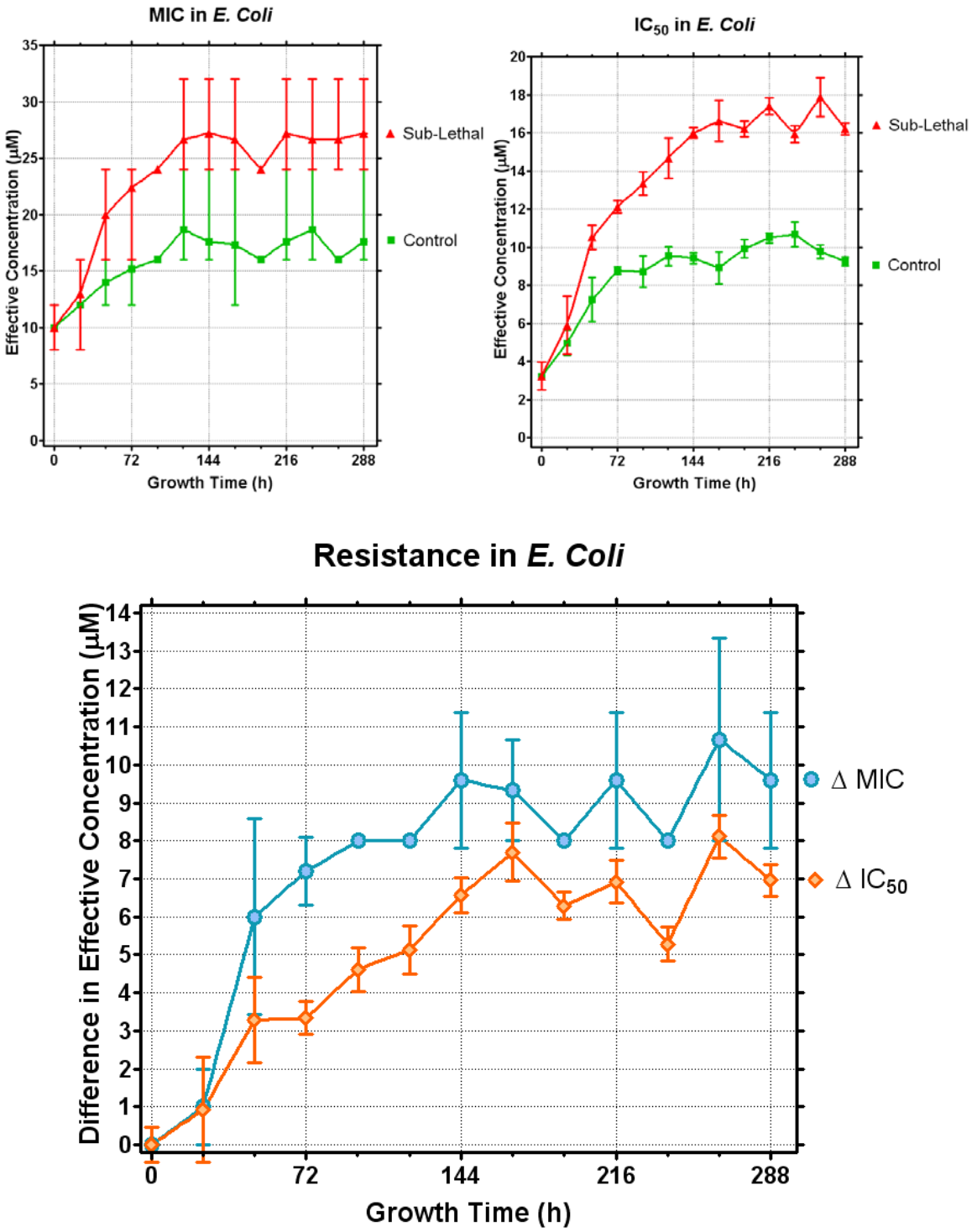

Figure 5.12 *(Top) Change in the measured MIC (left) and IC_{50} (right) over time for cultures grown in the presence of hydraphile* ***1*** *and 1% ethanol (triangles, "sub lethal") and 1% ethanol only (squares, "control"). MIC error bars represent the range of replicates recorded, IC_{50} error bars represent the standard deviation from the curve fit to the data points at each time point. (Bottom) Difference in effective concentrations of the MIC (open circles) and IC_{50} (open diamonds) between the control and test.*

Conclusions

The investigation of activity in biological systems is an overarching goal of chemical biologists. The ability of a synthetic transmembrane ion transporting agent to elicit antimicrobial activity is just one example of how this goal can be realized. As demonstrated by these investigations, not all ion transport agents effect antimicrobial activity. Compounds that exhibit ion transport activity in biological model systems, such as phospholipid vesicles and phospholipid planar bilayer membranes, are, by definition, membrane active. However, due to the heterogeneous character of natural systems with membrane proteins and sugars, a wider variety of phospholipids,[34] efflux proteins that actively pump toxic substances out of the cell,[35] and (in the case of *E. coli* and other Gram negative organisms) a second bilayer membrane forming the bacterial cell wall, complications can certainly arise. The fact that any of these compounds exhibit membrane activity at all is surprising, given the complexity of these systems and their defenses.

While previous work has established that cation channels, as well as cation carriers, can effect antimicrobial activity, the compounds surveyed in the present study show that neither anion channels nor anion carriers can reproduce the effect. Conceivably, the disruption of the balance of anions within a target system would impair growth or cause apoptosis. However, the anionic nature of bacterial membranes can impede the ability of anion carriers and channels to effect their intended chloride transport purpose in bacteria.

The co-application with the synthetic anion transporter, *p*-nitro substituted dicipicolinic dianiline **24** with a cation transporter, C_{12} diazacrown **28**, shows that the antimicrobial activity of the latter is completely negated when applied at 2 μM. As shown in Chapter 3, the unsubstituted dianilide, **23**, does not bind chloride as strongly or transport

chloride as efficiently in phospholipid vesicles, but the antimicrobial activity of **28** is likewise mitigated in the presence of **23**, albeit to a lesser extent. The simultaneous transport of chloride and sodium by each species is implicated in the negation of the antimicrobial activity of **28**. Presumably, the disruption of the sodium gradient by **28** is eliminated as an environmental stressor by the presence of **24** as a chloride transporter or as a transport blocker, interacting directly with **28**.

Finally, these studies show that *E. coli* evolve resistance to C_{12} benzyl channel, compound **1,** over extended periods of constant exposure to a sub-lethal concentration, but the development of resistance does not continue to develop after an initial time period. Using either the MIC or IC_{50} as a gauge, *E. coli* has developed only a two-fold resistance to compound **1** over 288 h. The assays also show that resistance develops continuously until about 144 h, or 6 days of growth, and then begin to plateau. This characteristic is promising as the individuals that are resistant to the effects of the antibiotic are not being selected for, and application of a high enough concentration of hydraphile **1** continues to elicit bactericidal function even after a continuous application of high, but sub-lethal, concentrations of the drug.

The sensitivity of the MIC assays used in the original antimicrobial studies is improved by utilizing intercalated two-fold dilutions. The IC_{50} spectrophotometric assays show a level of sensitivity that is not reached with the stepped threshold levels seen in the MIC assays and better precision is more readily attained.

These spectrophotometric assay methods can be applied to both standard antibiotics or other hydraphiles for a relevant comparison. If C_{12} benzyl channel performs better over continued sub-MIC exposure times than standard antibiotics, then there may be some

advantage that the compound and related structures possess that circumvent the downfalls of other antibiotics.

Experimental

General

All UV-Vis absorbance spectra were recorded on a Beckman Coulter DU 7400 Spectrophotometer. All microbiological assays are performed using sterile technique. All equipment and growth media solutions are autoclaved to 121°C with sterilizing conditions confirmed by autoclave tape. Equipment that is prepackaged as sterile is not similarly sterilized and assumed usable as delivered. All transfers are performed with sterile equipment that is flamed (passed over a Bunsen burner a number of times in rapid succession) before and after transfers, and all unique transfers use a new micropipette tip. Before each liquid transfer or inoculation, the liquid is vortexed for at least 3 seconds to ensure proper mixing and even distribution of nutrients, agents, and/or bacteria. To ensure accuracy and reproducibility, all assays are replicated from 3 to 5 times at each relevant concentration.

The study tests the viability of *Escherichia coli* DH5α cells with a plasmid expressing ampicillin resistance. Unless otherwise noted, all inoculations are of the standard inoculum size of 5×10^{5} CFU ml^{-1}. This is measured as an approximate optical density of 0.5 at 600nm compared to growth media blank. Cultures grown from frozen stock are thus grown to an optical density of between 0.45 and 0.55.

The growth media used in all experiments is LB Miller broth, which contains 10g L^{-1} casein peptone, 10 g L^{-1} sodium chloride, and 5 g L^{-1} yeast extract. The growth media

is made selective for ampicillin resistance by the addition of 50μM ampicillin, and is pH balanced at 7.0 by 10mM 4-(2-hydroxyethyl)-1-piperazineethanesulfonic acid (HEPES) buffer.

Compounds Studied

Compound 1

This compound was synthesized by Dr. Wei Wang and was used as received. Synthetic details are reported in the literature. [36]

Compounds 2-9

These compounds were synthesized by Dr. Wei Wang and were used as received. Synthetic details are reported in the literature.[2]

Compounds 10-11

These compounds were synthesized by Dr. Wei Wang and were used as received. Synthetic details are reported.[37]

Compound 12

This compound was synthesized by Dr. Wei Wang and was used as received. Synthetic details are reported in the literature.[38]

Compound 13

This compound was synthesized by Dr. Lei You and was used as received. Synthetic details are reported in the literature.[39]

Compound 14

This compound was synthesized by Dr. Lei You and was used as received. Synthetic details are reported in the literature.[40]

Compounds 15-17

These compounds were synthesized by Dr. Oleg Kulikov and were used as received. Synthetic details are reported in the literature.[41]

Compounds 18-17

These compounds were synthesized by me, as detailed in Chapter 2 of this work.

Compounds 23-27

These compounds were synthesized by me, as detailed in Chapter 3 of this work.

Compound 28

This compound was synthesized by Dr. Wei Wang and was used as received. Synthetic details are reported in the literature.[42]

Serial Dilutions

The compound of interest is dissolved in either ethanol or DMSO at a concentration one hundred times the desired in-culture concentration. A volume of 20 μL is added to each culture, which in total has a volume of 2000μL. Two-fold serial dilutions of the test antibiotic are established using either the macrobroth dilution method or the stock solution dilution method. The latter entails diluting the stock solution down a series of solutions containing the solvent used for the antibiotic. These pre-diluted solutions are then each added to the series of growth media. The macrobroth method involves the same dilution aspect, but is performed with pre-inoculated liquid media in each culture tube. Two different series of dilutions can be used to establish two series of intercalated concentrations. In most experimental replications, the macrobroth dilution method is used to create two intercalated series for testing, though for at least one replication of each assay the stock solution dilution method is used to validate both the macrobroth method and

statistical distribution. The standard dilution concentrations for the intercalated series are 2 μM and its two-fold multiples (128, 64, 32, 16, 8, 4, 2, 1, 0.5) and 3 μM and its two-fold multiples (96, 48, 24, 12, 6, 3, 1.5, 0.75).

Minimum Inhibitory Concentration

The minimum inhibitory concentration (MIC) is determined using a modification of the methods outlined by the NCCLS.[32] The modification entails using two intercalated series of serial two-fold dilutions of a given antibiotic instead of the standard single series. The use of intercalated series is expected to yield more sensitive results. The MIC is determined by inoculating each test tube in the series with a standard inoculum size and growing at 37°C, while agitating at 200 rpm for 16 hours. The MIC is determined by a visual inspection of turbidity. An antibiotic concentration at which the resulting solution is cloudy (turbid) is one in which growth has not been inhibited. A concentration at which the resulting solution is transparent is a concentration at which growth is inhibited. The lowest concentration at which this latter scenario is true is thus determined as the MIC. If growth is present at the highest concentration at both series, the MIC is listed as higher than that concentration and, for all intents and purposes, the compound is inactive.

Spectrophotometric Assays

Using the same dilution and growth procedures as used for MICs (the same grown cultures can be used, as well), the optical density (absorbance) at 600nm is measured for each dilution using a UV/Vis spectrophotometer. All readings are compared to a blank consisting of uninoculated growth media with the test compound present.

The spectrophotometric data were normalized by subtracting the absorbance of uninoculated culture and 1% ethanol as the blank for all values before dividing by the blank-adjusted absorbance of an inoculated culture grown with 1% ethanol to yield the adjusted and normalized growth percentages. Using the graphing software GraphPad, data points from all of the replications were plotted against the logarithmic concentration of **1** and, using non-linear regression analysis with equation 1, fit to a variable-slope sigmoidal dose-response curve as previously described.[1]

$$Y = \text{Bottom} + \frac{(\text{Top} - \text{Bottom})}{1 + 10^{(\text{LogEC50}-X)\cdot\text{HillSlope}}} \quad \textbf{(eq.1)}$$

Values are fit to equation 1 where "Y" equals the percentage of growth, "X" equals log[hydraphile] of each dilution, "Top" is the maximal growth (100%), normalized to the results of the ethanol blank and "Bottom" is the minimum growth (or 0%). The resulting value, "LogEC50," is converted to a micromolar concentration for reporting in Table 5.3 and Figure 5.12.

Continuous Growth

E. coli from stock culture is used to inoculate two growth cultures—one containing a sub-MIC concentration (8 μM) of C_{12} benzyl channel hydraphile, **1**, in ethanol and one containing a blank with only ethanol added (1% present in culture). Each culture, with compound solution and inoculum added, has a volume of 2mL. This first generation is incubated for 24h at 37°C while agitating at 200 rpm.

After one 24h cycle, an 100 μL inoculum (5% of volume) is transferred from the first generation culture to fresh growth media with the appropriate amount of compound present. The concentrations for growth after the first cultures are adjusted to be additive with compound already present in previous growth that is transferred over with the

inoculum so that a constant 8 μM is present. This second set of growth cultures is again incubated for 24 h at 37°C while agitating at 200 rpm, and the process is repeated for a total of twelve sets of growth cultures.

Meanwhile, the remnants of these growth cultures (1900 μL) are frozen to –80°C using glycerol added to yield 15% volume as a cryoprotectant. A portion of these frozen cultures are revived at a later date by adding 50 μL of thawed culture to fresh growth media. These are grown out to mid-logarithmic phase (OD_{600} = 0.5) and used to inoculate cultures grown for the MIC and IC_{50} studies, using a different thawed culture for each replication.

Growth Curves

The methodology for this investigation uses a modified procedure from an earlier study comparing antibiotics and investigating synergistic effects.[29] Using regular (non-selective) growth media without ampicillin, *S. epidermidis* was grown from stock culture to mid-logarithmic phase, and is subsequently used to inoculate ten growth cultures. Three cultures were grown containing only diaza-crown 28 at three concentrations: 16 μM, 4 μM and 2 μM—the first being the pre-determined MIC of 16 μM in *S. epidermidis* and the latter two below the MIC. Two cultures were grown containing either dipicolinic dianilide **23** or **24** alone, each at 50 μM. Six cultures were grown containing a combination of **23** or **24** (at 50 μM) and diaza-crown **28** at the three tested concentrations. For cultures with only one type of transporter present, the solvent used for the other transporter type is thus added to eliminate experimental differences. Finally, a control culture was grown with no compounds present in 0.5% DMSO and 0.5% ethanol.

Each culture was measured for growth by the optical density at 600 nm assay

method. Absorbance readings above 2.5 approach higher deviation from linearity and can be thought of as “full growth” for this purpose.

1 Leevy, W. M.; Donato, G. M.; Ferdani, R.; Goldman, W. E.; Schlesinger, P. H.; Gokel, G. W. *J. Am. Chem. Soc.* **2002,** *124*, 9022-9023.

2 Wang W.; Yamnitz, C. R.; Gokel, G. W. *Heterocycles* **2007,** *73*, 825-839.

3 Shales, D. M.; Dale, N. G.; John, J. F. *et al*.; *Clin. Infect. Dis.* **1997**, *25*, 584-599.

4 (a) Goossens, H.; Ferech, M.; Vander Stichele, R.; Elseviers M. *Lancet* **2005**, *365*, 579-587. (b) Ferber, D. *Science* **2002**, *295*, 27-28.

5 Matagne, A.; Dubus, A.; Galleni, M.; Frère, J.-M. *Nat. Prod. Rep.* **1999**, *16*, 1-19.

6 Marr, A. G. *Microbiol. Rev.* **1991**, *55*, 316-333.

7 Tenover, F. C. *Am. J. Med.* **2006**, *119*, S3-S10.

8 Thomson, J. M.; Bonomo, R. A. *Curr. Opin. Microbiol.* **2005**, *8*, 518-524.

9 Tenover, F. C. *Am. J. Med.* **2006**, *119*, S3-S10.

10 (a) Polk, R. E.; Healy D. P.; Schwartz, L. B.; Rock, D. T.; Garson, M. L.; Roller, K. *J. Infect. Dis.* **1988**, *157*, 502-507. (b) Alván, G.; Nord, C. E. *Drug Saf.* **1995**, *12*, 305-313.

11 Levine, D. P. *Clin. Infect. Dis.* **2006**, *42*, S5-S12.

12 Sieradzki, K.; Roberts, R. B.; Haber, S. W.; Tomasz, A. *N. Engl. J. Med.* **1999**, *340*, 517.

13 Zasloff, M. *Nature* **2002**, *415*, 389-395.

14 Cirz, R. T.; Chin, J. K.; Andes, D. R.; de Crécy-Lagard, V.; Craig, W. A.; Romesberg, F. E. *PloS Biology* **2005**, *3*, 1024-1033.

15 (a) Schönfeld, J. K.; Peuchen-Drost, N.; Büchli, E. *Ant.van Leeuwenhoek* **1957**, *23*, 150-160. (b) Michael, J. G.; Massell, B. F.; Perkins, R. E. *J. Bacteriol.* **1963**, *85*, 1280-1287.

16 Kohanski, M. A.; DePristo, M. A.; Collins, J. J. *Mol. Cell* **2010**, *37*, 311-320.

17 Leevy, W. M.; Weber, M. E.; Gokel, M. R.; Hughes-Strange, G. B.; Daranciang, D. D.; Ferdani, R.; Gokel, G. W. *Org. Biomol. Chem.* **2005**, *3*, 1647-1652.

18 (a) Gokel, G. W. *Chem. Commun.* **2000**, 1-9. (b) Leevy, W. M; Donato, G. M. Ferdani, R.; Goldman, W. E.; Schlesinger, P. H.; Gokel, G. W. *J. Am. Chem. Soc*. **2002**, *124*, 9022–9023. (c) Leevy, W. M; Gokel, M. R.; Hughes-Strange, G. B.; P. H. Schlesinger, P. H.; Gokel, G. W. *New J. Chem.* **2005**, *1*, 205–209.

19 Watanakunakorn, C. *J. Infect. Dis.* **1971**, *124*, 581-586.

20 (a) Djedovic, N.; Ferdani, R.; Harder, E.; Pajewska, J.; Pajewski, R.; Weber, M. E.; Schlesinger, P. H.; Gokel, G. W. *New J. Chem.* **2005**, *29*, 291-305. (b) Ferdani, R.; Gokel, G. W. *Org. Biomol. Chem.* **2006**, *4*, 3746-3750.

21 Morrison, D. C.; Jacobs, D. M. *Immunochem.* **1976**, *13*, 813-818.

22 Makovitzki, A.; Baram, J.; Shai, Y. *Biochemistry* **2008**, *47*, 10630-10636.

23 Ghuysen, J.-M.; Hakenbeck, R. eds. *Bacterial Cell Wall*, Elsevier; Amsterdam, Netherlands, **1994**.

24 De Lucca, A. J.; Walsh, T. J. *Antimicrob. Agents Chemother.* **1999**, *43*, 1-11.

25 Pajewski, R.; Garcia-Medina, R.; Brody, S. L.; Schlesinger, P. H.; Gokel, G. W. *Chem. Commun.* **2006**, 329 – 331.

26 Li, R.; Kulikov, O.; Gokel, G. W. *Chem. Commun.* **2009**, 6092-6094.

27 Yamnitz, C. R.; Negin, S.; Carasel, I. A.; Winter, R. K.; Gokel, G. W. *Chem. Commun.* **2010**, *46*, 2838-2840.

28 Klevems, R. M.; Morrison, M. A.; Nadle, J. *et al.*; *J. Am. Med. Assoc.* **2007**, *298*, 1763-1771.

29 Chalkley, L. J.; Koornhof, H. J. *Antimicrob. Agents Chemother.* **1985**, *28*, 331-342.

30 Ameyama, M.; Shinagawa, E.; Matsushita, K,; Adacji, O. *Agric. Biol. Chem.* **1984**, *48*, 3099-3107.

31 Leevy, W. M.; Gammon, S.; Levchenko, T.; Daranciang, D. D.; Murillo, O.; Torchilin, V.; Piwnica-Worms, D.; Huettner, J. E.; Gokel, G. W. *Org. Biomol. Chem.* **2005**, *3*, 3544-3550.

32 National Committee for Clinical Laboratory Standards, *Methods for Dilution Antimicrobial Susceptibility Tests for Bacteria that grow Aerobically*, NCCLS, Wayne, Pennsylvania, **2000**,5th edn., M7-A5.

33 Contois, D. E. *J. Gen. Microbiol.* **1959**, *21*, 40-50.

34 Ghuysen, J.-M.; Hakenbeck, R. eds. *Bacterial Cell Wall*, Elsevier; Amsterdam, Netherlands, **1994**.

35 M. A. Webber, L. J. V. Piddock; *J. Antimicrob. Chemother.* **2003**, *51*, 9-11.

36 Murray, C. L.; Gokel, G. W. *J. Supramol. Chem.* **2001,** *1*, 23-30.

37 Wang W.; Doctoral Dissertation **2008**, Chapter 4.

38 Wang W.; Li, R.; Gokel, G. W. *Chem. Commun.* **2009,** 911-913.

39 Schlesinger, P. H.; Ferdani, R.; Liu. J.; Pajewska, J.; Pajewski, J.; Saito, M.; Shabany, H.; Gokel, G. W. *J. Am. Chem. Soc.* **2002**, *124*, 1848-1849.

40 You, L.; Li, R.; Gokel, G. W. *Org. Biomol. Chem.* **2008**, *6*, 2914-2923.

41 Kulikov, O. V.; Daschbach, M. M.; Yamnitz, C. R.; Rath, N.; Gokel, G. W. *Chem. Commun.* **2009**, 7497-7499.

42 Leevy, W. M.; Huettner, J. E.; Pajewski, R.; Schlesinger, P. H.; Gokel, G. W. *J. Am. Chem. Soc.* **2004,** *126*, 15747-15753.